Contributions to

IPAC15

Richmond, Virginia, USA – May 3rd – 8th 2015

TITLE / AUTHORS **PAGE**

NUMERICAL OPTIMIZATION OF ACCELERATORS WITHIN oPAC

C.P. Welsch#

Cockcroft Institute, Daresbury, UK and The University of Liverpool, Liverpool, UK
on behalf of the oPAC Consortium

Abstract

Powerful simulation tools are required for every accelerator and light source to study the motion of charged particles through electromagnetic fields during the accelerator design process, to optimize the performance of machine diagnostics and to assess beam stability and non-linear effects. The Optimization of Particle Accelerators (oPAC) Project is funded by the EU within the 7th Framework Program and currently supports 23 Fellows that are based at institutions across Europe. This large network carries out R&D that closely links beam physics studies with the development of diagnostics and beyond state-of-the-art simulation tools. This contribution presents selected research outcomes from oPAC, including the numerical optimization of beam loss monitor locations along the European Spallation Source's 5 MW proton linac, results from tracking studies for the LHeC lattice that allow beam stability to be assessed, and multi-objective optimization of the linear and non-linear beam dynamics of the synchrotron SOLEIL. In addition, an overview of recent and future oPAC events is given.

INTRODUCTION

oPAC – Optimization of Particle Accelerators – is a Training Network funded by the European Union [1]. With a budget of almost €6M shared between 12 beneficiary partners over a 4-year period, it brings together 34 institutions across the industry and academia to provide formation on particle accelerators to a total of 23 early stage researchers. The main objective of the oPAC network is to train the next generation of accelerator scientists and engineers for the increasingly demanding community of accelerator facilities while strengthening the bonds within this community. oPAC is also strongly engaged in raising public awareness on the importance of particle accelerators for society, through their applications in health, industry, security, energy, and fundamental knowledge.

Each of the Fellows is developing a project set in one of the following topics: research of beam dynamics, development of beam diagnostics, numerical simulation tools, and accelerator control and data acquisition systems. In addition to the research in their home institution, the Fellows undertake secondments in any of the other partner institutions, complementing their formation and fostering collaborative research. Moreover, the Fellows receive regularly specific training on complementary skills and techniques through a series of topical workshops and schools that are held at different venues across the network. The Fellows together with the central management team are also carrying out an intensive program of outreach and dissemination, through the internet and social media, but also through the organization of events and participation in conferences, trade fairs, exhibitions, etc.

*This project has received funding from the European Union's Seventh Framework Programme for research, technological development and demonstration under grant agreement no 289485.

#carsten.welsch@cockcroft.ac.uk

RESEARCH

As outlined before research within the network is carried out across four thematic work packages. The following subsections highlight progress made by three exemplar Fellows across these work packages.

Beam Loss Monitoring at ESS

The linear accelerator of ESS will produce a 5 MW proton beam. Beam of this power must be strictly monitored by a specialized Beam Loss Monitoring (BLM) system to detect any abnormal losses and to ensure that operational losses do not exceed a limit of 1 W/m. In order to optimize the detectors layout in terms of their numbers and locations a series of beam loss simulations was performed using the MARS Monte Carlo code. Different loss scenarios were considered and yielded an indication of the energy deposition along the ESS linac.

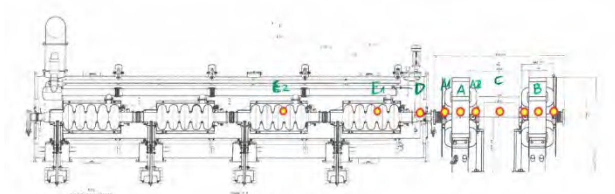

Figure 1: Loss point locations.

Different beam loss simulations were performed for four different energies in the ESS cold linac, ranging from 220-2,000 MeV [2]. For all of these energies 10 different possible locations along a cryomodule-quadrupole doublet were chosen, see Fig.1. At these locations three points on the beam pipe were considered as possible loss points. Losses were then simulated for 3 different angles: 1 mrad, 3 mrad and 1°. The power deposited in air around a loss was used as primary indicator for suitable BLM locations as it is proportional to the BLM signal within certain limits. For more accurate results, an approach using particle flux-to-generated charge converters shall be applied in the future. BLMs were placed around the cryomodule-quad assemblies in a way that optimizes three figures of merit: Distinguishability of individual losses, volume coverage and sensitivity. The aim is to avoid missing any loss (full volume coverage), ability to differentiate between individual losses, and detecting even smallest losses which are just above the noise level.

This was done by a custom-written MATLAB algorithm utilizing a matrix representation of the loss cases and detectors that are being considered. This algorithm was then compared to a brute force method which simply evaluates the root mean squares for pairs of detectors, see [2] for further details.

Tracking Studies in the LHeC Lattice

An interaction region design for the LHeC was proposed in the Conceptual Design Report [3]. The aim of this design was to achieve head-on electron-proton collisions in the interaction region 2 (IR2) at a luminosity of $L=10^{.}33cm^{-2}s^{-1}$ which requires a low β*=10 cm. This was achieved by implementing a new set of quadrupoles closer to the interaction point, called the inner triplet (IT), at a distance L* from the IP. A first integration of the LHeC IR into the HL-LHC lattice was performed. This integration consisted in an extension of the ATS was done in the arc 23 to perform a telescopic squeeze to further reduce the value of β*in IP2 while leaving the HL-LHC insertions (IP1 and IP5) undisturbed. Achieving a value of β*=10 cm for IP2 and β* of 15 cm in IP1 and IP5.

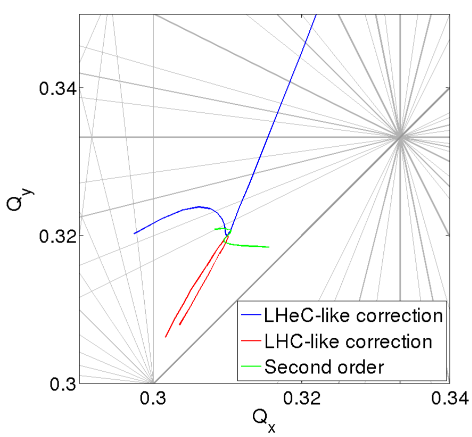

Figure 2: Calculated variation in horizontal and vertical tune for different corrections.

The flexibility of this design was studied in terms of minimizing β* to study the reach in luminosity, and in terms of increasing L* to reduce the synchrotron radiation. This work explores the different types of chromatic corrections for the nominal case with β*=10 cm and L*=10 m by studying its impact on the stability of the beam via the dynamic aperture and the effect of non linearities via frequency map analysis. Three different chromatic corrections were studied. The first one, named "LHC-like" performs the chromatic correction similar to the LHC by changing the focussing and defocussing families by the same amount. The second correction, named the "LHeC-like" adds a further constraint to control the Montague functions in the collimation insertions and allows each sextupole family to change by a different amount. And finally, the third one contemplates correcting the second order chromaticity.

DA studies were computed by E. Cruz from the Cockcroft Institute/University of Liverpool for three chromatic correction schemes in SixTrack using a polar grid of initial conditions with 30 particles for each 2σ interval and 5 different phase angle, over 10^5 turns [4]. The momentum offset was set to 2.7×10^4. Concerning the magnetic errors, 60 different realizations (seeds) were considered for the LHC magnets. Results show a similar behavior at small angles for all three cases. On the other hand it was observed that at bigger angles the second order correction gives a bigger dynamic aperture for angles ~75°, although not that different from the LHeC-like correction, while the LHC-like correction shows a negative impact for angles >50°. Frequency map analysis studies were then performed in SUSSIX and applied to calculate the variation in tunes over 5,000 and 10,000 turns for a sample of initial amplitudes via the diffusion factor. Similarities were again found for the LHeC-like and second order correction, except for the stable region observed at Qx ~Qy, where the latter case presents better results. Also, for bigger angles (Ix=0-5 σ and Iy ~20 σ) where the second order correction does not show the instability region observed in the LHeC-like case caused by resonance line (-1,4). The same regions are also different for the LHC-Like case. In this scenario the region for larger angles shows a higher instability, but the main difference is observed in the region with Qx ~Qy in which a stable region seen in the other corrections is no longer present, see Fig. 2.

Beam Dynamics Optimization at SOLEIL

The purpose of the project of X. Gavalda who is based at the Synchrotron SOLEIL, near Paris in France, is to optimize the linear and non-linear beam dynamics of the light source using Multi-Objective Genetic Algorithms (MOGA) [5] and the tracking code ELEGANT [6]. In general, the optimization of a storage ring lattice is a multi-objective problem that involves a high number of constraints and a multi-dimensional parameter space defined by the optimization variables. The introduction of the sextupole magnets to correct the strong focusing affects two important parameters of the beam dynamics: the dynamic and the momentum aperture. Both parameters are strongly related with the injection efficiency and the Touschek lifetime, respectively. In our case, the optimization objectives are the dynamic aperture and the Touschek lifetime, the variables are the settings of the quadrupole and sextupole magnets.

Genetic Algorithms [7] are a heuristic search that mimics the process of natural selection and generates solutions to optimization problems using techniques inspired by natural evolution, such as mutation, selection and evolution. Starting from an initial stable lattice called starting point (SP), MOGA searches the optimized lattices changing randomly the settings of variables: the focusing strength of the quadrupole and sextupole families. From this initial population, the algorithm chooses the best lattices that will become the parents of the next generation. With this process, the algorithm converges to the group of solutions with the best compromise between all objectives, the so called Pareto front. The process is iterative and stops when the maximum number of generations is achieved.

After the installation of MOGA at the SOLEIL cluster and the study of the preliminary optimized results, a complete comparison between ELEGANT and TRACY3 [8] has been done. The discrepancies observed between both codes in the calculation of the momentum acceptance and the vertical chromaticity were reduced introducing 6D tracking in the optimization process and changing the energy model of the dipole edge focusing, respectively. Thereafter, new lists of optimization solutions have been tested on the control room of SOLEIL using beam-based experiments to check their completeness. A complete study of the relation between the total beam, the Touschek and the gas lifetime was necessary to process these experimental data. The initial experimental results do not show an improvement of the Touschek lifetime provided by the simulations due to the proximity of the horizontal and vertical tunes to the integer resonance lines. A further study of the optimization process is necessary to improve the quality of MOGA and search the multi-dimensional space in a more complete way as defined by the quadrupole and sextupole families of the SOLEIL storage ring. These new solutions will then be tested experimentally in the near future.

TRAINING EVENTS

The League of European Research Universities, the UK-based Russel Group of research-led Universities and other similar networks recognize that best practice researcher training involves cohorts of candidates rather than individuals. The ITN structure is ideal for this and to achieve the aspirations of the EU Principles for Innovative Doctoral Training oPAC takes best advantage of industry participation and by providing regular network training to bring the Fellows together.

International Schools

All Fellows received a general introduction to the physics and technology of accelerators either through the CERN Accelerator School or the Joint Universities Accelerator School (JUAS) in 2013 or 2014. In addition, the network organized an Advanced School on Accelerator Optimization at Royal Holloway University of London in July 2014. It was attended by more than 70 delegates from within and outside of oPAC. The participation of external participants ensures knowledge exchange with a wider community and turned out to be an ideal opportunity for establishing links to other researchers working on similar topics. The school covered beam physics, instrumentation R&D and charged particle beam simulations at an advanced level [9].

Topical Workshops

oPAC has already organized a series of Topical Workshops across its work packages over the past 3 years. This includes a workshop on the Grand Challenges in Accelerator Optimization which took place at CERN, Geneva in June 2013 [10], a workshop on Beam Diagnostics hosted by CIVIDEC [11] and one on Libera Technology at Instrumentation Technologies. Most recently, a workshop on Computer-Aided Optimisation of Accelerators (CAoPAC) was held at the GSI Centre for Heavy Ion Research in Darmstadt, Germany from 10 – 13 March 2015. This was a special event for the network as it was organized by the Fellows of the network, providing them with the opportunity to take charge of a whole event from scratch, with a limited time-frame, limited resources, and the challenge of offering an interesting event to attract a good number of participants. The workshop brought together 51 participants from 18 institutions across Europe. It included talks about optics and beam dynamics modelling, control systems and data analysis, techniques for modelling accelerator components, such as diagnostics, as well as the generation and propagation of synchrotron light. A poster session and a visit of the GSI accelerator infrastructure complemented an exciting event. Two hands-on workshops have been provided by Bergoz on Beam Instrumentation and by CST their Particle Studio simulation suite. Finally, the University of Liverpool will host a workshop on Technology Transfer later in 2015 in conjunction with an outreach symposium.

Conference and Symposium

An international conference will be hosted by the national accelerator center (CNA) in Seville, Spain between 7-9 October 2015 [12]. It will promote all research outcomes from the network and enable the Fellows to engage with other university groups and private companies. The conference will also present an opportunity for follow-up activities between the oPAC partners and participating scientists from outside the network and thus serve as a career platform for all Fellows. An outreach Symposium on 26 June 2015 on Accelerators and Lasers for Science and Society will be organized at the Liverpool Convention Center as a finale to the outreach activities undertaken during the course of oPAC [13]. This will present the main project findings in an understandable way for the general public emphasizing the possible applications of the technologies concerned.

SUMMARY AND OUTLOOK

The Marie Curie network oPAC is currently in its final year and will conclude at the end of November 2015. The project has trained 23 early stage researchers in accelerator optimization and three examples of recent research results have been presented in this contribution.

In addition to a broad and interdisciplinary research program, oPAC also organizes a series of international events which have also been summarized in this paper. Despite the significant training effort provided through the network, it is clear from studies such as TIARA that many more training initiatives like oPAC will be needed to satisfy the high demand in skilled accelerator experts across Europe and around the world.

REFERENCES

[1] http://www.opac-project.eu
[2] M. Jarosz, et al., MOPTY047, Proc. IPAC, Richmond, USA (2015).
[3] LHeC Conceptual Design Report, J Physics G 39 (7) 075001 (2012).
[4] E. Cruz, et al., MOPJE079, Proc. IPAC, Richmond, USA (2015).
[5] C.M. Fonseca, P.J. Fleming, “Multi-objective genetic algorithm”, IEEE colloquium on ‘Genetic Algorithms for Control Systems Engineering’, Digest No 1993/130, (1993).
[6] M. Borland, “Elegant: A Flexible SDDS-Compliant Code for Accelerator Simulation”, Advanced Photon Source LS-287 (2000)..
[7] Konak A. et al. “Multi-objective optimization using genetic algorithms: a tutorial”, Reliability Engineering and System Safety 91 (2006) 992-1007.
[8] L. Nadolski and J. Zhang, TRACY3 Manual – SOLEIL version.
[9] indico.cern.ch/conferenceDisplay.py?confId=297045
[10] indico.cern.ch/conferenceDisplay.py?confId=243336
[11] indico.cern.ch/conferenceDisplay.py?confId=293158
[12] indico.cern.ch/conferenceDisplay.py?confId=380975
[13] indico.cern.ch/conferenceDisplay.py?confId=368273

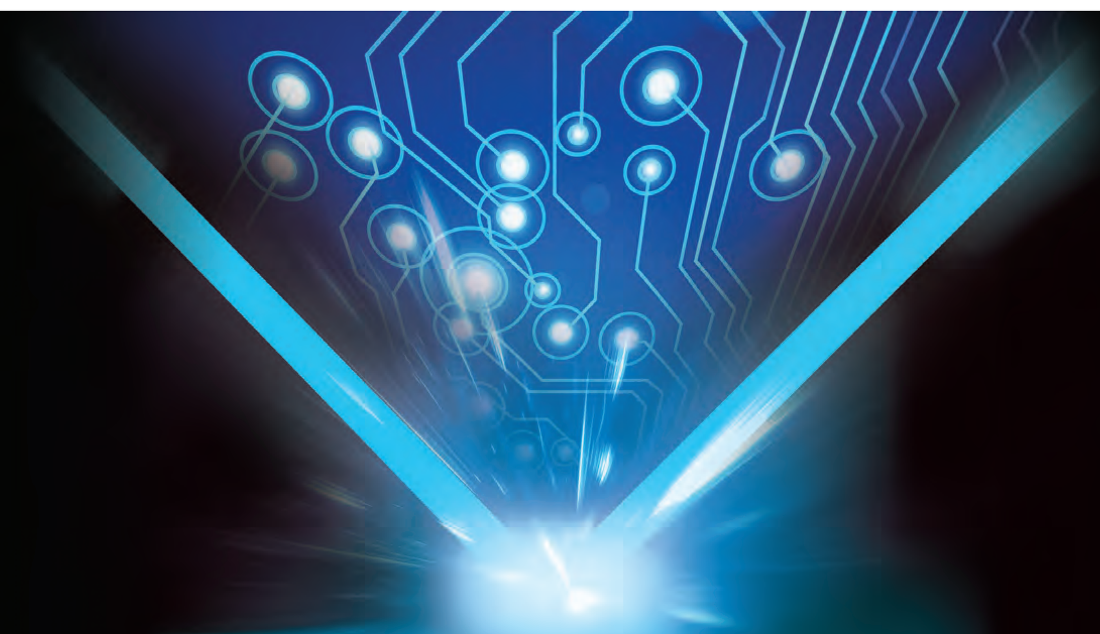

Numerical Optimization of Accelerators within oPAC

C.P. Welsch, Cockcroft Institute and The University of Liverpool, UK
on behalf of the oPAC Consortium

Abstract

Powerful simulation tools are required for every accelerator and light source to study the motion of charged particles through electromagnetic fields during the accelerator design process, to optimize the performance of machine diagnostics and to assess beam stability and non-linear effects. The Optimization of Particle Accelerators (oPAC) Project is funded by the EU within the 7th Framework Program and currently supports 23 Fellows that are based at institutions across Europe. This large network carries out R&D that closely links beam physics studies with the development of diagnostics and beyond state-of-the-art simulation tools.
This contribution presents selected research outcomes from oPAC, including the numerical optimization of beam loss monitor locations along the European Spallation Source's 5 MW proton linac, results from tracking studies for the LHeC lattice that allow beam stability to be assessed, and multi-objective optimization of the linear and non-linear beam dynamics of the synchrotron SOLEIL. In addition, an overview of recent and future oPAC events is given.

Research

oPAC is structured into four R&D work packages: beam physics, beam diagnostics, simulation tools and accelerator control and data acquisition systems. Fellow R&S stretches across these work packages and targets the optimization of existing and future accelerator-based infrastructures. Here, recent results from a few selected projects are presented.

Beam Loss Monitoring at ESS

M. Jarosz - ESS, Sweden

Project Aims: Optimize beam loss monitoring system along the ESS main linac. Identify best monitor technologies for identified loss point locations.

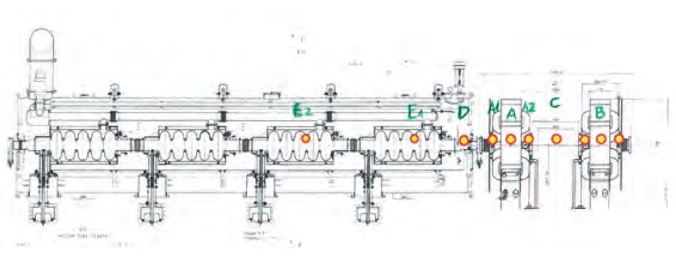

Overview of loss point locations.

Studies carried out:

- Monte Carlo simulations using MARS into different loss scenarios;
- Study of losses as function of beam energy between 220 - 2,000 MeV;
- Investigation into loss patterns at 10 locations, see figure to the left;
- Power deposited in air was used as primary indicator for suitable locations.

Results: Optimization done for 3 figures of merit: Distinguishability of individual losses, volume coverage and sensitivity using a custom-written MATLAB algorithm based on a matrix representation of the losses and detectors. Results were then compared to a brute force method evaluating the root mean squares for pairs of detectors [MOPTY047].

Tracking Studies in the LHeC Lattice

E. Cruz, Cockcroft Institute/University of Liverpool, UK

Project Aims: Optimize the flexibility of the design of the LHeC interaction regions in terms of minimizing β* to understand the reach in luminosity, and in terms of increasing L* to reduce the synchrotron radiation.

Studies carried out:

- Different chromatic corrections for the nominal case with β*=10 cm and L*=10 m were considered;
- Impact on the stability of the beam was studied via dynamic aperture simulations;
- Effect of non-linearities was investigated via frequency map analysis.

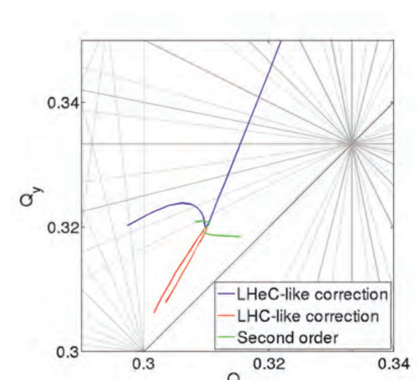

Calculated variation in horizontal and vertical tune for different corrections.

Results: Similar behavior was found at small angles for all considered cases. Tunes variation was observed over 5,000/10,000 turns in studies using SUSSIX for a sample of initial amplitudes via the diffusion factor. Similarities were again found for LHeC-like and 2nd order correction, except for the stable region observed at $Q_x \sim Q_y$, where the latter case presented better results [MOPJE079].

Beam Dynamics Optimization at SOLEIL

X.N. Gavalda, SOLEIL, France

Project Aims: Optimize the linear and non-linear beam dynamics of the synchrotron light source SOLEIL using Multi-Objective Genetic Algorithms (MOGA) and the tracking code ELEGANT.

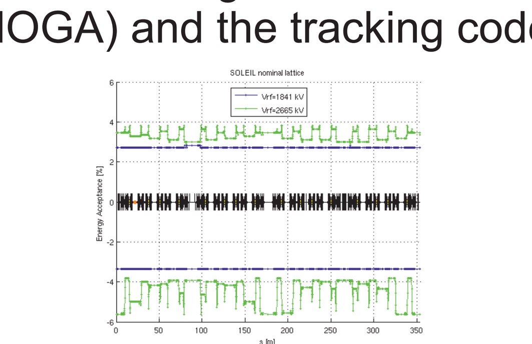

Energy acceptance of two filling patterns (and two RF voltages) at SOLEIL from beam-based measurements

Studies carried out:

- Comparison between results from ELEGANT and TRACY3 was done;
- 6D tracking included in optimization process and energy model of dipole edge focusing improved.

Results: Optimization routines have been verified in the SOLEIL control room in beam-based experiments. The relation between the total beam, Touschek and rest gas lifetime was studied. However, so far no significant improvement of Touschek lifetime was observed and studies are ongoing.

Training

It is recognized that best practice researcher training involves cohorts of candidates rather than individuals. The ITN structure is ideal for this and to achieve the aspirations of the EU Principles for Innovative Doctoral Training oPAC takes best advantage of industry participation and by providing regular network training to bring the Fellows together.

International School on Accelerator Optimization

Royal Holloway University of London, UK

At the start of their training all oPAC fellows participated in either the CERN Accelerator School or the Joint Universities Accelerator School. An **oPAC School on Accelerator Optimization** was organized by the consortium between **7th-11th July 2014** at Royal Holloway University of London, UK. It covered advanced techniques for the optimization of particle accelerators.

All Fellows followed a **Skills School** in Liverpool, UK in **June 2013**. During the week-long school they were provided with subject-specific training in addition to generic topics, including project management, scientific writing, problem solving techniques and building bridges between academia and industry. A similar school is now offered to all PGR students in the School of Physical Sciences at University of Liverpool and discussions with other HEIs are ongoing with the aim to let more researchers benefit from this successful scheme which also commended as a **success story** by the EU.

Topical Workshops

Venues across the network

A workshop on the **Grand Challenges of Accelerator Optimization** was held in **June 2013** at CERN and gathered more than 120 participants to review the state-of-the-art in accelerator R&D. CERN IndicoID: 243336. Expert **training days** on 'Simulation Tools' and 'Beam Diagnostics' were held for all Fellows, hosted by CST AG and Bergoz, respectively.

In **April 2014 a Workshop on Libera** was offered by Instrumentation Technologies and one on **Beam Instrumentation** by CIVIDEC in Vienna, in **May 2014** (293158). **Computer-Aided Optimisation of Accelerators** was a the focus at GSI in **March 2015**; this was a special event for the network as the event was organized by the Fellows (333414).

Full details and information about all events and the project's research can be found in the network's quarterly **newsletter** and its **Facebook** page. In order to subscribe, please send an email to the coordinator or ‚like' the project.

International Conference on Accelerator Optimization

Cockcroft Institute/*University of Liverpool, UK*

In **October 2015** an international **Conference on Accelerator Optimization** will be organized at CNA in Seville, Spain. It will cover beam physics, diagnostics, computer simulations and control systems.
Registration is now open (380975) **!**

Adjunct partners can still join the network and participate in the network's research activities and benefit from a wide ranging training program. Information on how to join can be obtained from the coordinator.

carsten.welsch@cockcroft.ac.uk

This project has received funding from the European Union's Seventh Framework Programme for research, technological development and demonstration under grant agreement no 289485.

http://www.opac-project.eu

STUDIES INTO ELECTRON BEAM GENERATION, ACCELERATION AND DIAGNOSTICS WITHIN LA³NET*

C.P. Welsch#, Cockcroft Institute and the University of Liverpool, UK
on behalf of the LA³NET Consortium

Abstract

The Laser Applications at Accelerators Network (LA³NET) is receiving funding of up to 4.6 M€ from the European Union within the 7th Framework Program to carry out R&D into laser-based particle sources, laser acceleration schemes and laser-based beam diagnostics. This international network joins universities, research centers and private companies and has been training 19 early stage researchers at network nodes across Europe since 2011. This contribution presents research outcomes from LA³NET's main work packages, covering electron beam generation, acceleration and diagnostics. Results from surface studies of photocathodes for photo injector applications in the framework of the CLIC project are presented along with information about expected accelerating gradients in dielectric laser-driven accelerators as identified for non-relativistic and relativistic electron beams using the CST and VSIM simulation codes. Initial results from energy measurements using Compton backscattering at the ANKA Synchrotron at KIT are also presented. In addition, a summary of recent and upcoming international events organized by the consortium is also given.

INTRODUCTION

The LA³NET Fellows are hosted by 11 partner institutions all over Europe and although their work focuses on research, they are provided not only with scientific supervision and opportunities of secondments to other institutions involved in the project, but also complementary training through network-wide events [1]. This includes international schools and topical workshops, as well as a final project conference and numerous outreach events. Through the involvement of almost 30 associated and adjunct partners the project gains an interdisciplinary dimension including strong links to industry. The network carries out many dissemination and outreach activities aimed at interesting a wide audience in science and to raise public awareness of the application of lasers and accelerators in many different fields that have influence on everyone's life, such as medicine, electronics, energy and the environment. LA³NET trains accelerator experts for academia and industry, joins the accelerator and laser communities and to raises public awareness of the importance of this research for society. In the following section examples of recent research results from across the consortium are given.

RESEARCH

The Fellows carry ou research within one out of 5 thematic work packages within LA³NET. These are particle sources, acceleration, beam diagnostics, system integration and detector technology.

Surface Characterization of Photo Cathodes for Photoinjector Applications

Within the CLIC (Compact Linear Collider) project, feasibility studies of a photoinjector option for the drive beam are on-going, covering both, the laser and the photocathode side. The main challenge is to achieve high bunch charges, long trains and high bunch repetition rates together with sufficiently long cathode lifetimes. Cs_2Te cathodes, sensitive to ultra-violet (UV) laser beam that were produced at CERN showed good quantum efficiency and reasonable lifetime [2]. However, the available laser pulse energy in the UV for 140 μs long pulse trains is currently limited due to a degradation of the beam quality during the 4th harmonics conversion process. Using green laser beam in combination with Cs_3Sb cathodes would overcome this limitation. Cs_3Sb and Cs_2Te photocathodes were produced at CERN by co-deposition process and tested in the PHIN RF photoinjector, see [3]. LA³NET Fellow I. Martini who is based at CERN led a detailed analysis of cathode surface composition through X-ray Photoelectron Spectroscopy (XPS) and correlated the findings to the cathode performance [4]. The Quantum Efficiency (QE) map shows an overall efficiency reduction in used cathodes as compared to newly produced ones, see Fig. 1 as an example. This can be explained by changes in the composition of the photoemissive layer.

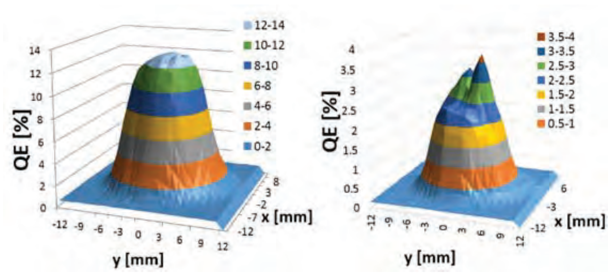

Figure 1: QE maps of Cathode #198 (Cs_2Te) as newly produced (left) and used in the RF photoinjector (right).

The XPS studies showed that both cathodes were oxidized during operation. Moreover, the detailed analysis

* This project has received funding from the European Union's Seventh Framework Programme for research, technological development and demonstration under grant agreement no 289191.
# carsten.welsch@cockcroft.ac.uk

of the XPS spectra measured on the used cathodes identified as contribution to the surface composition some compounds with the wrong stoichiometry that could explain the poor photoemissive properties. Further studies on newly produced photocathodes are planned to better understand if degrading effect during photoinjector operation, , such as backscattered high energy ions or also inaccuracies in the deposition process, lead to the formation of different compounds.

Dielectric Laser Acceleration

Dielectric laser-driven accelerators (DLA) based on a grating structure have good potential as ultra-compact electron accelerators, benefitting from high acceleration gradients of up to GV/m and mature lithographic techniques for the fabrication of the microstructures. Within LA³NET, A. Aimidula has carried out initial studies into the optimization of such gratings structures, modifying a range of geometry parameters and critically assessing their impact on the acceleration efficiency [5]. Fellow Y. Wei from the Cockcroft Institute/University of Liverpool is building up on this early work and investigates acceleration of relativistic and non-relativistic electrons in double gratings silica structures, using different harmonic modes of the accelerating field [6]. When a double grating structure is driven by two transverse magnetic (TM) polarized lasers from opposite sides, different harmonic modes of the accelerating electric field are simultaneously excited, see Fig. 2.

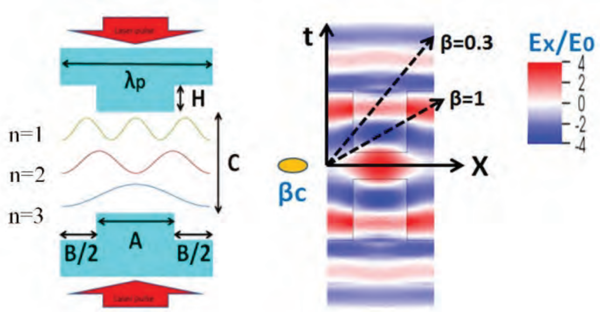

Figure 2: Illustration of the first, second and third spatial harmonic mode in one grating period, driven from opposite sides by laser.

Assuming an erbium-fiber laser emitting a wavelength of λ_0=1550 nm and Silica with a refractive index of n=1.528 as substrate simulations were carried out into the acceleration efficiency using the commercial CST and VSim simulation codes. Both codes yielded very similar results over a wider range of parameters, supporting the findings of earlier studies. For highly relativistic electrons a maximum achievable acceleration gradient of around 2.2 GV/m was found. For non-relativistic electrons at β=0.3 the first spatial harmonic gave access to the largest acceleration gradient of around 0.33 GV/m, as compared to 0.25 GV/m for the second harmonic and 0.16 GV/m for the third harmonic. Taking into account manufacturing constraints a grating period of 930 nm was found to be optimum in terms of simplicity of production and acceleration efficiency. This work will now be extended towards multistage acceleration.

Beam Energy Measurements Using Compton Back Scattering

For Compton back scattering (CBS) measurements at storage rings, the electron beam energy of the stored beam can be determined from the known values of the electron rest energy, the laser photons energy, and the measured collision angle φ and Compton edge energy. LA³NET Fellow C. Chang and colleagues from ANKA at KIT have now used a High Purity Germanium (HPGe) spectrometer to determine the energy of the emitted photons [7]. Figure 3 shows a typical spectrum that was acquired from a 1.3 GeV electron beam over 120 seconds. The mechanical centers of two quadrupoles were used as reference line and the laser direction measured relative to this line with a laser tracker and a camera. In addition beam position monitors were used to check the electron orbit orientation relative to the reference line.

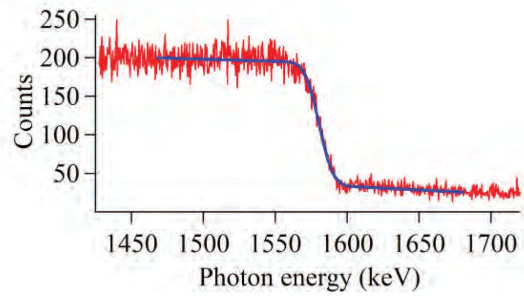

Figure 3: Measured CBS spectrum at 1.3 GeV with fit to determine the Compton edge energy. Signal integrated over 120 seconds.

The collision angle φ was determined from this measurement and yielded an average value of the beam energy of 1287.0 MeV ± 0.2 MeV. As compared to conventional CBS methods for energy measurement, a compact setup based on a transverse scheme has been successfully tested at ANKA. These measurements have been extended to beam energies of 0.5 GeV, 1.6 GeV and 2.5 GeV and gave promising initial results. It was shown that longer acquisition times can help further reduce statistical uncertainties in the Compton edge and hence beam energy. This might give access to measurements uncertainties to below a few10^{-5} in the future.

TRAINING EVENTS

Training within the LA³NET network is primarily through cutting edge research. In addition, the network organizes a number of network-wide events that are also open to the wider community, including international schools on laser applications at accelerators and workshops on specific topical areas, as well as an international conference and symposium that take place in 2015.

International Schools

A first international school on laser applications was held at GANIL, France in 2012 and was reported on in the Proceedings of IPAC13 [8]. Between 29 September and 3 October 2014 the consortium held an Advanced School on Laser Applications at Accelerators. The event was hosted by the Spanish Pulsed Lasers Centre (CLPU) in Salamanca, Spain and attracted over 70 participants from all over the world. The school started with lectures about an introduction to lasers, the history of accelerator development in Europe, accelerator applications, as well as beam generation, acceleration and diagnostics – all given by internationally renowned lecturers. Day two included lectures on laser ion sources, photo injectors and Free Electron Lasers (FELs), in addition to a two-hour study session giving delegates a chance for a hands-on look at some of the topics covered. An outreach talk about "attosecond science" by Prof. Luis Plaja in the evening on the main University of Salamanca campus attracted more than 100 students from the university and local high schools in addition to the school participants. The following days covered more advanced topics in ion and electron acceleration, commonly used simulation codes for accelerator design and optimization, as well as industry applications of accelerators and lasers. This was complemented by a Laserlab-sponsored visit to the facilities at CLPU, a second study session and a lively poster display and industry exhibition, sponsored by Danfysik. The School drew to a close with talks on THz applications, compact X-ray sources and the Extreme Light Infrastructure (ELI) project. The School stimulated many fruitful discussions throughout the week and was an excellent addition to the many scientific events the network has organized to date. All presentations can be found on the school's indico page [9]. In addition, the network has organized two researcher skills schools for all Fellows, covering wider skills, such as presentation skills, scientific writing, project management or CV writing. These schemes were specifically praised by a number of bodies, including the REA, HEA and UKRO and has since been implemented for many additional student cohorts at partner universities.

Topical Workshops

The network also organizes workshops on specific R&D areas that are covered in the network's different work packages, including particle sources (2013), novel acceleration techniques (2013) and laser technology (2014). Between 16-18 November 2014 a "Scientists Go Industry" workshop explored a slightly different area. It was hosted by the Helmholtz Association in Berlin with thirteen invited speakers from industry and the commercial world talking about their own career pathways and what their work entails. This provided the Fellows and external delegates with an insight into the full range of job opportunities available for them outside of academia. The event was a sell-out showing that there is an appetite for investigating such alternative career paths. The speakers stepped up to the mark to paint a bright picture of the spectrum of career pathways available with each session generating plenty of questions and some lively discussion. The presentations are available from the workshop website as a resource for any physicist pondering their future [10].

The penultimate events for LA^{3}NET took place in Mallorca at the end of March 2015 with a 2-day long Topical Workshop on Beam Diagnostics kicking off a week dedicated to lasers and accelerators. The first day saw presentations about the state of the art in optical diagnostics, beam profile and emittance measurements using optical radiation, laser wire scanner R&D, Compton backscattering and the use of optical techniques for ultra-short bunch diagnostics. On the second day longitudinal measurements of ultra-short Bunches, novel sensors and technologies and advanced diagnostics technologies were covered [11].

Wednesday welcomed the opening of the LA^{3}NET Conference on Laser Applications at Accelerators [12]. This event brought together around 70 experts to discuss the state of the art in the network's R&D area. All LA^{3}NET Fellows presented the outcomes of their research in form of talks and the conference also featured presentations by research leaders from around the world. Sessions were organized along the network's research work packages and triggered many interesting and stimulating discussions.

Finally, the project will host an outreach symposium in Liverpool on 26 June 2015 [13]. There, the network will present its research results to a very wide audience to help promote researcher careers in the field of accelerator science and technology.

SUMMARY

The LA^{3}NET project is one of the largest Marie Curie initial training networks ever funded by the European Union. It has been training 19 early stage researchers in an interdisciplinary area and organized numerous events for the wider scientific community. This paper gave 3 examples of recent research results by LA^{3}NET Fellows. Stretching across beam generation, acceleration and diagnostics, the network provides a unique framework for international cooperation across sectors.

Identified as a European 'success story' by the REA as part of formal reviews in a number of key areas, including Fellow R&D, international dissemination, project management and coordination, the project is providing a high quality training program to its Fellows, giving them an excellent basis for their future careers.

REFERENCES

[1] http://www.la3net.eu
[2] C. Hessler et al., TUPPD066, Proc. of IPAC’12, New Orleans, Louisiana USA (2012).
[3] C. Hessler et al., TUPJE039, these proceedings, Proc. of IPAC’15, Richmond, Virginia, USA (2015).
[4] I. Martini et al., TUPJE040, these proceedings, Proc. of IPAC’15, Richmond, Virginia, USA (2015).
[5] A. Aimidula et al., Physics of Plasmas **21**, 023110 (2014).
[6] Y. Wei et al., WEPWA051, these proceedings, Proc. of IPAC’15, Richmond, Virginia, USA (2015).
[7] C. Chang et al., MOPHA040, these proceedings, Proc. of IPAC’15, Richmond, Virginia, USA (2015).
[8] C.P. Welsch, THPWA044, Proc. of IPAC’13, Shanghai, China (2013).
[9] indico.cern.ch/conferenceDisplay.py?confId=285698
[10] indico.cern.ch/conferenceDisplay.py?confId=318719
[11] indico.cern.ch/conferenceDisplay.py?confId= 340153
[12] indico.cern.ch/conferenceDisplay.py?confId= 340381
[13] indico.cern.ch/conferenceDisplay.py?confId= 368273

LA³NET

IPAC15

Studies into Electron Beam Generation, Acceleration and Diagnosticswithin LA³NET

C.P. Welsch, Cockcroft Institute and The University of Liverpool, UK

on behalf of the LA³NET Consortium

Abstract

The Laser Applications at Accelerators Network (LA³NET) is receiving funding of up to 4.6 M€ from the European Union within the 7th Framework Program to carry out R&D into laser-based particle sources, laser acceleration schemes and laser-based beam diagnostics. This international network joins universities, research centers and private companies and has been training 19 early stage researchers at network nodes across Europe since 2011. This poster presents research outcomes from LA³NET's main work packages, covering electron beam generation, acceleration and diagnostics. Results from surface studies of photocathodes for photo injector applications in the framework of the CLIC project are presented along with information about expected accelerating gradients in dielectric laser-driven accelerators as identified for non-relativistic and relativistic electron beams using the CST and VSim simulation codes. Initial results from energy measurements using Compton backscattering at the ANKA Synchrotron at KIT are also presented. In addition, a summary of recent and upcoming international events organized by the consortium is also given.

Research

R&D within LA³NET is split into 5 work packages: Laser-based particle sources, laser driven particle beam acceleration, laser-based beam diagnostics, system integration and laser and photon detector technology. Here, examples of recent research highlights are given.

Surface Characterization of Photo Cathodes

I. Martini, CERN, Switzerland

Project Aims: Identify photo cathode materials suitable for achieving high bunch charges, long bunch trains and high bunch repetition rates together with sufficiently long cathode lifetimes.

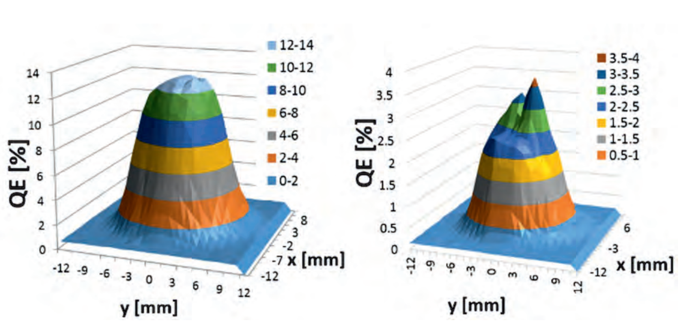

QE maps of Cathode #198 (Cs_2Te) as newly produced (left) and used in the RF photoinjector (right).

Studies carried out:

- Cs_3Sb and Cs_2Te photocathodes were produced by co-deposition process and tested in the PHIN RF photoinjector;
- A detailed analysis of cathode surface composition through X-ray Photo-electron Spectroscopy was carried out and correlated to cathode performance.

Results: Quantum Efficiency (QE) map showed an overall efficiency reduction in used cathodes as compared to newly produced ones. XPS indicated oxidization during operation. Wrong stoichiometry might explain poor photoemissive properties. Further measurements on newly produced cathodes are planned to complete these studies [TUPJE040].

Dielectric Laser Acceleration

Y. Wei, Cockcroft Institute/University of Liverpool, UK

Project Aims: Investigate acceleration of relativistic and non-relativistic electrons in double gratings silica structures and analyze optimum scheme using different harmonic modes of the accelerating field.

Studies carried out:

- Using an erbium-fiber laser (λ_0=1550 nm) and Silica (n=1.528) simulations were carried out into the acceleration efficiency using CST and VSim codes
- Structures driven by two lasers were considered, using spatial harmonics n=1-3.

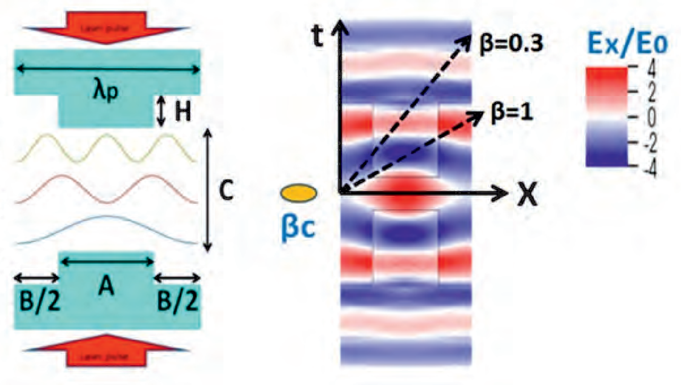

Illustration of the first, second and third spatial harmonic mode in one grating period, driven from opposite sides by laser.

Results: Both codes gave similar results over a wider parameter range. For highly relativistic electrons a maximum acceleration gradient of 2.2 GV/m was found. Taking into account manufacturing constraints a grating period of 930 nm using the second harmonic was found to be optimum for non-relativistic electrons in terms of simplicity of production and acceleration efficiency, providing a gradient of 250 MV/m. This work will now be extended towards multistage acceleration [WEPWA051].

Beam Energy Measurements by Compton Backscattering

C. Chang, KIT, Germany

Project Aims: Determine the energy of a stored electron beam from Compton back scattering measurements in a transverse configuration.

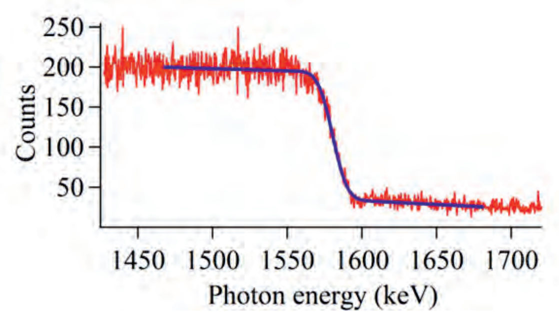

Measured CBS spectrum at 1.3 GeV with fit to determine the Compton edge energy. Signal integrated over 120 seconds.

Studies carried out:

- A High Purity Germanium spectrometer was used to determine the energy of the emitted photons at various beam energies.

Results: A compact setup based on a transverse scheme has been successfully tested at ANKA at energies between 0.5-2.5 GeV. Longer acquisition times help further reduce statistical uncertainties in the Compton edge and hence beam energy [MOPHA040].

Training

Training of all LA³NET Fellows is mostly through specific project-based research realized by the respective host institutions with specific secondments to other partners for specialized techniques and cross-sector experience. In addition, the consortium organizes a number of network-wide events that are open to the wider community.

International Schools

GANIL, France, University of Liverpool, UK and CLPU, Spain

An **Advanced School on Laser Applications** was held in **September 2014** at CLPU in Spain and covered advanced laser technologies, in particular the combination of different fundamental techniques (CERN indico: 285698).

Topical Workshops

Venues across the network

A "Scientists Go Industry" workshop was hosted in Berlin in **November 2014** and organized by the network Fellows with thirteen invited speakers from industry talking about their own career pathways and what their work entails. This provided the participants with an insight into the full range of job opportunities available for them outside of academia (CERN indico: 318719).

A workshop on **Laser-based Beam Diagnostics** was held on Majorca, Spain in **March 2015**. It covered optical diagnostics, beam profile and emittance measurements, laser wire scanner R&D, Compton backscattering and the use of optical techniques for ultra-short bunch diagnostics (CERN indico: 340153).

International Conference and Symposium on Laser Applications

University of Liverpool, UK

A 3-day **international conference** on laser applications at accelerators was held **on Majorca in March 2015**. 70 experts discussed the state of the art in the network's R&D areas (CERN indico: 340381).

An **Outreach Symposium** in Liverpool on 26 June 2015 will be the project's final event. It will present the LA³NET R&D to a wide audience to help promote careers in accelerator science and technology (CERN indico: 368273).

The consortium will award an annual LA³NET cash **prize** of 1,000 € for an outstanding contribution to the field of laser applications at accelerators to a researcher in the first five years of their professional career. Applications for the **2015 prize** can be submitted until **7. June 2015**.

The network produces a quarterly **newsletter and is present in Facebook** - in order to subscribe for the former, simply send an email to the coordinator.

carsten.welsch@cockcroft.ac.uk

This project has received funding from the European Union's Seventh Framework Programme for research, technological development and demonstration under grant agreement no 289191.

http://www.la3net.eu

NON-INVASIVE BEAM PROFILE MONITORING

C.P. Welsch[#1], T. Cybulski[1], A. Jeff[1,3], V. Tzoganis[1,2], H. Zhang[1]
[1] Cockcroft Institute and The University of Liverpool, UK
[2] RIKEN, Nishina Center, Wako, Japan
[3]CERN, Geneva, Switzerland

Abstract

Highest energy and intensity accelerators require new approaches to transverse beam profile monitoring as many established techniques will no longer work due to the high power stored in their beam. In addition, many accelerator applications such as ion beam cancer therapy or material irradiation would benefit significantly from the availability of non-invasive beam profile monitors. Research in the QUASAR Group has focused on this area over the past 5 years. Two different approaches were successfully developed: Firstly, a supersonic gas jet-based monitor was designed and commissioned. It enables the detection of the 2-dimensional transverse beam profile of essentially any charged particle beam with negligible disturbance of the primary beam and accelerator vacuum. Secondly, a monitor based on the Silicon strip VELO detector, originally developed for the LHCb experiment, was tested as an online beam monitor at the Clatterbridge Cancer Center in the UK. The design of both monitors and results from measurements are presented in this contribution.

INTRODUCTION

Least intrusive beam profile measurement techniques that allow continuous operation of an accelerator whilst providing comprehensive information about the particle beam would be ideal for many applications, ranging from high energy/high intensity accelerators such as the LHC at CERN and its future upgrades or the high power proton driver linac at ESS where conventional diagnostics would simply not work. Various non-invasive methods have been developed for the determination of the transverse beam profile. These include Ionization Profile Monitors (IPM) [1] which are based on the collection of the ions produced by impact ionization of rest gas by the main beam and the Beam Induced Fluorescence Monitor (BIF) [2] which relies on the detection of the light produced from the excited residual gas. IPM's are truly non-invasive devices which can operate parasitically if the residual gas pressure is sufficiently high and offer very good spatial resolution down to 100 µm and time resolution in the order of 10 ms with a fast camera or a few µs with a fast readout system. However they are usually limited to high energy accelerators. BIF's are parasitical as well, but require higher residual gas pressures in excess of 10^{-6} mbar and longer signal integration times.

*Work supported by the EU under grant agreement 215080 and 289485, HGF and GSI under contract number VH-HG-328, the STFC Cockcroft Institute Core Grant No. ST/G008248/1, and a RIKEN-Liverpool studentship.

#carsten.welsch@cockcroft.ac.uk

Gas Jet-based Beam Profile Monitor

A possible approach to overcome these limitations is to utilize a cold (< 20 K) neutral supersonic gas jet shaped into a thin curtain. The core of this monitor consists of an expansion of a room temperature high pressure gas (1-10 bars) into vacuum through a nozzle with 30 µm diameter, resulting in an adiabatic expansion and the formation of a jet with a very stable and cold inner core.

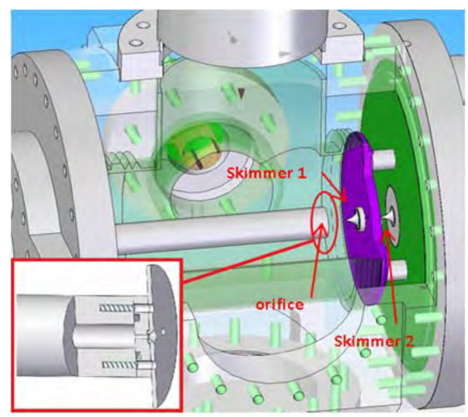

Figure 1: CAD drawing of the nozzle chamber where the first two skimmers are highlighted.

This jet is then further shaped by several skimmers. The first part of the experimental setup is illustrated in Fig. 1. Skimmers separate several differentially pumped vacuum chambers through which the jet passes until it reaches a final "reaction chamber", held at a pressure of 10^{-9}-10^{-12} mbar [3]. When entering this chamber the jet has already been shaped by a final rectangular skimmer into a curtain that crosses the primary beam to be analyzed under an angle of 45°. In this interaction impact ionization of the jet particles occurs and the resulting ions are imaged by a moderate electric field of some kV/m onto a position-sensitive double layer Micro Channel Plate (MCP) detector. The MCP provides signal amplification of up to 10^6. Finally, the resulting beam profile is observed by a Phosphor screen-camera combination that is mounted on the top of the reaction chamber, see Fig. 2.

At low energies of the primary beam the extraction electric field can lead to its displacement when passing through the reaction chamber. This is compensated by deflecting electric fields before and after the interaction region (not shown in the figure).

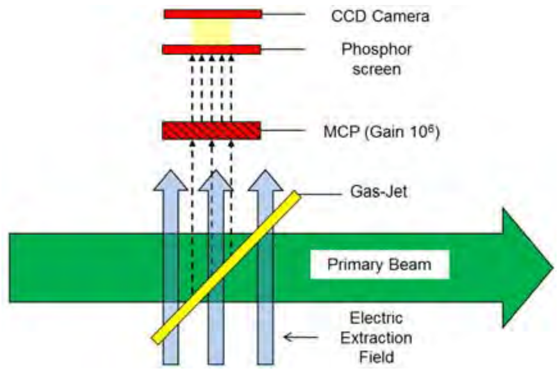

Figure 2: Illustration of the gas jet monitor operation principle. The gas jet is travelling into the page.

Proof-of-principle measurements were recently completed at the Cockcroft Institute [4]. An example profile obtained by crossing the gas jet with a 5 keV electron beam is shown in Fig. 3 [5]. It shows the profile of the electron beam as measured with the gas jet, as well as a signal obtained from ionization of the residual gas.

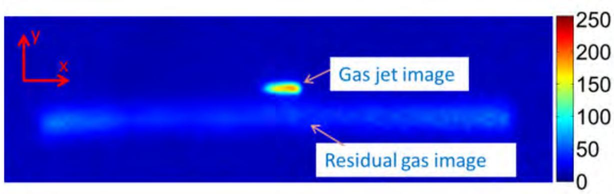

Figure 3: Beam profile of a 5 keV electron beam as measured with the gas jet and the residual gas.

The broadening of the image and resulting poorer signal quality caused by the thermal velocity of the residual gas particles as compared to the signal from the cold jet can be clearly observed. Also, a higher intensity from the jet as compared to the signal from the residual gas can be seen. Note that the lateral displacement between the two profiles is a direct result of the high jet velocity.

One initial challenge was the high gas load from the inlet nozzle onto the overall system. Gas reflections from the surrounding vacuum chamber walls caused instabilities in the jet and contributed to general alignment problems. This was overcome by the addition of a Festo solenoid pulsed valve. By synchronizing the camera with the pulse valve and setting a proper shutter time, it was shown that the signal ratio between the supersonic gas-jet and the residual gas can be increased significantly. Current studies focus on the optimization of the electric extraction field, impact of different gas species on signal quality and studies into the gas dynamics. In addition, the monitor is being adapted for integration into the HL-LHC and under consideration for the ESS main linac.

Silicon Strip Detector as Beam Monitor

The VErtex LOcator detector (VELO) is the most proximal device to the interaction region of the LHCb experiment. It provides track coordinates of the secondary vertices from B-mesons decays in the investigations of CP violations and other rare phenomena [6]. Its design allows precise measurements to be taken a few millimeters from the primary beam, without affecting it.

VELO is a multi-strip silicon detector and has been tailored to meet both the stringent requirements of the operation in a high-level radiation environment and facilitate data collection at high frequencies, matched with the bunch crossing at LHC. Each sensor embeds 2048 diode strips resolving the position of the hit in r – and φ-coordinates. The r – measuring side is divided into four 45° sections, thus lowering the overall strip capacitance and occupancy [7]. The φ – side consists of inner- and outer- section of radially oriented strips with a skew angle being introduced between the regions to support the ghost hit recognition algorithms. VELO has a central hole through which the primary beam passes and the detector surface surrounding this area. The geometry of the sensors allows approaching the beam to as little as 8.2 mm radial distance. Such high proximity enables resolving track vertices with high spatial resolution. This special detector geometry has also proven to be advantageous for applications as a non-invasive beam monitor for medical applications. Acting as a proton counter in the tail distribution of the beam, the monitor can serve as a beam position, profile and halo monitor, and potentially – once signals have been cross-calibrated against absolute current measurements from another detector – as an online intensity and hence dose monitor. This would add significant benefit as intensity could be monitored non-invasively during patient treatment, hence effectively eliminating setup and calibration times.

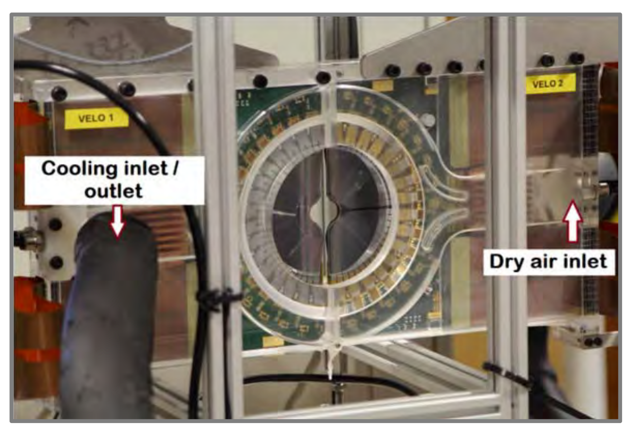

Figure 4: Photograph of the VELO detector after a local positioning, ventilation and cooling system has been added.

During normal operation the LHCb VELO detector works under LHC vacuum conditions. Its integration into the treatment beam line of an ion beam center, however, requires it to work under ambient pressure and at room temperature. Therefore, a designated support structure was developed, encompassing a 3D positioning system, remote read-out, together with a local ventilation and cooling system [8]. Performance tests carried out in the Cockcroft Institute laboratories yielded noise levels at a bias voltage of -100V at the level of 2–3 analogue to digital counts (ADCs).

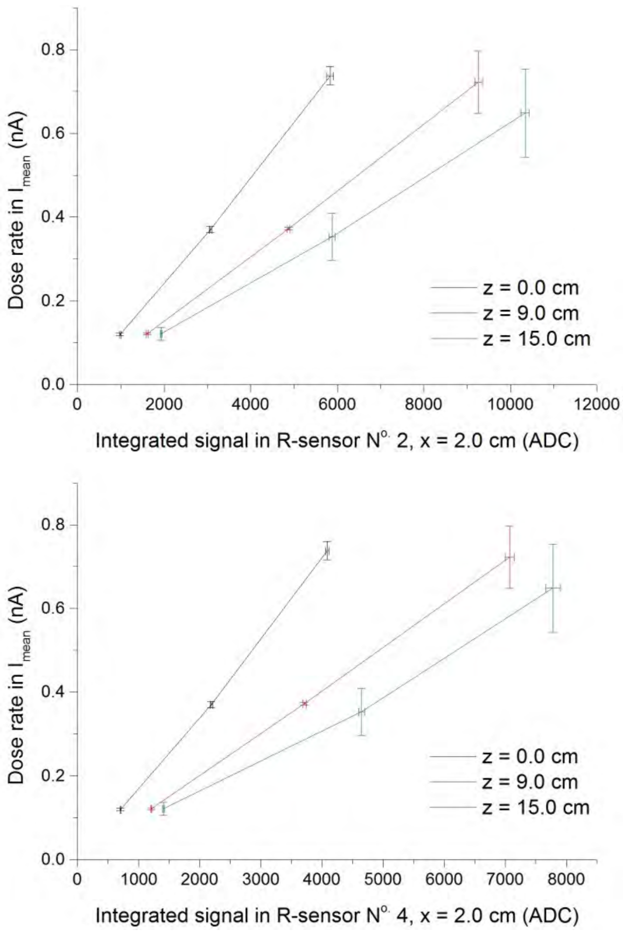

Figure 5: Signal of two sensors at x = 2.0 cm around the beam axis. Sensors No. 2 and 4 are on opposite sides of the beam.

With a maximum energy of 62 MeV, provided by a Scanditronix MC-60 PF cyclotron, the Clatterbridge Cancer Center (CCC) is specialized in the treatment of ocular tumors. As part of the preparations for measurements with VELO, studies into beam transport through the CCC treatment line have been carried out [9]. For measurements with beam the whole detector assembly was then integrated into the CCC treatment beam line in 2014. The detector was placed at the isocenter. It was mounted on a 3D translation stage that allowed for transverse movement, as well as shifting the whole assembly to different positions near the isocenter that corresponded to the range typically used for treatment.

An example from these measurements is shown in the above Fig. 5 which shows the measured dose rate as a function of total counts at three different longitudinal positions z=0.0/9.0/15.0 cm and at a radial distance of 2 cm from the beam center. The two sensors were located on opposite sides of the beam. A good linearity between integrated signal and delivered dose can be seen. The dose was obtained by a Faraday Cup used for absolute intensity measurements.

Initial analysis of this data supports the idea that the proton beam halo produced by a passive beam delivery system based on scattering for a medical accelerator can be used for an estimation of the beam current and hence dose delivered to the patient. Benefiting from VELO's unique semi-circular architecture it was shown that clear signals can be obtained without causing detector saturation or excessive noise levels. Further measurements are now planned to better understand the correlation between the halo and core reading and to develop automated algorithms for signal processing.

CONCLUSION AND OUTLOOK

Two new technologies for least invasive beam monitoring have been developed by the QUASAR Group and were successfully tested with beam. The particular advantages of the gas jet monitor are that integration into beam lines and storage rings operating at vacuum pressures as low as 10^{-12} mbar is possible, that the 2D transverse beam profile of the primary beam can be obtained in a least invasive way, and that the monitor can essentially be used for any type of beam, starting at lowest keV energies, and stretching all the way up to TeV energies. Beam and gas jet densities, together with the interaction frequency and respective ionization cross sections will then determine the event rate for a specific application. Optimization studies are currently being undertaken and focus on the integration into the HL-LHC vacuum environment and the impact from space charge on image quality in the case of high current beams, as found e.g. at ESS.

Furthermore, the LHCb VELO detector has been developed into a stand-alone monitor for use in treatment beam lines and was tested at the Clatterbridge Cancer Centre. Initial data taken during a beam time in summer 2014 shows a clear correlation between halo readings and dose delivered to the patient. More measurements are however required to fully understand intensity limitations, noise levels and automate signal processing.

REFERENCES

[1] T. Tsang et al., Phys Rev. STAB 16 (2014).
[2] P. Forck, et al., Proc. IPAC2010, TUZMH01, Kyoto, Japan, http://www.jacow.org/
[3] V. Tzoganis, et al., VACUUM 109 (2014) .
[4] V. Tzoganis and C.P. Welsch, APL 104 204104 (2014).
[5] H. Zhang, et al., MOPWI006, Proc. IPAC2015, Richmond, USA, http://www.jacow.org/
[6] LHCb VELO Technical Design Report, CERN/LHCC 2001-0011, LHCb TDR 5, Geneva
[7] T. Cybulski, et al., TUPG011, Proc. BIW2012, Santa Fe, USA, http://www.jacow.org/
[8] T. Cybulski, et al., THPME185, Proc. IPAC2014, Dresden, Germany, http://www.jacow.org/
[9] T. Cybulski, et al, MPOWA059, Proc. IPAC2013, Shanghai, China, http://www.jacow.org/

Non-invasive Beam Profile Monitoring

C.P. Welsch, T. Cybulski, A. Jeff[1], V. Tzoganis[2], H. Zhang, *Cockcroft Institute and The University of Liverpool, UK*
[1]*also: CERN, Geneva Switzerland* [2]*also: Nishina Center, Wako, Japan*

Abstract

Highest energy and intensity accelerators require new approaches to transverse beam profile monitoring as many established techniques will no longer work due to the high power stored in their beam. In addition, many accelerator applications such as ion beam cancer therapy or material irradiation would benefit significantly from the availability of non-invasive beam profile monitors.
Research in the QUASAR Group has focused on this area over the past 5 years. Two different approaches were successfully developed: Firstly, a supersonic gas jet-based monitor was designed and commissioned. It enables the detection of the 2-dimensional transverse beam profile of essentially any charged particle beam with negligible disturbance of the primary beam and accelerator vacuum. Secondly, a monitor based on the Silicon strip VELO detector, originally developed for the LHCb experiment, was tested as an online beam monitor at the Clatterbridge Cancer Center in the UK. The design of both monitors and results from measurements are presented here.

Ultra-cold Gas Jet

A possible approach to overcome these limitations is to utilize a cold (< 20 K) neutral supersonic gas jet shaped into a thin curtain. The core of this monitor consists of an expansion of a high pressure gas (1-10 bars) into vacuum.

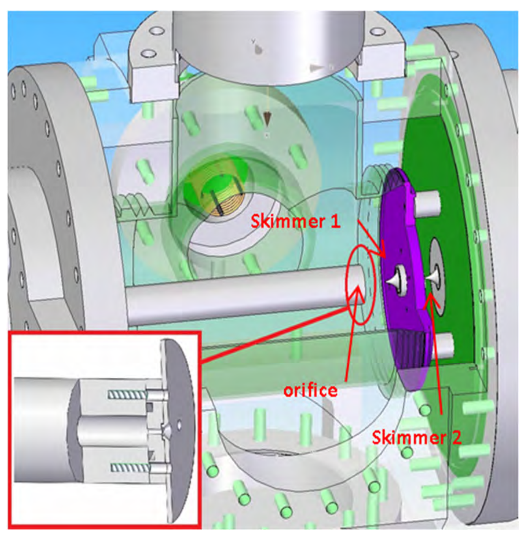

CAD drawing of the nozzle chamber with first two skimmers.

This jet is shaped by a system of nozzle and skimmers. The first part of the experimental setup is illustrated to the left. Skimmers separate differentially pumped vacuum chambers before the jet reaches a final "reaction chamber", held at a pressure of 10^{-9}-10^{-12} mbar.

In this chamber the jet has been shaped by a final rectangular skimmer into a curtain that crosses the primary beam to be analyzed under an angle of 45°. After impact ionization the resulting ions are imaged by a moderate electric field onto an MCP detector for imaging via a Phosphor screen-camera combination.

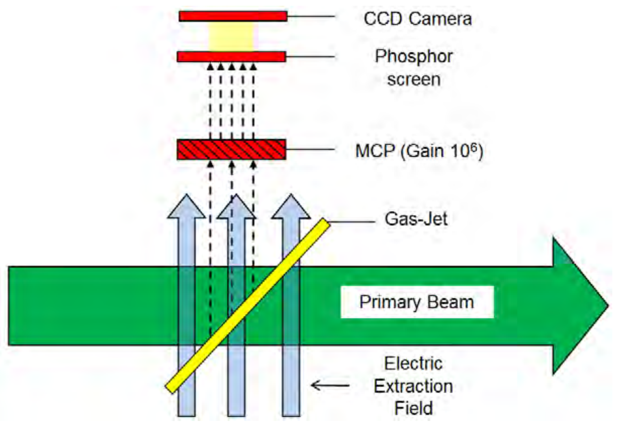

Illustration of the gas jet monitor operation principle.

Proof-of-principle measurements were recently completed at the Cockcroft Institute. An example profile obtained by crossing the gas jet with a 5 keV electron beam is shown below.

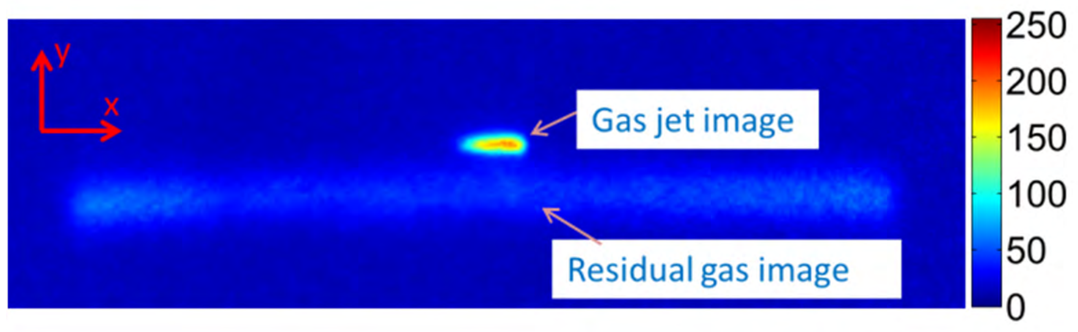

Beam profile of a 5 keV electron beam as measured with the gas jet and the residual gas.

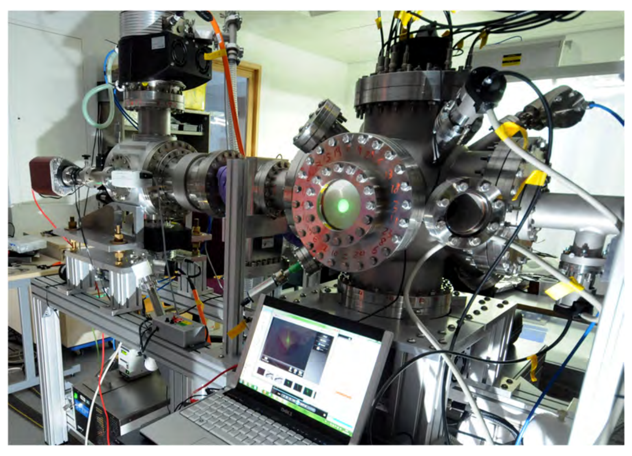

Challenges included:
- Alignment of the system
- High gas load from the inlet nozzle

Solutions:
- Laser-based based alignment, supported by 3D observation of chamber movement
- Installation of pulsed valve.

Studies into the jet dynamics using a vacuum gauge mounted on a 3D translation stage, as well as laser self-mixing based techniques are currently being carried out.
Future work will focus on the optimization of the electric extraction field and the impact from different gas species on signal quality . The monitor is currently being adapted for integration into the HL-LHC and under consideration for the ESS main linac.

VELO Detector

The VErtex LOcator detector (VELO) is the most proximal device to the interaction region of the LHCb experiment. Its design allows taking precise measurements a few millimeters from the primary beam, without affecting it. VELO is a multi-strip silicon detector, tailored to meet the requirements of the operation in a high-level radiation environment and facilitate data collection at high frequencies.

We have adapted it for integration into in the treatment beam line of an ion beam cancer therapy center. A 3D positioning system, remote read-out, local ventilation and cooling system were developed. Performance tests were carried out in the Cockcroft Institute laboratories to study noise and signal levels.

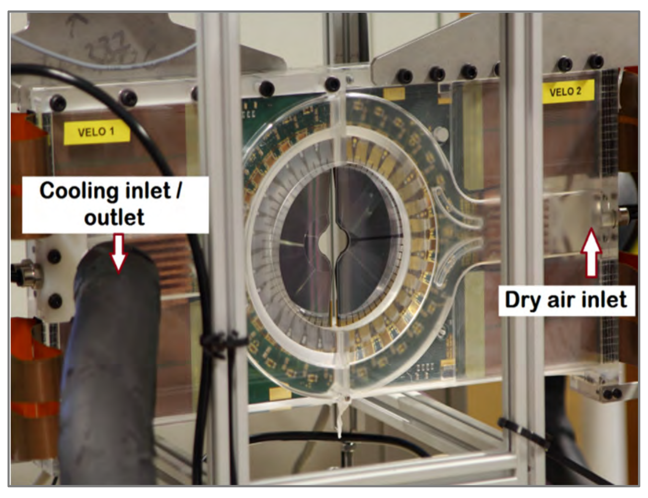

Photograph of the VELO detector after a local positioning, ventilation and cooling system has been added.

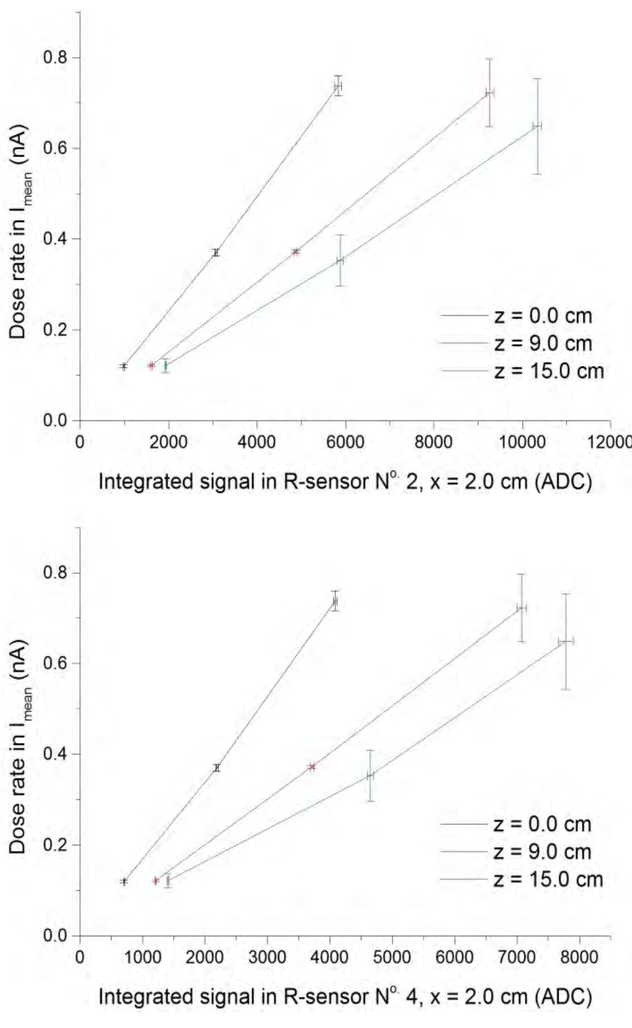

Signal of two sensors at x = 2.0 cm around the beam axis. Sensors No. 2 and 4 are on opposite sides of the beam.

Measurements with beam have been carried out at the Clatterbridge Cancer Center, see an example to the left. The linear dependency of dose rate as a function of total counts at three different longitudinal positions z=0.0/9.0/15.0 cm and at a radial distance of 2 cm from the beam center can clearly be seen. The dose was obtained by a Faraday Cup used for absolute intensity measurements.

Initial analysis of this data supports the idea that the proton beam halo produced by a passive beam delivery system based on scattering for a medical accelerator can be used for an estimation of the beam current and hence dose delivered to the patient.

Benefiting from VELO's unique semi-circular architecture it was shown that clear signals can be obtained without causing detector saturation or excessive noise levels. Further measurements are now planned to better understand the correlation between the halo and core reading and to develop automated algorithms for signal processing.

Work supported by the EU under grant agreement 215080 and 289485, HGF and GSI under contract number VH-HG-328, the STFC Cockcroft Institute Core Grant No. ST/G008248/1, and a RIKEN-Liverpool studentship.

http://www.cockcroft.ac.uk
http://www.quasar-group.org
carsten.welsch@cockcroft.ac.uk

QUALITY AND STABILITY STUDIES OF THE BEAMS IN THE ELENA RING TRANSFER LINES

J. R. Hunt, O. Karamyshev, J. Resta-López, C. P. Welsch
Cockcroft Institute and The University of Liverpool, UK

Abstract

The Extra Low Energy Antiproton (ELENA) ring will initially provide eight different experiments at CERN with extra low energy (~100 keV) antiprotons by utilising electron cooling techniques. As a result, a system of transfer lines is being designed to ensure each experiment receives a beam consistent with specified properties. In this paper, particle tracking simulations are performed to explore the effects of different lattice imperfections, e.g. element misalignment, electric field errors and matching errors, on the beam quality and orbit stability. Specific values for the upper limits of inaccuracies are obtained as a guide for the construction of the transfer lines, and will enable further optimization.

INTRODUCTION

ELENA is a low energy storage ring designed to increase the efficiency of the antimatter experiments at CERN [1]. Currently under construction, ELENA will accept antiprotons from the Antiproton Decelerator (AD) [2] and employ the use of an electron cooler to further decelerate them from a kinetic energy of 5.3 MeV to 100 keV. At these lower energies, fewer antiprotons will be lost to degrader foils at the end of the deceleration process and as a result the anti-hydrogen experiments will receive higher intensity beams.

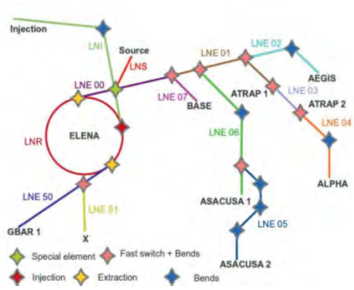

Figure 1: Schematic layout of transfer lines.

A system of transfer lines will carry these extra low energy beams to eight different locations within the AD hall. The low beam energy after ejection from ELENA allows the use of electrostatic elements. Reasons for this design choice include cost of construction, low power consumption, easy operation and good possibilities for shielding elements against stray magnetic fields. [1]

Nine separate lattices make up the transfer lines, two of which are directly connected to ELENA. The studies undertaken in this paper focus on the lattice 'LNE00' as it is connected directly to ELENA and the beams for all but one experiment will pass through this section,see Fig. 1. The only working optical elements present along LNE00 in these simulations are the quadrupoles in a configuration used to pass the beam through to LNE01.

TRACKING CODE

For this study Polymorphic Tracking Code (PTC) [3] was used to track a series of beams through a complete MAD-X [4] model of LNE00 obtained from [5]. For each simulation, a Gaussian beam of 10,000 particles with initial ε_x and ε_y = 1 mm·mrad, momentum spread = 5×10^{-4} and no x-y coupling, was generated using Monte-Carlo methods. After tracking, the beam data was passed to a custom Matlab code for analysis.

ELEMENT POSITION OFFSETS

The positions of the quadrupoles were offset in the x and y planes separately. Monte-Carlo methods were used to offset each element by a random amount corresponding to a Gaussian spread. The magnitude of the offsets was increased and the effect on the particle losses in the beam was observed (Fig. 2). For each point the result of 10 runs with varying random offsets were averaged to capture overall effect of the position errors.

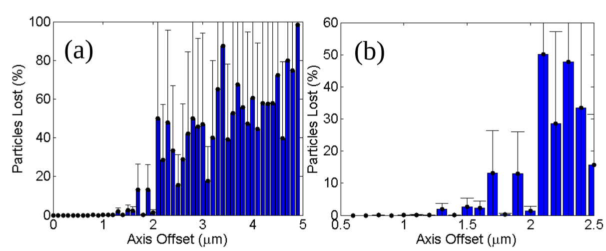

Figure 2: Horizontal losses at the end of LNE00 for increasing quadrupole offsets. The vertical losses results have similar features. (a) shows the full scan and (b) shows more detail around 1.5 µm.

The effects of the quadrupole offsets on the beam losses at the end of the transport line remain steady until they significantly increase around 1.8 µm, with the average reaching just below full beam loss by 5 µm. The first significant losses occur at 1.3 µm where for one particular run almost 18% of the beam was lost, however the other 9 runs lost only 0.56% in total, bringing the average down.

As this simulation only includes the physical aperture and we would expect a dynamic aperture at a smaller

Work supported by the EU under Grant Agreement 624854 and the STFC Cockcroft Institute core grant No. ST/G008248/1.
james.hunt@cockcroft.ac.uk

radius we suggest a preliminary maximum position error of 1 μm for the quadrupoles in LNE00. This will decrease when considering other configurations of the optics of the line, particularly when transferring to LNE07 using kickers. It should be noted that for other lines along the transfer system, elements such as kickers and bending magnets will also contribute to particle losses which must be taken into account when performing additional studies across the transport system.

BEAM INJECTION MISMATCH

A good match between the lattice parameters of the extracted beam and the beam transfer lines is essential to minimize particle losses. In this section we explore the effects of a mismatch of the beam which could occur for a variety of reasons, e.g. due to non-optimum voltage or magnet settings and fluctuations in power supplies.

In order to study the effects of a β-function mismatch upon entering the transfer line, three series of 100 beams each with a range of β_x, β_y and momentum spread values were generated separately. The β_x and β_y variations lead to maximum mismatch parameters (B_{mag}) of 2.4821 and 1.1905, respectively. The mismatch parameter was calculated using:

$$B_{mag} = \frac{1}{2}\left[\left(\frac{\beta}{\beta_*}+\frac{\beta_*}{\beta}\right)+\left(\alpha_*\sqrt{\frac{\beta}{\beta_*}}-\alpha\sqrt{\frac{\beta_*}{\beta}}\right)^2\right], \qquad (1)$$

where the * subscripts denote the mismatched lattice parameters [6].

The emittance for each of these beams was calculated and plotted. The effect of the mismatching on the emittance was negligible even beyond values that correspond to a beta mismatch of almost 50%.To further understand the effects of a β-function mismatch the profiles of the beams in phase space were considered (Fig. 3). It can clearly be seen that the β_x-function mismatch has a detrimental effect on the projected beam sizes as we would expect – they increase with increasing B_{mag}. However in the case of a β_y-function mismatch the effect is much less pronounced. This is because although the β values have both been varied by the same percentage amount, the B_{mag} value they correspond to is different due to a dependence on α, α_x is much larger than α_y.

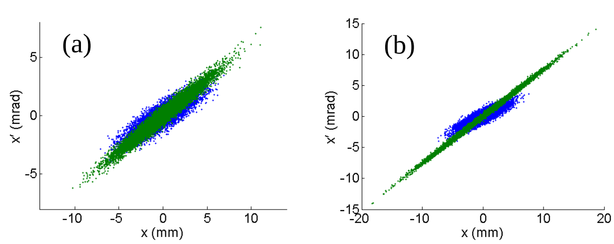

Figure 3: Beams in phase space for (a) B_{mag} = 1 (blue) & 1.8 (green) and (b) B_{mag} = 1 (blue) & 7 (green) due to a β_x mismatch.

An investigation into particle losses was also carried out with a more significant β mismatch – a pessimistic case of a 200% increase, corresponding to $B_{mag} \approx 7$ for β_x. Particle losses begin to rise steadily from $B_{mag} \approx 3$, and although the errors are large due to a low number of realisations per point, a clear trend can be seen (Fig. 4).

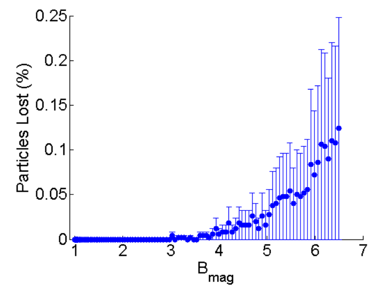

Figure 4: Horizontal losses at the end of LNE00 due to significant β_x mismatching.

QUADRUPOLE FIELD STRENGTH ERRORS

Fluctuations in the field strength of quadrupoles along LNE00 were also simulated. With the Gaussian smearing method used in the element position offsets study, the strengths of each quadrupole were varied independently from each other. This was repeated for 10 random iterations before the strength of the error was increased by 1%.

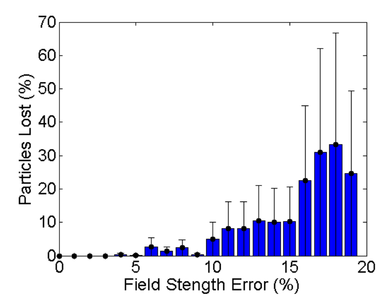

Figure 5: Results of the quadrupole field strength scan along LNE00, the large error bars are due to the random nature of the variations, but a clear overall trend can be seen.

Figure 5 shows the results of the scan along LNE00, the large error bars are due to the random nature of the variations, but a clear overall trend can be seen. Significant particle loss does not occur until a field strength error of around 11%. However, significant particle loss did occur earlier than this for specific runs. This is due to configurations of field error that are by chance more effective at blowing the beam up, for example the first and second elements (LNE.ZQMF.0002 and LNE.ZQMD.0005) have an extremely large error in the same direction. These cases are relatively rare (around one in thirty), but could be explored in future studies, perhaps to identify particularly error sensitive elements or combinations along the line.

FINITE ELEMENT SIMULATIONS & MULTIPOLAR COMPONENTS

Studies to determine the multipolar components of the electrostatic elements are underway [7]. The finite element program COMSOL Multiphysics was used to create a test quadrupole with the geometry of those used along LNE00 (Fig. 6). For now, arbitrary voltages of ±500 V were applied to the opposing poles and a cylindrical shaped shield was added 10 mm from the ends of the element.

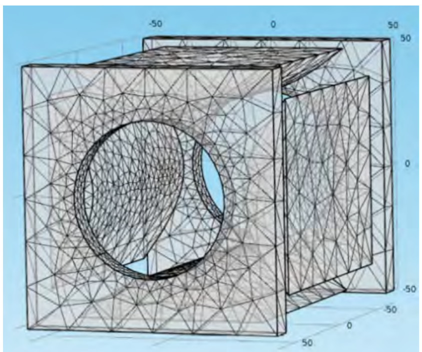

Figure 6: COMSOL Multiphysics model of LNE00 quadrupole with initial mesh.

In order to find the different components of the field, the electric potential around a transverse circle ($\varphi = 0..2\pi$) at fixed z and radius was calculated. The multi-polar components can then be found in a Taylor expansion of the electric potential in cylindrical co-ordiantes:

$$V(R,\varphi,z) = \frac{q}{2E_{kin}} \sum \frac{1}{n!} A_n(z) R^n e^{in\varphi}, \qquad (2)$$

where A_1 = dipole, A_2 = quadrupole, A_3 = sextupole, A_4 = octupole… components.

Fitting the circular scan of $V(R,\varphi,z)$ with

$$V(R,\varphi,z) = K\cos(2x) + D\cos(6x)\,, \qquad (3)$$

gives the quadrupole, K, and dodecapole, D, components of the field. K and D were then calculated along z and the effective overall quadrupole and dodecapole coefficients k_{eff} and d_{eff} were found by using the integrals in Eq. (4).

$$k_{eff} = \int \frac{2qLK(z)}{2E_{kin}R^2} dz \quad d_{eff} = \int \frac{6!\,qLD(z)}{2E_{kin}R^6} dz. \quad (4)$$

This process was repeated for a model with quadrupole shaped shields, the results are shown in Table 1.

Table 1: Field Co-efficients For Different Electrode Shapes

Shield Shape	**k_{eff} (m^{-1})**	**d_{eff} (m^{-5})**
Cylindrical	0.6018	3.4210×10^6
Quadrupolar	0.6069	1.6354×10^5

Analytically calculating k_{eff} for a hard edge quadrupole using Eq. (5) gives us

$$k_{eff} = \frac{qU_{total}}{2E_{kin}R^2} L = 0.5556\ (m^{-1}) \qquad (5)$$

This result is in good agreement with those obtained numerically with the finite element methods, within 10%. However, we expect some disagreement as the hard edge model is a simplified case.

These coefficients can be easily implemented to the MAD-X model of the ELENA transfer lines for a continuation of the studies presented in earlier sections.

CONCLUSION AND OUTLOOK

The work presented in this paper represents the first steps in developing a multi-knob simulation platform for carrying out a detailed analysis of the impact from various factors on the resulting beam quality in electrostatic transfer lines. First tests were done for the example of the ELENA beam lines and in particular LNE00 has been studied in its most basic configuration, with no kickers or deflectors enabled. However, the work on the quadrupoles provides a good blueprint for the implementation of additional optical elements, such as kickers and bending elements, along the whole of the transfer system. Furthermore, work to calculate the multipolar components of the quadrupole fields will also be extended to include these additional optical elements.

REFERENCES

[1] V. Chohan (editor), “Extra Low Energy Antiproton ring” and its Transfer Lines, Design Report,” CERN-2014-002 (2014).

[2] S. Maury (editor), “Design Study of the Antiproton Decelerator: AD,” CERN/PS 96-43 (AR), 1996.

[3] É. Forest et. “Introduction to the Polymorphic Tracking Code,” CERN-SL-2002-044 (AP).

[4] G. Roy (editor), “The MAD-X Program User’s Reference Manual”, Preliminary Draft: http://cern.ch/madx/madX/doc/latexuguide/madxuguide.pdf

[5] M. Fraser, online directory: http://mfraser.web.cern.ch/mfraser/public/ELENA/MADX/v1_8/

[6] A. Wu Chao, M. Tigner, *Handbook of Accelerator Physics and Engineering*, (World Scientific, 1999), 253.

[7] O. Karamyshev et. al “Optimization of Low Energy Electrostatic Beam Lines”, TUPRO071, Proceedings of IPAC 2014, Dresden Germany.

QUALITY AND STABILITY STUDIES OF THE BEAMS IN THE ELENA RING TRANSFER LINES

J. R. Hunt, O. Karamyshev, J. Resta-López, C. P. Welsch
Cockcroft Institute and the University of Liverpool, UK

Abstract

The Extra Low Energy Antiproton (ELENA) [1] ring will initially provide eight different experiments at CERN with extra low energy (~100 keV) antiprotons by utilising electron cooling techniques. As a result, a system of transfer lines is being designed to ensure each experiment receives a beam consistent with specified properties. In this paper, particle tracking simulations are performed to explore the effects of different lattice imperfections, e.g. element misalignment, electric field errors and mismatching errors, on the beam quality and orbit stability. Specific values for the upper limits of inaccuracies are obtained as a guide for the construction of the transfer lines, and will enable further optimization.

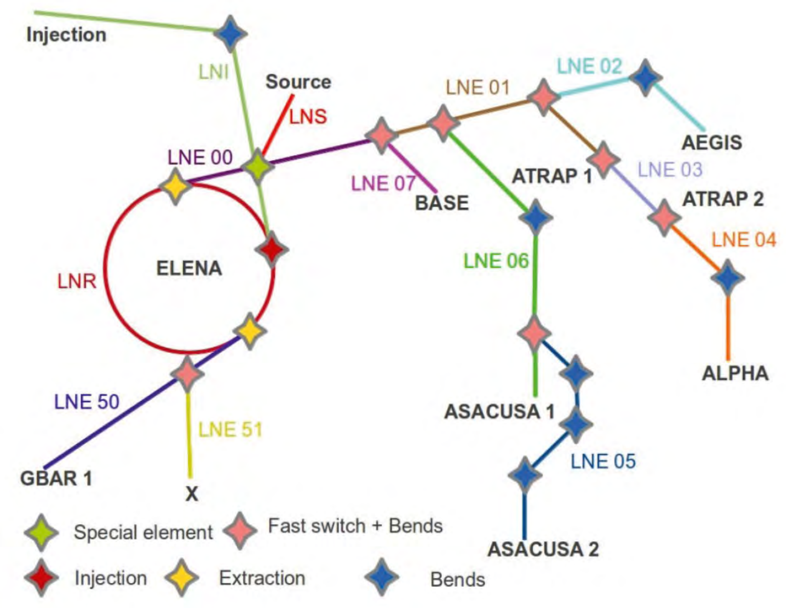

Schematic layout of the ELENA and it's transfer lines

Transfer Lines and Beam

- The transfer lines system is made up of electrostatic elements and split into 9 separate lattices. For this study LNE00 was used as it contains only quadrupoles and is directly connected to ELENA.
- For each simulation, a Gaussian beam of 10,000 particles with initial εx and εy = 1 mm·mrad, momentum spread = 5×10-4 and no x-y coupling was generated.

Tracking Code Methods

The main tracking code used was Polymorphic Tracking Code (PTC) [2], This was run from within the MAD-X [3] framework. The results were then passed to MATLAB for analysis.

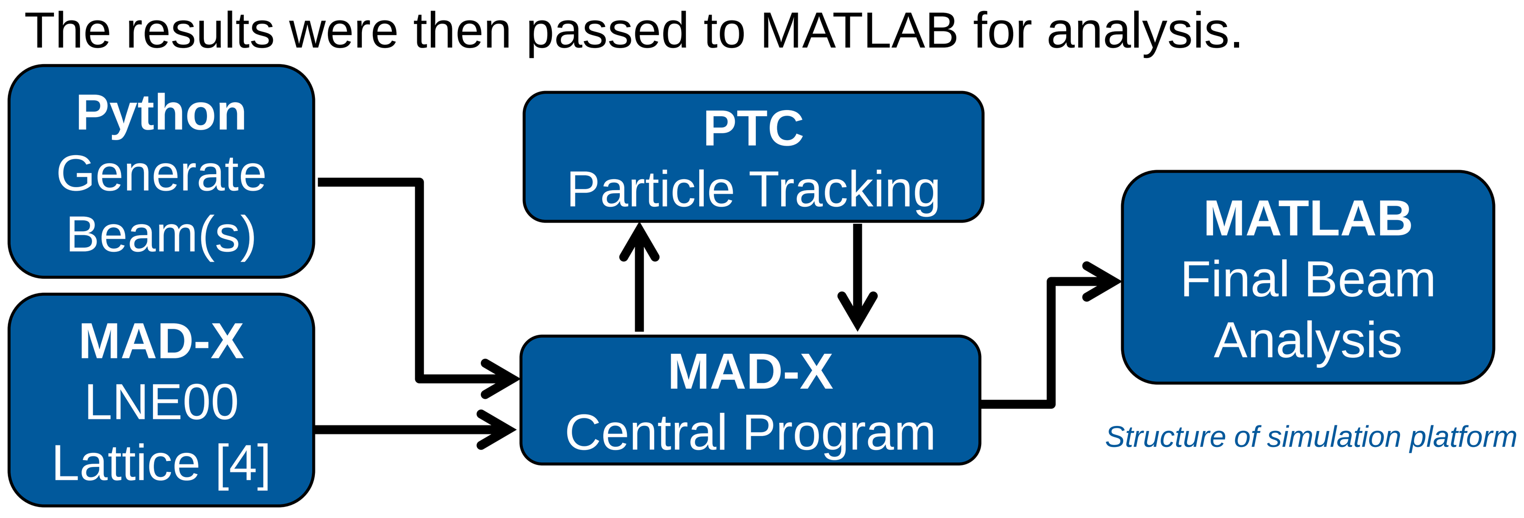

Structure of simulation platform

Element Position Offsets

- Positions of the quadrupoles were offset in the transverse x and y planes separately.
- Monte-Carlo methods were used to offset each quadrupole by a random amount corresponding to a Gaussian spread.
- 10 runs per offset amount were averaged to capture the effect of the errors.
- First significant losses at 1.3 µm – one run lost 18%.
- Losses climb from this point reaching almost full beam loss on average at 5 µm.
- Accounting for dynamic, aperture a maximum position error of 1µm is suggested.

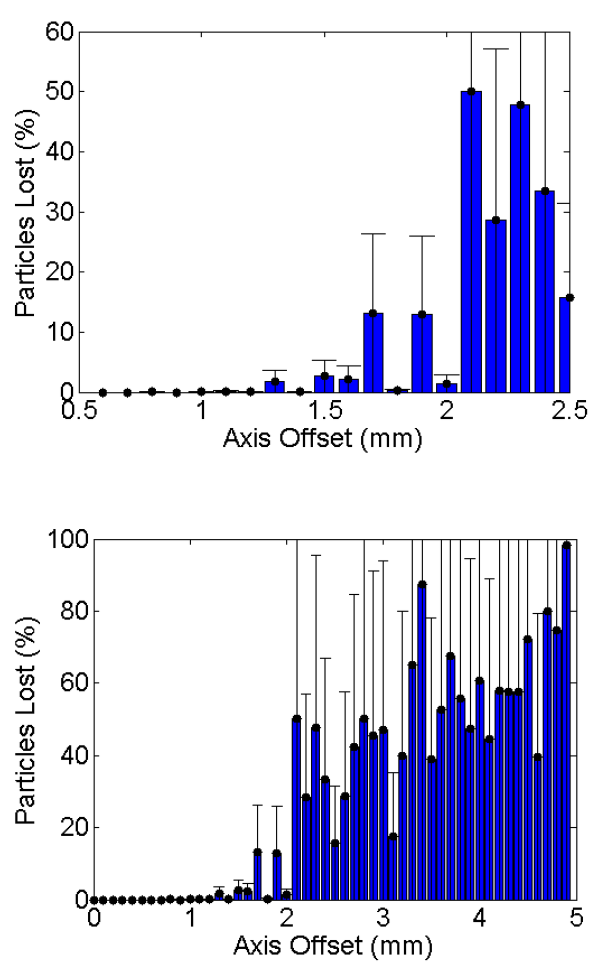

Particle losses for varying position offsets

Quadrupole Field Strength Errors

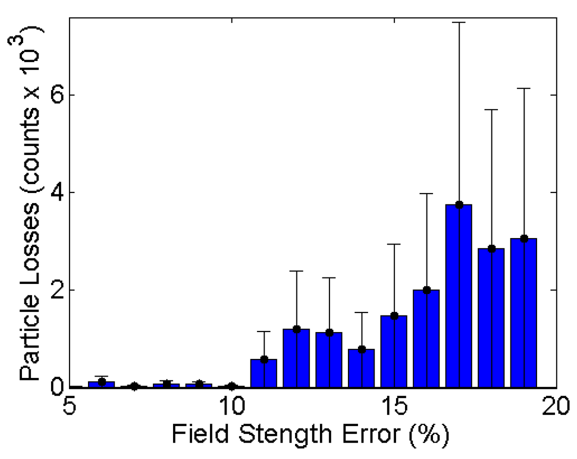

Particle losses for varying field strength error

- Strengths of each quadrupole were varied independently.
- 10 random iterations per 1% field strength error.
- Significant particle loss occurred around 11%.
- For certain configurations of field error particle loss occoured earlier.
- Configurations and elements more likely to lead to particle loss could be studied and highlighted.

Beam Injection Mismatch

- A β-function mismatch was simulated in the x and y planes.
- Mismatch expressed in terms of the mismatch parameter:

$$B_{mag} = \frac{1}{2}\left[\left(\frac{\beta}{\beta_*} + \frac{\beta_*}{\beta}\right) + \left(\alpha_* \sqrt{\frac{\beta}{\beta_*}} - \alpha \sqrt{\frac{\beta_*}{\beta}}\right)^2\right]$$

- The mismatch had no effect on the emittance of the beam up to $B_{mag} = 7$.
- A clear trend can be seen in increasing particle losses from $B_{mag} = 3$.

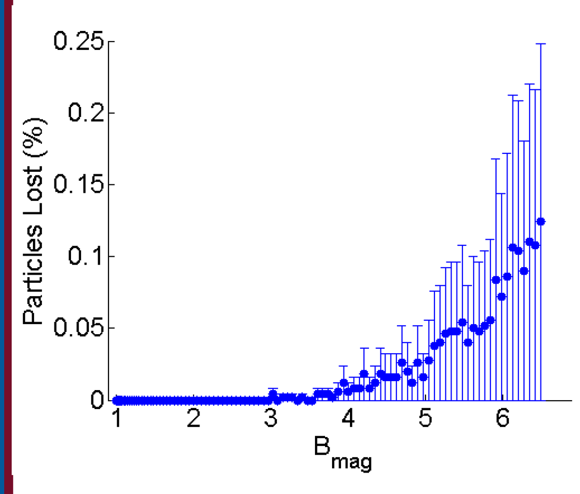

Particle losses for varying β_x mismatch

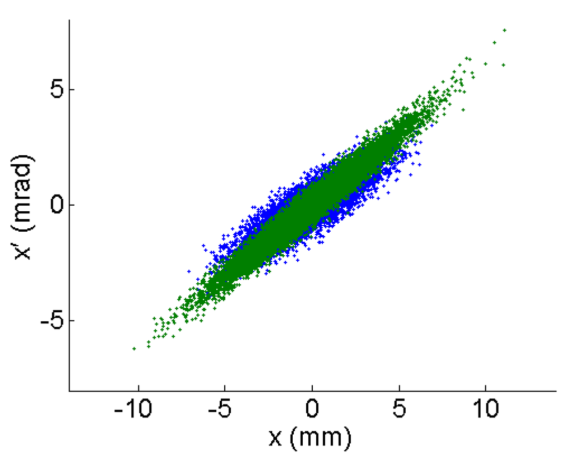

Phase space plots for B_{mag} = 1 (blue) and 1.8 (green)

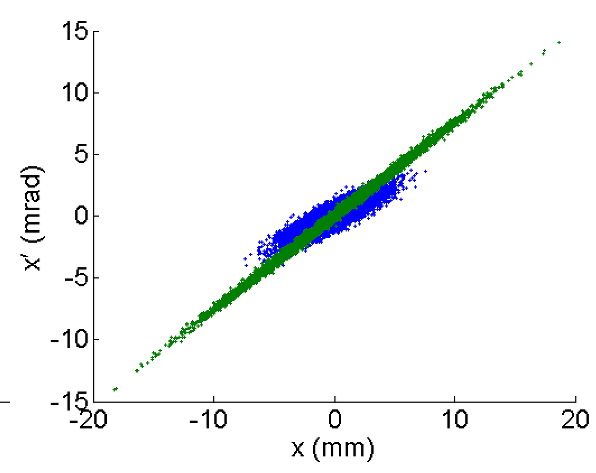

Phase space plots for B_{mag} = 1 (blue) and 7 (green)

Finite Element Simulations

- COMSOL Multiphysics was used to study the multipolar components of the quadrupoles using existing techniques [5].
- Two types of shield, cyclindrical and quadrupole shaped, were added 10mm from the ends of the quadrupoles.
- The quadrupole and dodecapole coefficients were calculated and compared with the hard edge model equivalent:

Shield Shape	k_{eff} (m^{-1})	d_{eff} (m^{-5})
Cylindrical	0.6018	3.4210×10^6
Quadrupolar	0.6069	1.6354×10^5
Hard edge model	0.5556	1.6354×10^5

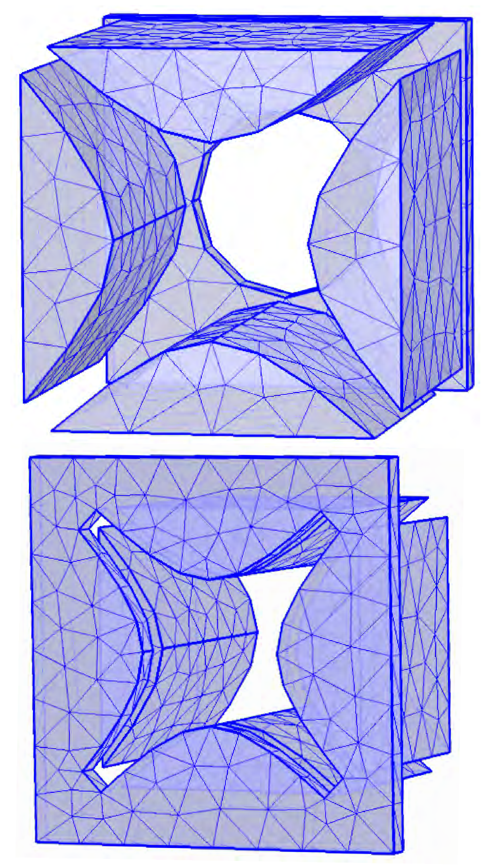

Initial Mesh COMSOL Models

Conclusion and Outlook

A multi-knob simulation platform has been developed for carrying out detailed analysis of the beam quality in ELENA's electrostatic beam transfer lines. Studies will be extended to the rest of the transfer line and include additional elements as well as multipolar components of the fields.

References:
[1] V. Chohan (editor), "Extra Low Energy Antiproton ring" and its Transfer Lines, Design Report," CERN-2014-002 (2014).
[2] É. Forest et. "Introduction to the Polymorphic Tracking Code," CERN-SL-2002-044 (AP).
[3] G. Roy (editor), "The MAD-X Program User's Reference Manual", Preliminary Draft: http://cern.ch/madx/madX/doc/latexuguide/madxuguide.pdf
[4] M. Fraser, online directory: http://mfraser.web.cern.ch/mfraser/public/ELENA/MADX/v1_8/
[5] O. Karamyshev et. al "Optimization of Low Energy Electrostatic Beam Lines", TUPRO071, Proceedings of IPAC 2014, Dresden Germany

Work supported by the EU under Grant Agreement 624854 and the STFC Cockcroft Institute core grant No. ST/G008248/1.
james.hunt@cockcroft.ac.uk

NOVEL SINGLE SHOT BUNCH LENGTH DIAGNOSTIC USING COHERENT DIFFRACTION RADIATION

R. Fiorito*, C. Welsch, H. Zhang, Cockcroft Institute, University of Liverpool, Daresbury, WA44AD, UK
A. Shkvarunets, IREAP, University of Maryland, College Park, MD, 20901, USA

Abstract

Current beam bunch length monitors that measure the spectral content of beam-associated coherent radiation to determine the longitudinal bunch form factor usually require wide bandwidth detection, Fourier transformation of spectral or interferometric data, phase retrieval algorithms and multiple beam pulses to obtain the bunch length. In this paper we discuss progress in the development of a novel single shot method that utilizes the frequency integrated angular distribution (AD) of coherent diffraction radiation (CDR) to measure the RMS bunch length directly. We also present simulation results that show how the AD changes with bunch length for two electron beam linacs, where we are planning to test this new method, our single shot measurement technique and plans for comparison to other bunch length monitors.

INTRODUCTION

Conventional RF accelerators as well as plasma wakefield accelerators have the ability to generate very short pulses of electrons (~10fs), and schemes are being developed to produce even shorter pulse lengths. A number of techniques have been developed to measure bunch length and even the longitudinal distribution of bunches down to ~10 fs in duration. These include Fourier transform interferometry, direct spectroscopy and various electro-optic techniques that sample either the Coulomb field of the bunch itself or the radiation field produced by the bunch interacting with a physical structure or an electromagnetic field. However, the experimental techniques required are usually complex and difficult to implement particularly for single shot measurements.

Frequently, measurement of the rms bunch length rather than the detailed longitudinal profile of the bunch is sufficient for tune up and accelerator monitoring. To meet this need we propose to develop a novel rms bunch length method that is noninvasive, easy to implement, simple to analyze, capable of bunch length measurements over a very wide range and has the potential for single-shot measurements.

BACKGROUND

For most cases of interest, the AD of the CDR can be calculated as the integrated spectral angular density of DR from single electron multiplied by the longitudinal form factor of the pulse:

$$\frac{dI_{bunch}^{CDR}}{d\Omega} \approx N_e^2 \int_{\Delta\omega} \frac{d^2 I_e^{DR}}{d\omega d\Omega} S_z(\sigma_z, \omega) d\omega \qquad (1)$$

The single electron spectral angular density, the first term of the integrand depends on the shape and size of the radiator as well as the frequency. This can be calculated for any size/shape radiator [1]. The second term of the integrand is the longitudinal bunch form factor, which is a function of the bunch length (σ_z). Assuming a model (e.g. a Gaussian) for the longitudinal bunch form factor and an appropriate frequency band, Eq. (1) can be integrated and fit to the measured AD data to produce the rms bunch length [1].

The method has been validated experimentally in a proof of principle experiment done at the Paul Scherrer Institute using repetitive picosecond electron beam pulses with energy E=100 MeV and a Golay cell to scan the angular distribution of the CDR in both the horizontal and vertical directions [2]. However, the measurement was time integrated, i.e. averaged over many repetitive macro-pulses and provided only 1D scans for the fit.

We propose to measure the entire AD projected onto the plane of an imaging detector to improve the accuracy of the measurement and to demonstrate single shot capability. The method will be tested at two accelerators with widely different bunch lengths and beam energies: the ALICE accelerator at Daresbury Laboratory and the FACET accelerator at SLAC.

EXPERIMENTS

ALICE

The beam parameters that are planned for our initial CDR AD imaging experiments on ALICE are: E=26 MeV, τ_{rms} = 0.7-1.3 ps, Q = 100 pC/micro-bunch, 1-4000 micro-bunches per macro-pulse and macro-pulse repetition rate τ_{rep} = 10 Hz.

CDR will be created as each picosecond micro-bunch passes through a simple circular annular aperture inclined at 45^0 to the velocity of the electron beam. The CDR will emerge at 90^0, passing through a vacuum window and be imaged onto a pyroelectric array.

We have calculated the frequency integrated AD of CDR for an annular radiator (outer radius = 8mm and inner radius = 4mm) over the wavelength band 18-200 μm, which corresponds to a frequency band 0.15 - 2 THz, for different bunch lengths. In this band the longitudinal bunch form factor is most sensitive to changes in the bunch size. The results of our calculations are shown in Figure 2. The widths of the three distributions correspond to rms bunch widths: 0.7, 1.0 and 1.3 ps. The intensities are normalized to their respective peak values.

*ralph.fiorito@cockcroft.ac.uk

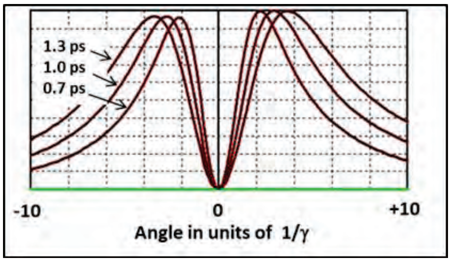

Figure 1: Horizontal line scans of the AD of CDR calculated for the ALICE accelerator parameters.

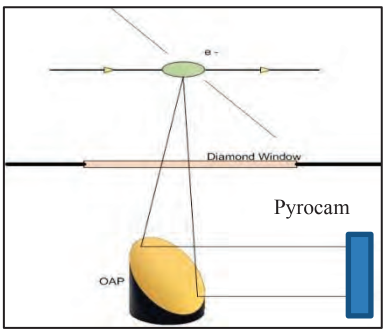

Figure 2: Set-up for direct imaging the AD of CDR passing through an annulus.

The experimental setup is shown in Figure 2. An off-axis parabolic reflector (OAP) with an effective focal length of 50mm will be used to focus the THz CDR AD onto a 12x12 mm, 124 x 124 element pyroelectric array (Pyrocam III). The 85 micron square pixels are sensitive to radiation with wavelengths from 1-3000 microns and have a minimum sensitivity of 7 nJ/pixel. When placed in the focal plane of the OAP the array will subtend an angular field of view $\Theta \sim 0.2$ radians or roughly half of the far field AD pattern shown in Figure 2. A single pixel of the array will be exposed to a calculated peak energy $E_p \sim 3 \times 10^{-6}$ J per micro-pulse per steradian and each pixel subtends about 3×10^{-6} sterad. Therefore for 1000 micropulses the signal to sensitivity ratio is about unity. To increase this ratio to ~10 we will use 3x3 binning on the Pyrocam. If more signal is needed we can increase the number of micropulses/macropulse.

The setup to test the proposed optics for our ALICE CDR AD imaging experiment is shown in Figure 3. A HeNe laser beam is first expanded using a two lens system to form a collimated beam. This beam is used to determine the focal plane of the 50 mm focal length OAP, i.e. the collimated laser beam is focused to a point at f = 50mm, where the Pyrocam is placed in order to image the AD of the CDR generated by the electron beam. The 10 X beam expander consists of f/25 and f/250 mm lenses spaced such that the distance between their principle planes is exactly 275mm. In practice this is achieved by varying the inter-lens spacing until a collimated laser beam is observed at several distances after the second (f/250mm) lens.

A 50/50 beam splitter (B.S.) directs the collimated beam from the expander to the Pyrocam and also transmits the ALICE internal alignment laser. The latter is setup up separately to follow the electron beam trajectory in the accelerator. When this beam is reflected by the radiator surface out of the vacuum chamber through an optical viewport, it can be used to align the OAP and Pyrocam to the direction of the central ray of the CDR AD pattern that will be observed in reflection from the radiator during the experiment.

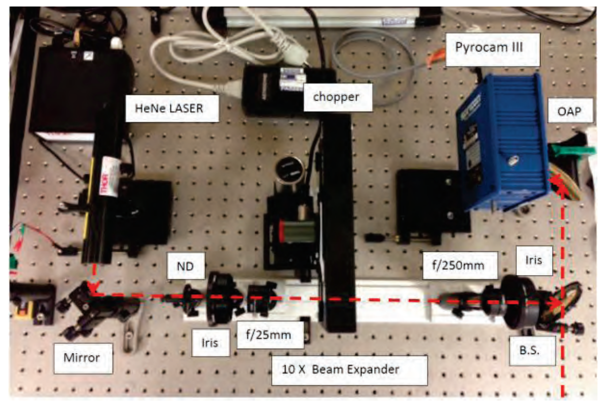

Figure 3: Optics setup to test and align the CDR AD imaging system for ALICE.

FACET

We also are planning CDR AD experiments to determine the bunch length of SLAC's FACET electron beam accelerator. The beam parameters are quite different than ALICE, i.e. E=20 GeV, $\tau_{rms} \sim$ 50-100 fsec and the number of electrons per bunch is 10^{10} or Q ~ 0.6 nC per bunch. We estimate the peak energy density of the CDR to be 134 J/sterad in the wavelength band 18-200 microns for a single bunch.

Two CDR radiators will be used to measure the bunch length: 1) an existing circular foil 25 mm in diameter and 2) an annular aperture with an outer radius of 12.5mm and inner radius 2.5mm. In contrast to ALICE we should easily be able to image the entire 2D angular distribution produced by a *single pulse* and analyze it to determine the bunch length. We will do this for a number of different bunch lengths and compare our results to those obtained with other techniques, e.g. a transverse deflecting cavity and an interferometer that are presently online.

A calculation of a horizontal scan of the CDR AD from the annular aperture is shown in Figure 4. Here we have calculated the frequency integrated AD of the CDR for three different bunch lengths over the same frequency band 0.15 - 2 THz used for the ALICE calculation above.

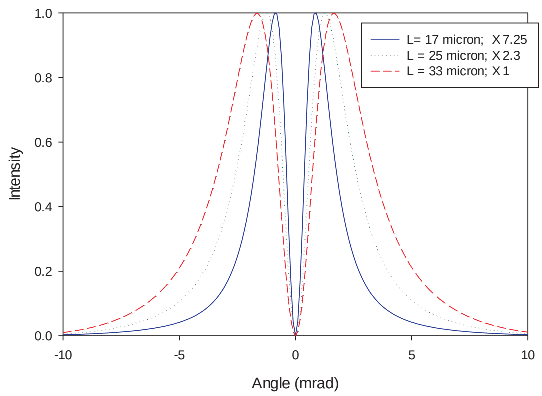

Figure 4: Calculated bunch length dependence of the AD of CDR from FACET for various bunch lengths; intensities are normalized to their peak values.

We will also employ an OAP to focus and image the AD with a Pyrocam III camera. However, since the beam energy is much higher than ALICE, the AD will be highly compressed in angle (cf. Figures 1 and 4). Thus a longer focal length (*f* ~ 1 meter) OAP is required to image the CDR AD. Our estimate for the peak CDR energy that will be seen by a single pixel of the Pyrocam per pulse is ~1 μJ, which is close to the saturation level of the pyroelectric elements, so that attenuation of the CDR may be necessary. Since the FACET pulse repetition rate is 10 Hz, it should be straightforward to capture the CDR AD of a single pulse with the Pyrocam, which can be readout at a 10 Hz rate and triggered to capture the CDR from the FACET electron beam pulse.

FUTURE PLANS

In follow-on experiments we plan to test an alternative method to perform single shot CDR AD imaging. It is an adaptation of a simple electro-optic (EO) technique that was previously developed to image CDR in the FIR-THz band. It utilizes the fact that the polarizability of an EO crystal is altered by incident CDR THz radiation. The polarization pattern imprinted on the crystal can be imaged on a CCD camera with the help of a polarized laser beam timed to overlap the beam pulse.

The optics that we will use to image the AD of CDR THz radiation is a simple variation of a technique that has been developed to image the source of coherent THz transition radiation (CTTR) [3]. Following the optical setup described above for ALICE, we will place an EO crystal in the focal plane of an OAP to image the THz CDR AD. The setup for the experiment is shown in Figure 5.

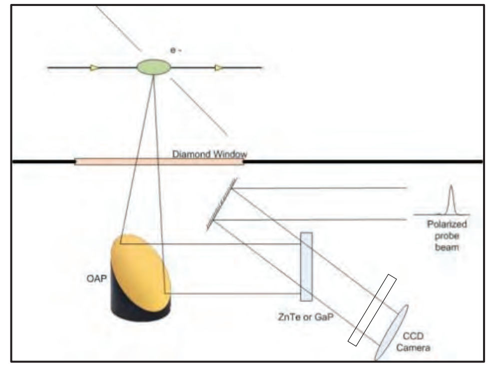

Figure 5: Proposed EO far field CDR AD electro-optic imaging system.

A similar technique has also been successfully applied to image the far field interference pattern of two overlapping AD distribution lobes of CTR produced by a single picosecond pulse. The Fourier transform of the interference pattern yields the autocorrelation and bunch length [4]. Hence the feasibility of far field EO imaging has already been demonstrated.

We will determine the required electric field strength needed to do the direct AD imaging required for our bunch length measurement method. Such a system could in principle be synchronized to select a single pulse from any RF accelerator or plasma wake-field accelerator and would provide a monitor for accelerator tune up and bunch compression.

ACKNOWLEDGEMENT

Work supported by the EU under grant agreement 624890 and the STFC Cockcroft Institute Core Grant No. ST/G008248/1.

REFERENCES

[1] A. Shkvarunets and R. Fiorito, Phys. Rev. ST Accel. and Beams, 11, 012801 (2008).

[2] A. Shkvarunets, R. Fiorito, et al., Proc. DIPAC2009, Venice, Italy, http://jacow.org/.

[3] J. van Tilborg, "Coherent THz radiation from laser wake field accelerated electron beams", Ph.D. thesis, Technishe Universiteit Einhoven (2006).

[4] D. Suetterlin, et al., Rev. Sci. Instrum, 81,105702 (2010).

Novel single shot bunch diagnostic using coherent diffraction radiation*

R. Fiorito†, C. Welsch, H. Zhang, *Cockcroft Institute and the University of Liverpool, Daresbury, UK*
A. Shkvarunets, *Institute for Electronics and Applied Physics, University of Maryland, College Park, MD, USA*

Abstract

Current beam bunch length measurement that use the spectral content of beam-associated coherent radiation to determine the longitudinal bunch form factor require wide bandwidth detection, Fourier transformation of spectral or interferometric data, phase retrieval algorithms and multiple beam pulses. In this paper we discuss progress in the development of a novel single shot method that utilizes the *angular distribution* (AD) of coherent diffraction radiation (CDR) to measure the RMS bunch length directly. We present simulation results that show how the AD changes with bunch length for two electron beam linacs: ALICE at Daresbury and FACET at SLAC where we are planning to image the 2D AD and our plans to apply the technique for single shot bunch length measurements.

Concept

The Angular Distribution of CDR from a slit or aperture can be calculated as the integrated spectral angular density of DR from single electron multiplied by the longitudinal form factor of the pulse:

$$\frac{dI^{CDR}_{bunch}}{d\Omega} \approx N_e^2 \int_{\Delta\omega} \frac{d^2 I_e^{DR}}{d\omega d\Omega} S_z(\sigma_z, \omega) d\omega$$

1) The single electron spectral angular density depends on the shape and size of the radiator as well as the frequency; this can be calculated for any radiator[1].

2) The longitudinal bunch form factor is a function of the bunch length (σ_z).

3) Assuming a model (e.g. a Gaussian) for the longitudinal bunch form factor and an appropriate frequency band, Eq. (1) can be integrated and fit to the measured AD data to produce the rms bunch length.

Previous CDR AD Line Scan Experiment

Setup for performing horizontal and vertical line scans of the AD of CDR from a slit at PSI's 100 Mev linac [2].

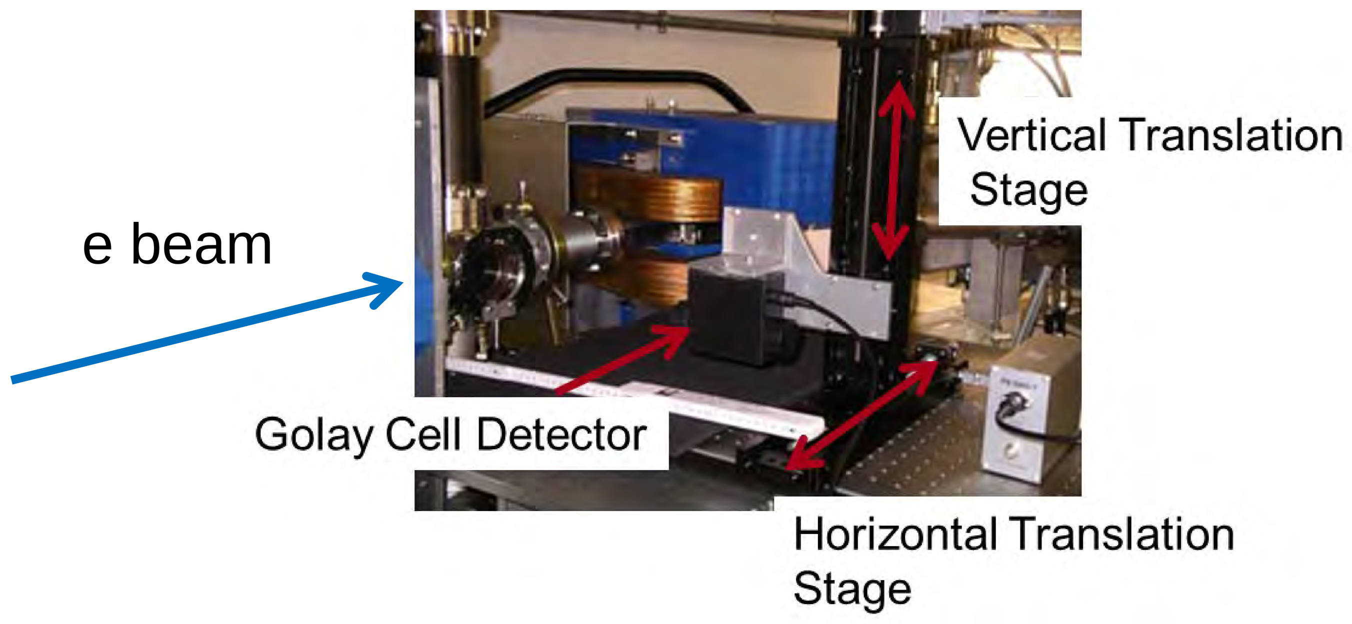

Fit of data (red) to a theoretical line scan of CDR AD (black) assuming a Gaussian pulse

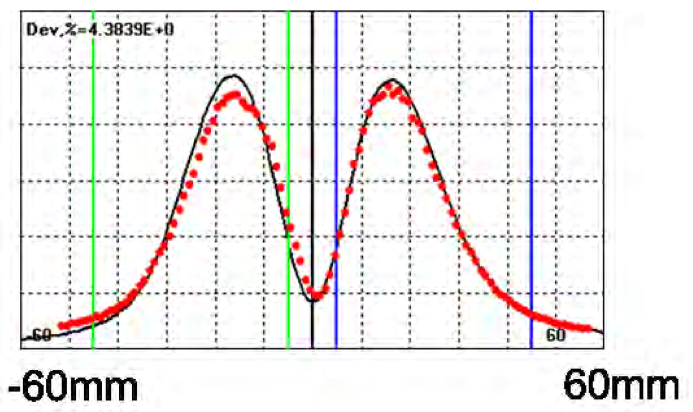

Comparison of CDR AD bunch length method with EO sampling technique

Method	Bunch Compressor Tune	T(ps) single Gaussian fit
AD CDR	PBU-0	0.8
E-O technique	PBU-0	0.75
AD CDR	PBU+3	1.0
E-O technique	PBU+3	1.0

*Work supported by the EU under grant agreement 624890 and the STFC Cockcroft Institute Core Grant No. ST/G008248/1.

† corresponding author: ralph.fiorito@cockcroft.ac.uk

CDR Imaging Experiments at ALICE and FACET

ALICE parameters:

E = 26 MeV;
micro-bunch width τ = 0.7-1.3 ps;
charge: Q = 100 pC;
no. of micro-bunches: 1-4000;
rep rate: f = 10 Hz

CDR peak energy density: 3 μJ/sterad
THz band: 18-200μ (0.15-2 THz)

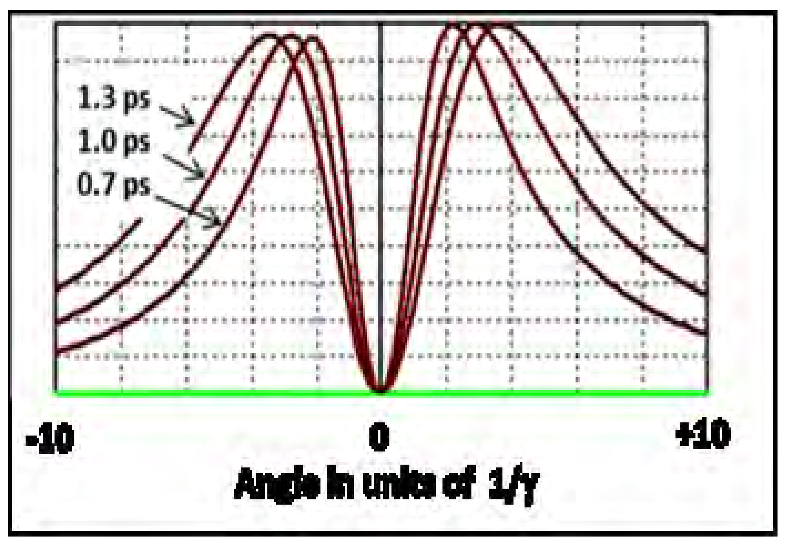

FACET parameters:

E = 20 GeV,
τ = 50-100 fsec ;
Q ~ 0.6 nC;
Single bunch;
rep rate: f = 10 Hz

CDR peak energy density: 134 J/sterad
THz band: 18-200μ (0.15-2 THz)

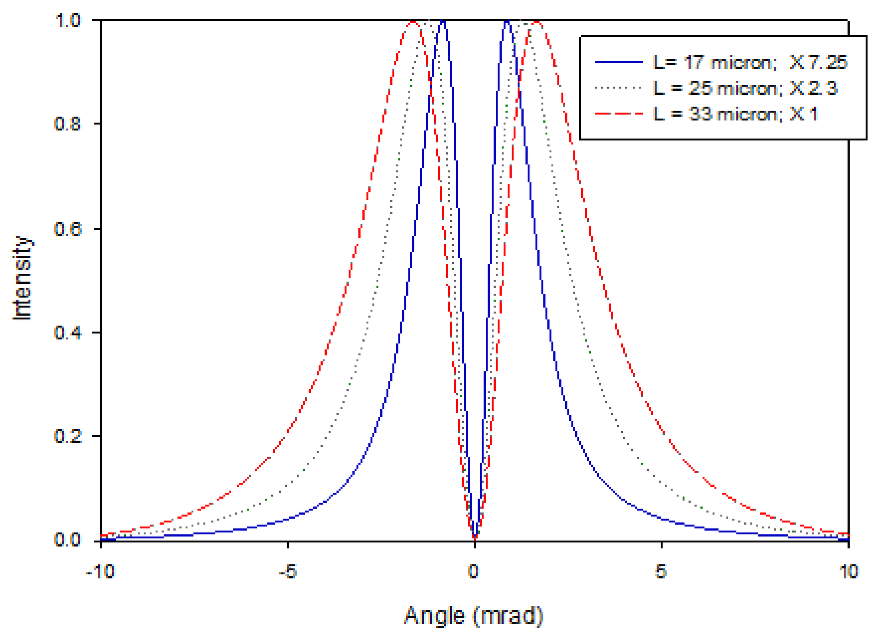

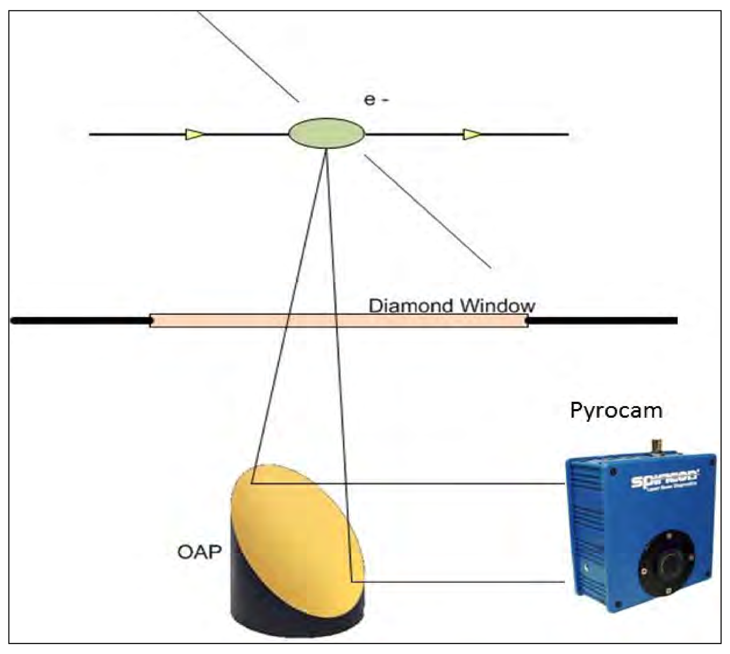

Setup to image AD of CDR from an electron beam with passing through an annular radiator.

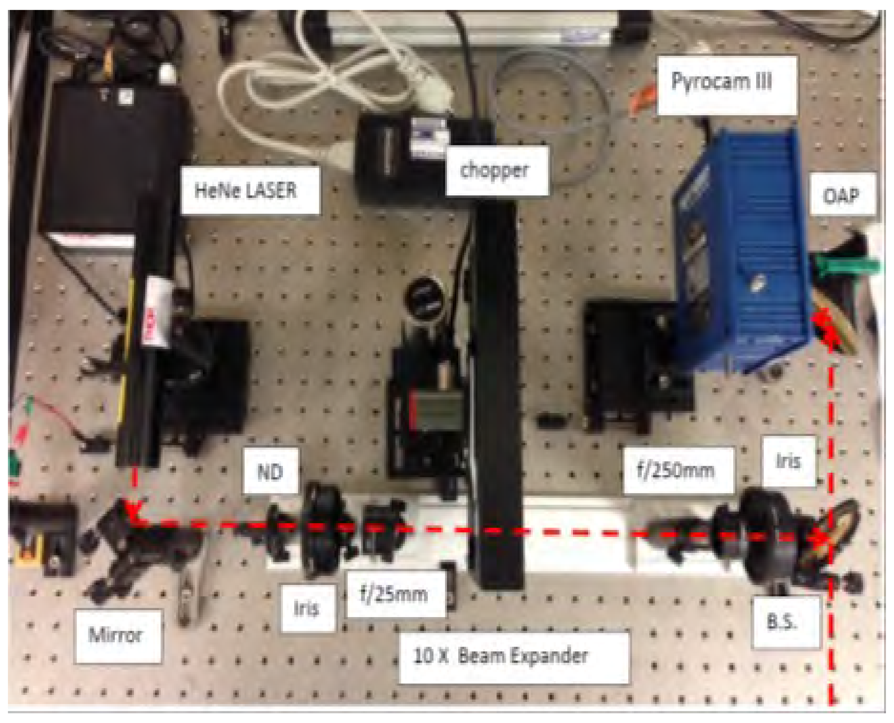

Optics setup to test and align the CDR AD imaging system for ALICE.

References

[1] A. Shkvarunets and R. Fiorito, Phys. Rev. ST Accel. and Beams, 11, 012801 (2008).
[2] A. Shkvarunets, R. Fiorito, et. al. Proc. of DIPAC07, Venice IT (2007).

DEVELOPMENT OF A SUPERSONIC GAS-JET MONITOR TO MEASURE BEAM PROFILE NON-DESTRUCTIVELY

H. Zhang[1,#], V. Tzoganis[1,2], A. Jeff[1,3], C. Welsch[1]
[1]Cockcroft Institute and university of Liverpool, Warrington, WA44AD UK
[2]RIKEN Nishina center, Japan
[3]CERN

Abstract

The measurement of the transverse beam profile is a great challenge for high intensity, high brightness and high power particle beams due to their destructive effects and thus non-destructive methods are desirable. Current non-destructive methods such as residual gas monitors and beam induced fluorescence monitors either requires a longer integration time or higher surrounding pressure to make a meaningful measurement. As a potentially improved technique, a supersonic gas-jet beam profile monitor has been developed by the QUASAR Group at the Cockcroft Institute, UK.

In this monitor, a 45 degree supersonic gas curtain is generated and interacts with beam when the beam crosses it. Ions generated by this process are then accelerated by an extraction electric field and finally collected by a Micro Channel Plate (MCP). Beam images are obtained via a phosphor screen and a CCD camera.

In this contribution, we briefly describe the working principles and present better beam profile measurement of a low energy electron beam using this monitor with newly installed pulsed valve.

INTRODUCTION

Beam profile monitoring is essential for any accelerator system in diagnosing the transverse property of particle beams. Many existing methods could be chosen based on the type, energy and lifetime of the specific particle beam as well as the system requirement such as vacuum condition and beam loss control. For an example, the beam diagnostic in the Ultra-low-energy Storage Ring (USR) [1] at GSI, in order to preserve a longer lifetime of the stored low energy antiproton beam, a vacuum condition of ~10^{-11} mbar is required. Meanwhile, considering the costly antiproton, a non-destructive method is preferred. These requirements basically limit the choice from the existing mature transverse diagnostics. Gas-based monitor, such as residual gas ionization monitor or fluorescent monitor, could be the potential candidate for USR project, because it reserves the vacuum condition quite well and disturbs the beam very little. However, a low ionization or fluorescent rate due to the low vacuum pressure requires a long integration time to obtain a meaningful profile and usually the measurement is in one dimension. In the USR case, the intrinsic integration time could be more than 100 ms which brings additional prerequisite for the primary beam stability. To reduce the integration time while keeping the non-destructive feature by using gas molecules, a novel 2-dimentional supersonic gas-jet ionization monitor is designed in Cockcroft Institute [2]. Previously, using the same principle, a magnetically focused oxygen molecular beam was implemented in HIMAC for fast heavy ion profile measurement [3] and a mechanically skimmed nitrogen beam in JPARC for the intense proton beam [4]. In this method, the localized gas intensity could increase by more than 5 orders of magnitude by the jet, which increases the ionization rate and thus shortens the integration time about the same order. Meanwhile, the vacuum is affected little due to the directionality of the supersonic gas-jet. In this paper, we will discuss the design and working condition of this monitor as well as recent results from an in-house low energy electron beam. Although the application is based on the USR due to its highly specialized requirement, this monitor could be generally used in any accelerators where the gas load is allowed.

WORKING PRINCIPLE AND TEST STAND

The schematic of the whole setup is shown in Fig. 1. The design is based on the Reaction Microscope [5]. To generate the supersonic gas flow, differential pumping technique is used in the nozzle chamber, the gas flow through a 30 um orifice from a high pressure area (few bar) to a low pressure area (about 10^{-1} to 10^{-2} mbar). With this large pressure difference, the gas will experience a free expansion process, and a supersonic flow will form inside a Mach disk. By placing the first conical skimmer (180 um in diameter) inside the Mach disk (less than 2 cm from the nozzle), we can guide a part of the supersonic flow into the following chambers to form a molecular flow and meanwhile avoid the effect from turbulence and other shock waves. An additional conical skimmer (400 um in diameter) is positioned 25 mm away from the first skimmer to further collimate the flow. In order to have a two dimensional measure of the primary beam profile, a third rectangular skimmer of 4*0.4 mm^2 is placed at 325 mm from the first skimmer before the interaction chamber under an angle of 45 degrees to create a screen-like jet. Detailed design and gas dynamics consideration including

#hao.zhang@cockcroft.ac.uk

pump usage and alignment procedures can be referred to [6, 7].

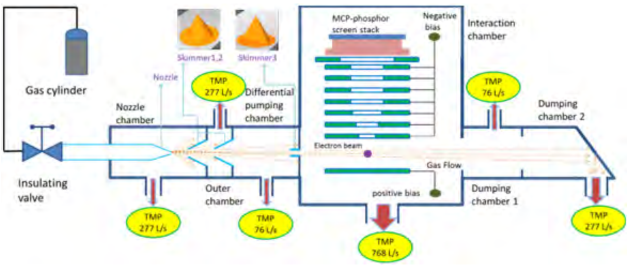

Figure 1: Schematic diagram of the supersonic gas jet setup.

In the interaction chamber, when the primary beam interacts with the supersonic flow, the gas molecules will be ionized. The ions generated in this ionization process are then accelerated by an extraction electric field. One circular solid metallic electrode is placed in the bottom of the reaction area and 8 parallel ring-shaped electrodes are above the reaction area. The bottom plate is positively biased while the top ones are biased with staged negative voltages to create a linear electric field of about 12 kV/m vertically. The top electrodes have central holes to let the ions pass through and the differences in the size of holes is to make the horizontal component of electric field small so as to minimize the distortion from the transverse distribution expansion of ions. The accelerated ions are collected by an MCP, and then the amplified signal reaches a phosphor screen. The finally image on the screen is recorded by a camera (Ueye 1024 x 768 8 bit CCD).

Figure 2 is a typical beam image from this monitor. Here, the initial pressure was 5 bar. The electron gun setting is 2.6 A filament current, 3.75 keV beam energy and 0.2 μA beam current. The camera setting is 70.0 ms shutter time, and 0 gain. In the current experiment environment, due to the out-gassing from the hot filament of the electron gun, the pressure inside the interaction chamber rises from $6.2{*}10^{-9}$ mbar to $1.2{*}10^{-8}$ mbar. Thus, a clear image of the primary beam from the residual gas can still be seen in the figure (the elongated line in x axis). In an actual application inside accelerator, such outgassing source can be eliminated and thus decrease the intensity of the residual gas image. The image from the supersonic gas-jet curtain is the top one with squeezed size which represents a more accurate measure of the primary beam in both directions. The shift from the residual gas image is due to the initial velocity of the ions from the gas jet.

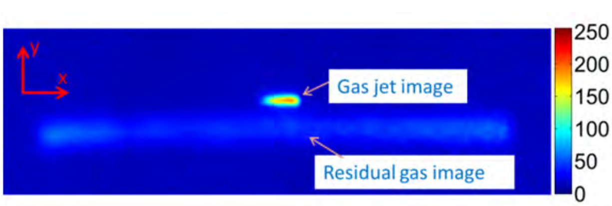

Figure 2: Beam profile from the supersonic gas-jet monitor.

NEWLY INSTALLED PULSE VALVE

Recently, we upgrade the insulating valve with a Festo solenoid pulsed valve. It features a maximum switching frequency of 280 Hz with 0.2 ms switching time, an operating pressure of 0-8 bar and a standard nominal flow rate of 200 l/min. We use a TGP110 pulse generator to trigger the pulsed valve externally. It has a frequency range from 0.1 Hz to 10 MHz and knobs for varying the period, pulse width and pulse delay individually. Its maximum output amplitude is 10 V which is less than the requirement of the pulsed valve operating voltage 24 V. Thus, a DC power supply (ISO-TECH IPS-3303) and a relay (Crydom DMO063) are used, together with the pulse generator to create a 24 V pulse. The electrical connection is shown in Fig. 3. The relay receives the 5 V trigger from the pulse generator and generates a 24 V signal from the power supply. A scope is used for monitoring the generated pulse.

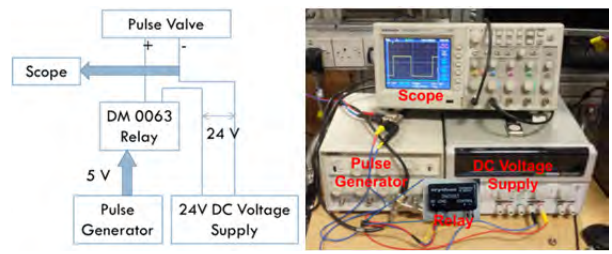

(a) (b)

Figure 3: (a) Diagram of the pulse valve module; (b) picture of the pulse generation setup.

Figure 4 shows the pressure response in the differential chamber and dumping chamber of the pulse valve with 0.8 s period, 50% duty cycle. Here, helium gas was used with an initial pressure of 2 bar from the gas cylinder. Initial tests of the pulse valve include varying the period, duty cycle and the initial pressure of the gas loading. These tests show a characteristic time of about half a second for the vacuum condition to restore after each firing of the gas-jet. The maximum pressures inside both the differential and dump chambers are quite linear with the initial gas loading pressure. These tests suggest that by synchronizing the camera with the pulse valve and setting a proper shutter time, the signal ratio between the supersonic gas-jet and the residual gas can be doubled at least.

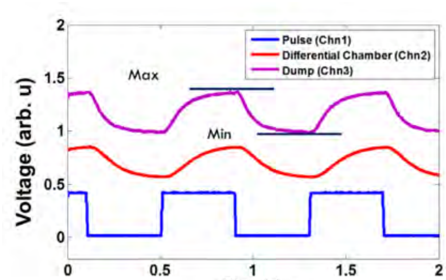

Figure 4: Time structure of the pulse valve and pressure response in the two chambers (as in voltage shown in scope).

MOVEABLE ION GAUGE COMPONENT

The gas curtain distribution is essential in estimating the final resolution of this method, especially the axis which perpendicular to the gas-jet direction. To investigate this distribution, a moveable ion gauge assembly has recently been added into the setup between the interaction chamber and the first dumping chamber. The whole assembly includes a translation stage outside the vacuum chamber (see Fig. 5 (a)) and the attached ion gauge aiming at the gas jet curtain (see Fig. 5 (b)). To sample the gas-jet curtain, two kind of gauge assembly could be used including the through gauge module and the compression gauge module.

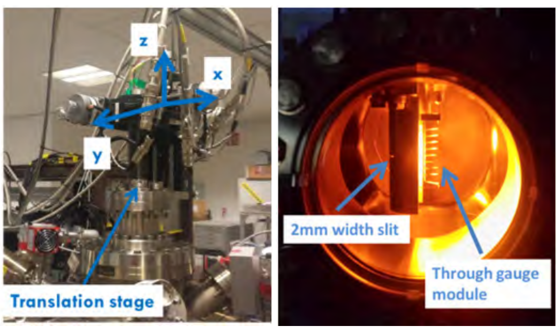

(a) (b)

Figure 5: Moveable ion gauge assembly: (a) 3D translation stage; (b) through gauge module inside.

The through gauge module, as seen in Fig. 6 (a), contains a slit in front of the Bayard-Alpert type ion gauge. In this configuration, only a small portion of the jet passes through the slit and its pressure is measured when the jet flow interacts with the gauge. The shortcoming is the competition of the signals from both the allowing portion of the gas jet and the surround pressure building up by the rest. Shorter pulses of the gas-jet could separate these two signals, but the real signal could be easily overlapped by noise.

For the compression gauge module, as seen in Fig.6 (b), the gauge is inside a small chamber with only a slit in the front to allow part of the jet to enter. The measured signal will be a time integration of the jet entering the slit. In this configuration, the pressure building up in the surrounding by the rest of the gas jet will have little influence on the measured signal. The only drawback is that we lose the time structure of the jet. These modules are currently installed into the whole setup.

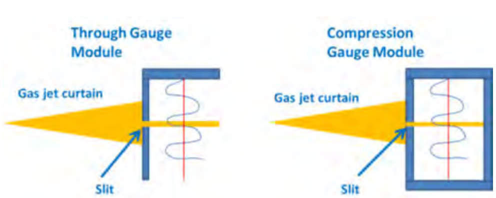

(a) (b)

Figure 6: (a) Through gauge module; (b) Compression gauge module.

CONCLUSION

In this paper, we discussed the working principle, beam experiment and recent development of a novel supersonic gas-jet beam profile monitor. We report new components which have been implemented in the system and detail experiments will be carried out.

Future plans include jet distribution measurement. These results will help to understand and maximize the resolution of this monitor and benchmark gas dynamics simulations. The benefit of the latter one is to optimise the design of nozzles, skimmers, as well as the whole vacuum system to implement this monitor into various types of particle beam and working environments.

ACKNOWLEDGMENT

This work is supported by the Helmholtz Association under contract VH-NG-328, the European Union's Seventh Framework Programme for research, technological development and demonstration under grant agreement no 215080 and the STFC Cockcroft core grant No. ST/G008248/1.

REFERENCES

[1] C.P. Welsch, M. Grieser, J. Ullrich, A. Wolf, 'An ultra-low-energy storage ring at FLAIR', NIM A 546 (2005) 405–417.

[2] V. Tzoganis, C. P. Welsch, 'A non-invasive beam profile monitor for charged particle beams', Applied Physics Letters 104, 204104 (2014).

[3] Y. Hashimoto, T. Fujisaw, T Morimoto, Y Fujita, T Honma, S Muto, K Noda, Y Sato, S Yamada, 'Oxygen gas-sheet beam profile monitor for the synchrotron and storage ring', NIM A 527 (2004) 289-300.

[4] Y. Hashimoto, Y. Hori, T. Toyama, T. Fujisawa, T. Murakami, K. Noda, D. Ohsawa, 'Development of a Beam Profile Monitor using a Nitrogen-Molecular Jet for the J-PARC MR. IBIC 2013, 2013, p. 848–51.

[5] J. Ullrich, R. Moshammer, A. Dorn, R. Dörner, L. Schmidt, H. Schmidt-Böcking, 'Recoil-ion and electron momentum spectroscopy: reaction-microscopes', Rep. Prog. Phys. 66 (2003) 1463.

[6] M. Putignano, K. Kühnel, C. Schröter, C. Welsch, 'A fast, low perturbation ionization beam profile monitor based on a gas-jet curtain for the ultra low energy storage ring', Hyperfine Interact 194 (2009) 189–93.

[7] V. Tzoganis, A. Jeff, C. P. Welsch, 'Gas dynamics considerations in a non-invasive profile monitor for charged particle beams', VACUUM, (2014) 1-8.

DEVELOPMENT OF A SUPERSONIC GAS-JET MONITOR TO MEASURE BEAM PROFILE NON-DESTRUCTIVELY

H. Zhang[1,#], V. Tzoganis[1,2], A. Jeff[1,3], C. Welsch[1]
[1]Cockcroft Institute and university of Liverpool, Warrington, WA44AD UK
[2]RIKEN Nishina center, Japan
[3]CERN

Abstract

The measurement of the transverse beam profile is a great challenge for high intensity, high brightness and high power particle beams due to their destructive effects and thus non-destructive methods are desirable. Current non-destructive methods such as residual gas monitors and beam induced fluorescence monitors either requires a longer integration time or higher surrounding pressure to make a meaningful measurement. As a potentially improved technique, a supersonic gas-jet beam profile monitor has been developed by the QUASAR Group at the Cockcroft Institute, UK. In this monitor, a 45 degree supersonic gas curtain is generated and interacts with beam when the beam crosses it. Ions generated by this process are then accelerated by an extraction electric field and finally collected by a Micro Channel Plate (MCP). Beam images are obtained via a phosphor screen and a CCD camera. In this contribution, we brief the working principles and present better beam profile measurement of a low energy electron beam using this monitor with newly installed pulsed valve.

Gas Jet Project

Motivation for transverse beam profiling

- Short life beams require a minimum interruption from beam diagnostics for living a longer life time.
- High energy, high luminosity and high power beams requires non-destructive diagnostic due to their destructive property .
- Fast time measurement usually require a single short measurement with short integration time.
- Two dimension measurement at the same time

Supersonic Gas-Jet Setup

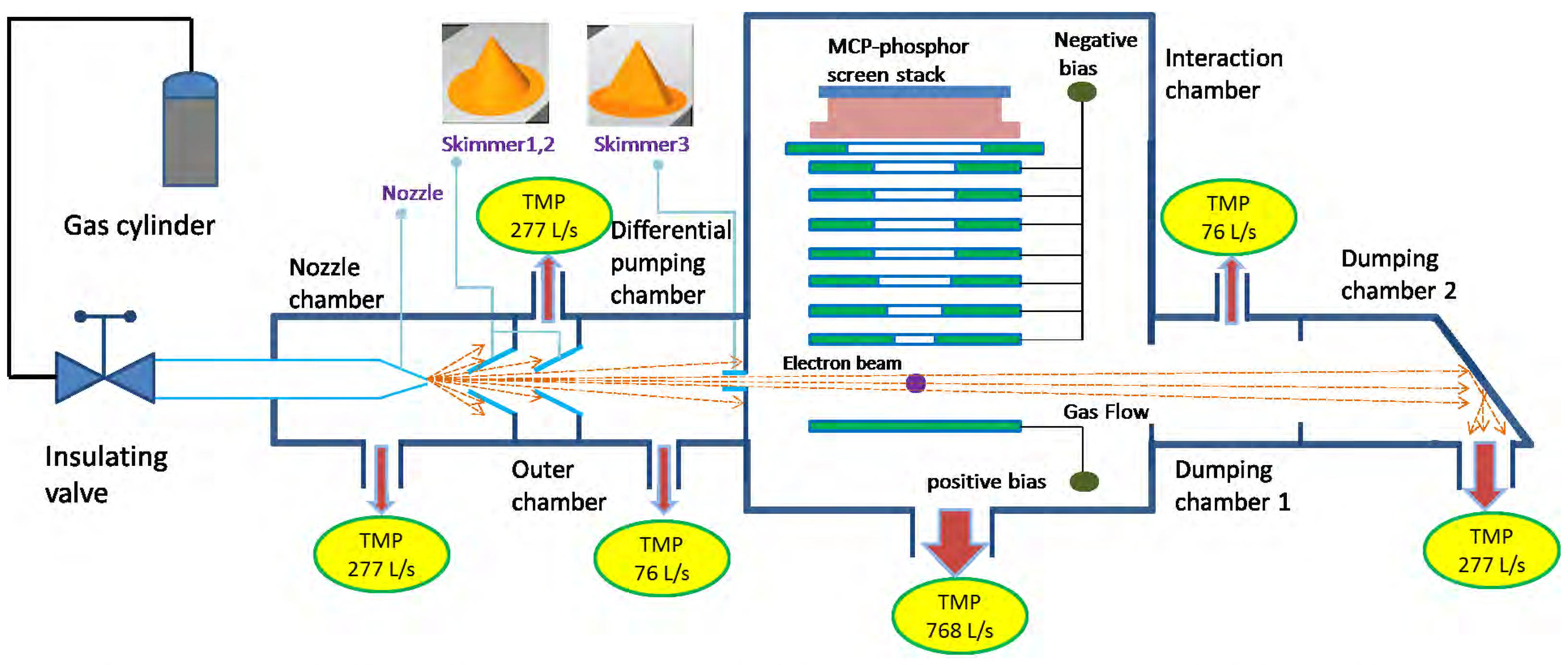

Nozzle: 30 um, round orifice ; Skimmer 1: 180 um, conical shape; Skimmer 2: 400 um, conical shape; Skimmer 3: 4*0.4 mm^2, pyramidal shape

Supersonic gas jet are formed when gas is free expanding from high pressure region to low pressure region through a nozzle. Additional collimation are performed by two conical skimmer. The third skimmer is to collimate the gas jet to a gas screen with an angle of 45 degrees.

Particle beam interacts with gas jet screen and causes gas molecules ionized. We accelerate the ions by extraction electrical field about 12 kV/m. The ions are finally collected by an MCP and phosphor screen stack and the image on the phosphor screen represent the transverse beam distribution. See below an beam image from this monitor with pulsed gas jet.

Beam profile measurement

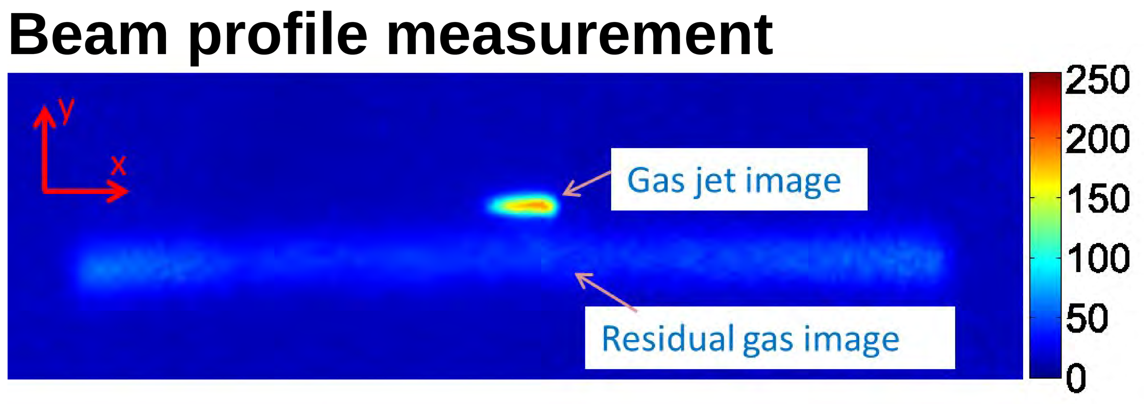

Electron beam:
Energy: 3.75 keV
Current: 0.2 μA
Gas jet setting:
Inlet pressure: 5 bar

Interaction chamber pressure: 6.2*10^{-9} mbar to 1.2*10^{-8} mbar

Conclusion

- Supersonic gas jet beam profile monitor could be potential candidate for any accelerator to monitor transverse beam profile.
- Recently installed pulse valve improve signal ratio.
- New installation of moveable ion gauge allows us investigate the gas dynamics about this jet.

Future plan

- Gas dynamic simulations and detail experiments about the gas jet distribution are scheduled for optimize the nozzle, skimmers designs, as well as the whole vacuum system.
- Simulate and optimize the ion collecting system.

Recent development

Pulse Valve

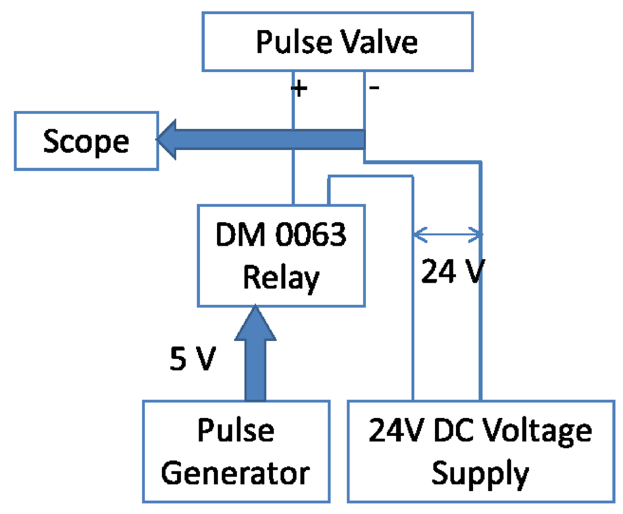

Pulse valve is used for minimizing the gas flow into the chamber. The recover time about 0.5 s and maximum gas inlet pressure about 8 bar are determined by measuring the pressure response in the differential chamber and dump chamber from different pulse valve setting such as period, duty cycle and inlet gas pressure.

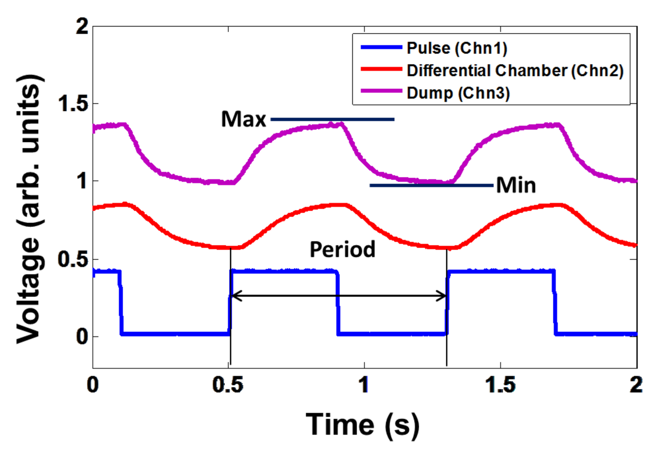

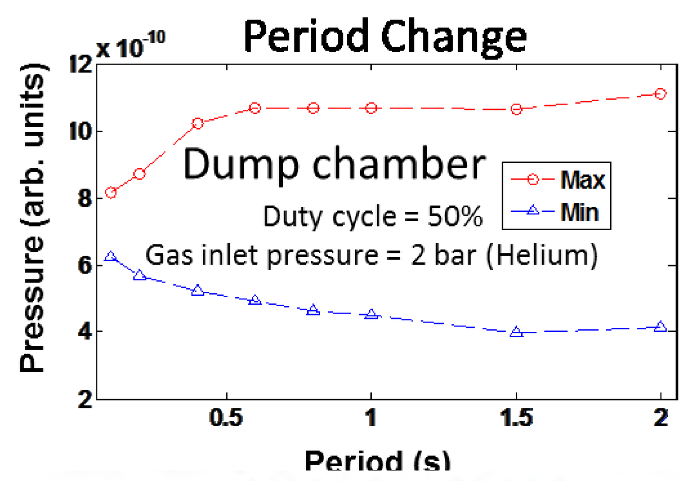

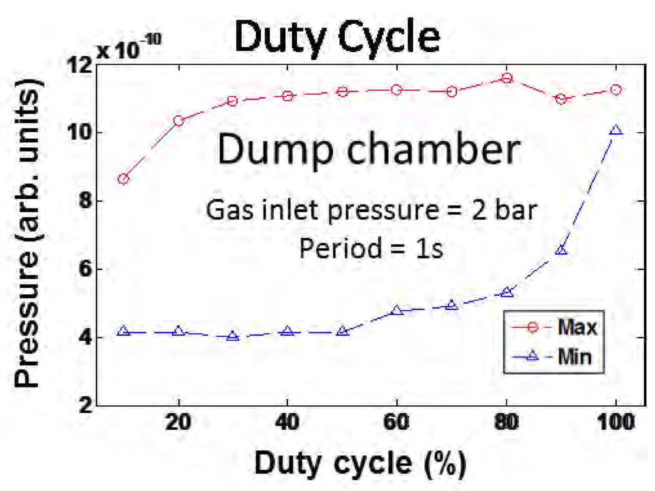

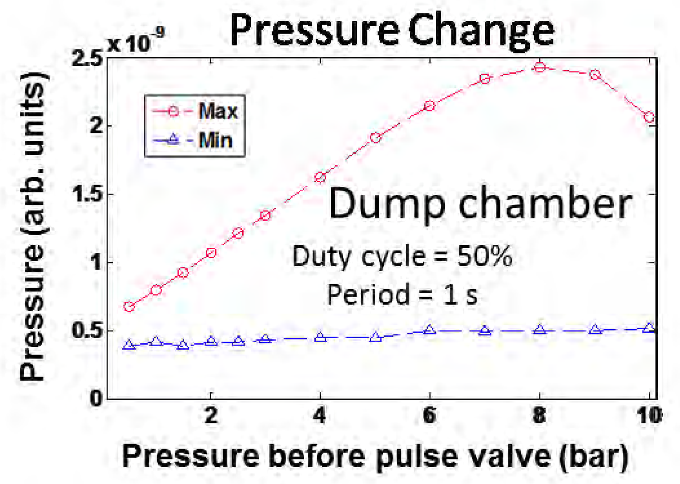

Moveable Ion Gauge

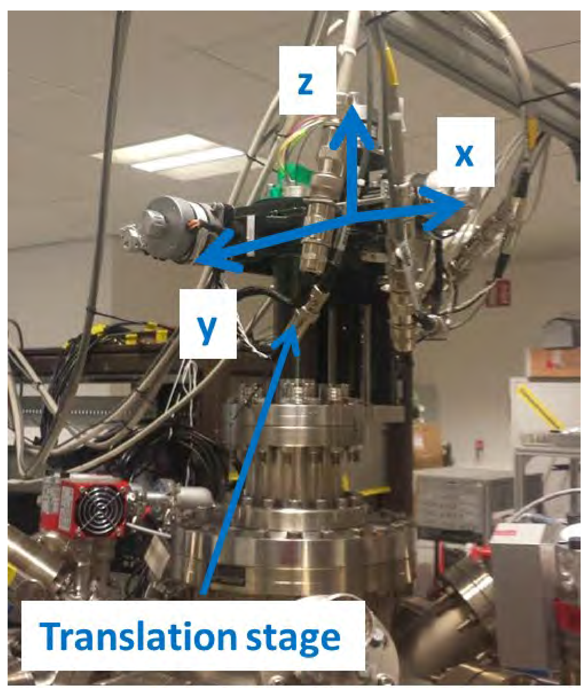

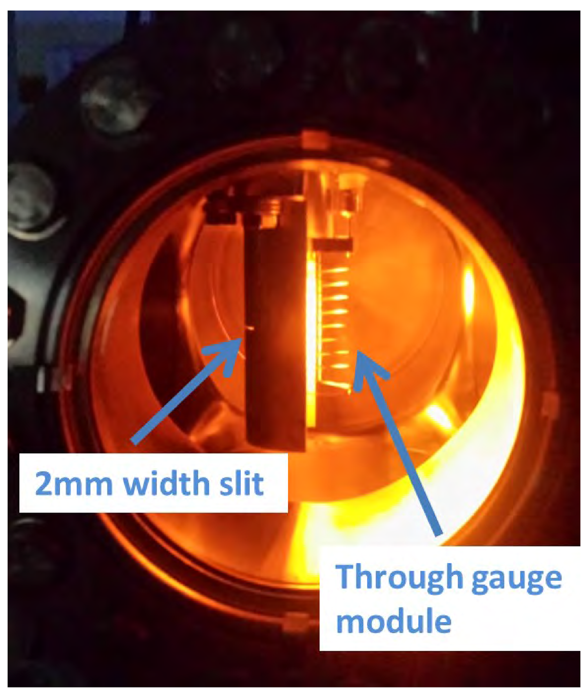

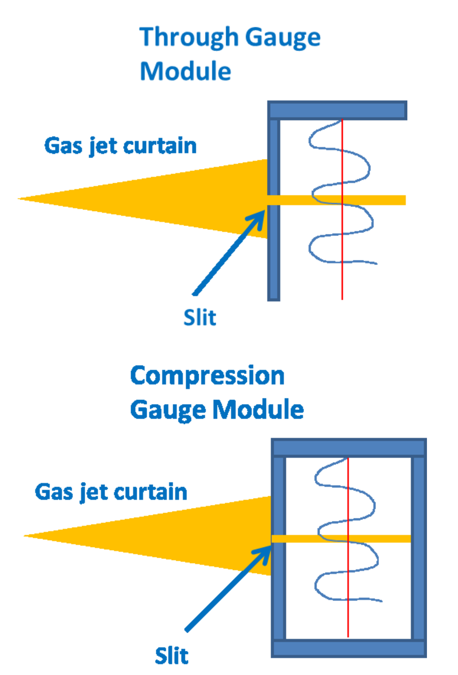

The resolution of this method is directed related with the gas jet distribution. We currently installed a moveable ion gauge component to measure the distribution. This component include a Bayard-Alpert type ion gauge attached with a external 3D translation stage. Two types of gauge modules including through gauge and compression gauge are under testing.

Work supported by the Helmholtz Association under contract VH-NG-328, the European Union's Seventh Framework Programme for research, technological development and demonstration under grant agreement no 215080 and the STFC Cockcroft core grant No. ST/G008248/1.

http://www.cockcroft.ac.uk
http://www.quasar-group.org
#hao.zhang@cockcroft.ac.uk

MODELING OF AN ELECTRON INJECTOR FOR THE AWAKE PROJECT

O. Mete*, G. Xia, †The University of Manchester, Manchester, UK
R. Apsimon, G. Burt, †Lancaster University, Lancaster, UK
S. Doebert, CERN, Geneva, Switzerland
R. Fiorito, C. Welsch, †The University of Liverpool, Liverpool, UK

Abstract

Particle-in-cell simulations were performed by using PARMELA to characterise an electron injector with a booster linac for the AWAKE project in order to provide the baseline specifications required by the plasma wakefield experiments. Tolerances and errors were investigated. A 3 GHz travelling wave structure designed by using CST code. Particles were tracked by using the field maps acquired from these electromagnetic simulations. These results are presented in comparison with the generic accelerating structure model within PARMELA.

INTRODUCTION

The AWAKE project is a proton driven plasma wakefield acceleration experiment by utilising the driver proton beam from CERN's SPS injector and a custom photo injector for the witness (trailing) electron beam [1, 2].

Figure 1 shows the layout of the injector consisting of an S-band standing wave RF gun (SW), previously used in CERN's PHIN photo injector [3], followed by laser optics to direct the laser onto the cathode. Beamline continues with beam current and position monitors and a pepper pot emittance measurement system suitable for a beam subject to space charge effects. A new S-band booster section (accelerating travelling wave structure, ATS) was designed by using CST suite [4] and introduced in the model to boost the beam energy to a region adjustable between 16 – 20 MeV. ATS is followed by a quadrupole triplet and a downstream screen to perform quadrupole scans for emittance measurement.

The tracking studies have been performed by using PARMELA [5]. For ATS the model provided by PARMELA and field maps extracted from CST were used and compared. Implementation of CST maps into PARMELA are discussed in the following sections.

BOOSTER LINAC

An S-band booster linac, ATS, was designed as a travelling wave structure with constant gradient of 15 MV/m through the entire structure (Fig.2) . It consists of 30 cells with 120° phase advance and varying radii matched to 1 μm precision. ATS was optimised for low reflection coefficient of about 2.5%. The multipole terms [7] due to transverse RF-kicks are 9.4241×10^{-7} mT, 7.8418×10^{-5} mT/m and 4.9×10^{-3} mT/m^2, respectively, from dipole to sextuple terms.

USING CST FIELD MAPS IN PARMELA

In order to use CST field maps in PARMELA tracking simulations, a MATLAB [6] script was prepared to format the standard CST field maps into the form required by PARMELA . The information that PARMELA requires on each line of a field map can be found in Table IV-2 from the program manual [5].

In PARMELA, two field maps must be provided for a travelling wave structure; one produced with Neumann boundary condition (cosine map) and the other with Dirichlet boundary condition (sine map). These fields which are shifted in phase by 90° are fed into PARMELA by using the TRWCFIELD command. A single TRWAVE line is used to represent the entire ATS including the bore tubes with lengths equal to a cell length at each end of ATS to account for the fringe fields.

BASELINE DESIGN

In order to maintain the balance between the emittance growth and the energy spread within ATS, a 10° off-crest phase was chosen for the baseline design by using the CST maps of the current design while the SW is optimised for the highest energy. In addition, the same beam dynamics conditions can be met with on-crest RF phase in the case of the PARMELA model for a travelling wave structure.

The space charge component of the emittance is compensated using the field produced by two solenoids located around the SW. Slightly different working points to satisfy the constant envelope condition were determined for the field distributions from PARMELA and CST models.

The beam dynamics specifications are presented in Table 1 in comparison with these two.

Table 1: Required specification and values produced with different models.

Parameter	Required	PARMELA Map	CST Map
E (MeV)	16	16	16
ΔE/E (%)	0.5	1.3	1.1
$\epsilon_{x,y}$ (mm mrad)	2	1.7,1.8	2.3, 2.5
$\beta_{x,y}$ (m)	5	4, 4	0.8, 0.8
$\alpha_{x,y}$	0	-0.2,-0.2	-1.4, -1.2

* oznur.mete@manchester.ac.uk
† and The Cockcroft Institute, Sci-Tech Daresbury, Warrington, UK

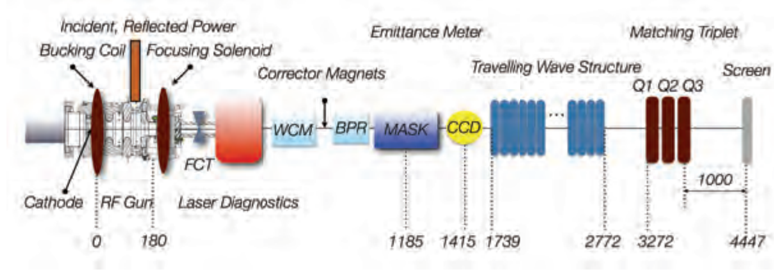

Figure 1: The layout of the photo injector and the booster linac section to provide a witness beam for the AWAKE plasma wakefield acceleration experiment.

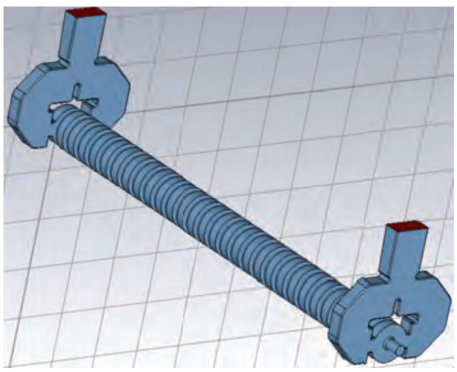

Figure 2: A snapshot from CST design of the S-band travelling wave structure as the energy booster linac for the electron injector.

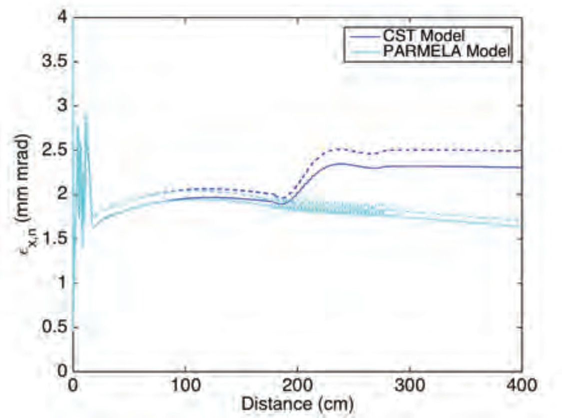

(a)

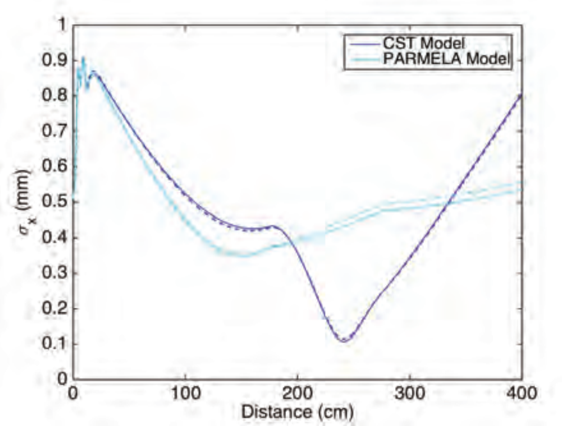

(b)

Figure 3: a) Transverse normalised emittance and b) the beam size as a function of the distance from the cathode. (Solid and dashed lines are x and y axes, respectively.)

RF PHASE ERRORS

Variations in the beam dynamics due to the RF phase errors induced on SW and ATS were investigated. As they are planned to be fed by the same klystron, the same phase error can be assigned to both structures. A typical phase error of 300 fs (1σ) was induced over a 500 samples assuming the RF jitter as the error source. Resulting variations were presented in Table 2. Especially time of flight errors are crucial to determine as they affect the synchronisation in the entrance of the plasma cell.

Table 2: Implications of the phase errors on various beam dynamics observable.

Parameter	1σ Error	Error/Degree of the phase jitter
E (keV)	1.4	5
ΔE/E (ppm)	28	93
$\epsilon_{x,n}$ (nm-rad)	2	7
Time of flight (fs)	57	190

EMITTANCE DIAGNOSTICS UNDER SPACE CHARGE

For a photo injector, the dominant limitation for the emittance diagnostics is the effect of space charge. Figure 5 shows the ratio of two defocusing terms from the envelope equation; the space charge and the outward pressure due to beam emittance. Different curves correspond to different bunch charges and lengths which are considered within the operational range of the injector. Although some cases are less space charge dominated (> 1) than others, in all cases considered, space charge is the dominating component of the total beam emittance. In the pre-booster region, a pepper-pot measurement system will be implemented as a standard technique to measure the emittance of space charge dominated beams. It is currently being designed at the Cockcroft Institute. For the post-booster region quadrupole scan technique is planned. The feasibility and reliability of this technique was assessed by simulations. Figure 6 compares the emittance values calculated from a simulated quadrupole scan and the rms emittance value at the same location. The

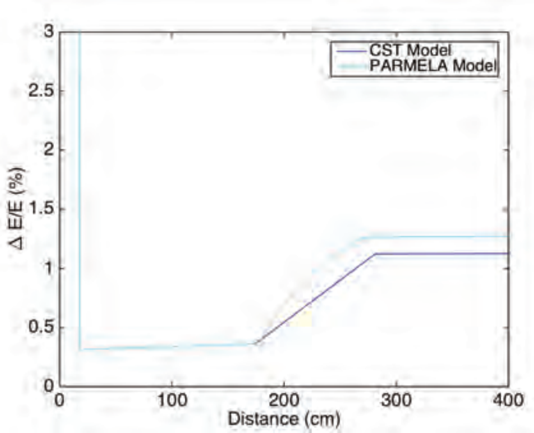

Figure 4: Evolution of the beam energy spread as a function of the distance from the cathode.

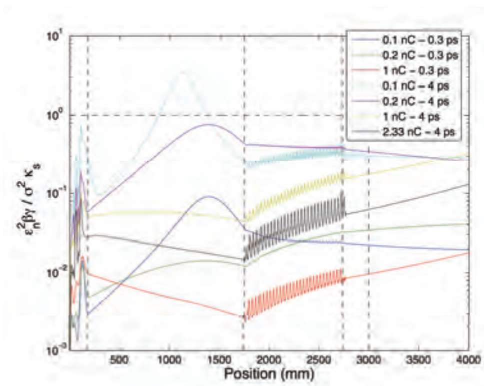

Figure 5: The ratio of space charge and emittance term of the beam envelope as a function of the distance from the cathode.

results differ 2% implying that emittance can be reliably measured within measurement error by using quadrupole scan in the post-booster region.

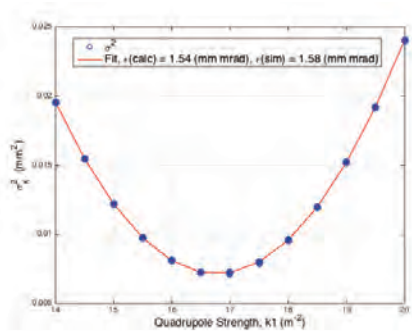

Figure 6: A simulated quadrupole scan result in the post-booster region.

We have also evaluated the Optical Diffraction Radiation Dielectric Foil Radiation Interference (ODR-DFRI) to measure the rms emittance. This technique which is a modified version of the Optical Transition Radiation Interference (OTRI) [8] technique extends the latter to lower beam energies and has the advantage of single shot operation. The

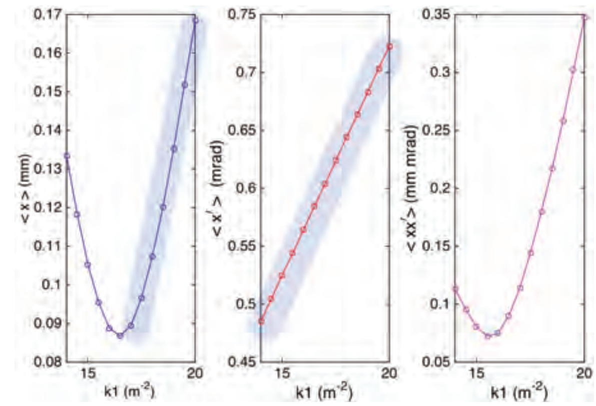

Figure 7: Beam size, divergence and the correlation terms for the range of working points of the injector.

technique can be used in conjunction with a new algorithm developed to use sparse data from a quad scan to measure the rms emittance of space charge dominated beams [9]. Thus, the lower limit of measurable divergence values is 0.3 mrad for the injector. Figure 7 shows the beam size, divergence and the correlations terms for a range of working points for the injector. As seen in the figure, the divergence values range from 0.5 and upwards implying that the ODR-DFRI technique could have been implemented for this system as a complementary technique to the conventional quadrupole scan in case of more severe space charge limitations.

CONCLUSIONS AND OUTLOOK

The tracking simulations for the injector were performed by using the field models from both PARMELA and CST. Slight discrepancies in the results are under investigation. Errors due to phase jitter were studied. Emittance diagnostics under space charge effect is studied for both low and higher energies.

ACKNOWLEDGEMENTS

This work was supported by the Cockcroft Institute Core Grant and STFC. Authors would like to express their gratitude to Janet Susan Smith and Stefano Mazzoni for useful communications on feasibility of beam diagnostics equipment during the course of this study.

REFERENCES

[1] A. Caldwell et al., CERN-SPSC-2013-013 (2013).

[2] O. Mete et al., Proc. of IPAC2014, MOPRI50 (2014).

[3] R. Roux, et al., CARE Note-2004-034-PHIN (2004).

[4] www.cst.com

[5] L. M. Young, LA-UR-96-1835 (2005).

[6] www.mathworks.co.uk

[7] R. G. Olave et al., Proc. of IPAC2013, WEPAC43 (2013).

[8] R. Fiorito et al., PRSTAB 9, 052802 (2006).

[9] K.Poorrezaie, et al., PRSTAB, 16, 082801 (2013).

Modeling of an Electron Injector for the AWAKE Project

Oznur Mete[1§], Guoxing Xia[1§], Robert Apsimon[2§], Graeme Burt[2§], Steffen Doebert[†], Ralph Fiorito[3§], Carsten Welsch[3§]

The University of Manchester[1], The University of Lancaster[2], The University of Liverpool[3]
The European Organization for Nuclear Research, CERN[†]
The Cockcroft Institute for Accelerator Science and Technology[§]

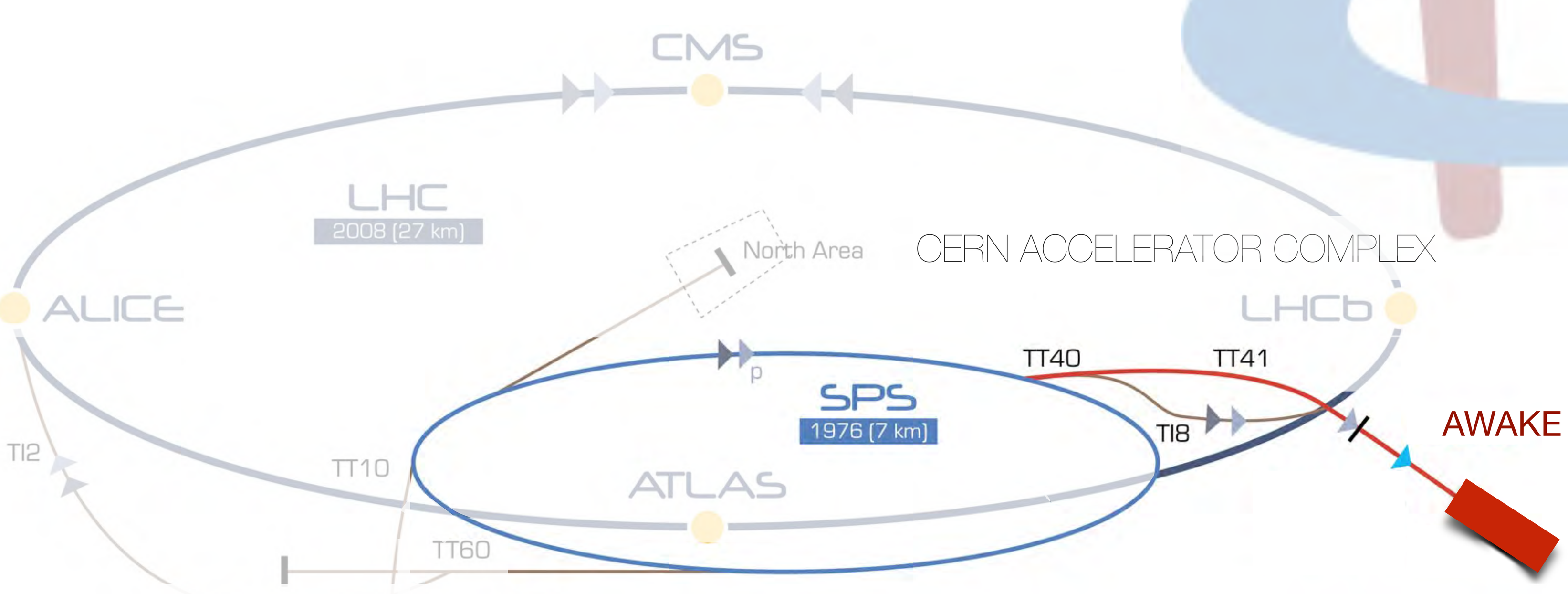

ABSTRACT Particle-in-cell simulations were performed by using PARMELA to characterise an electron injector with a booster linac for the AWAKE project in order to provide the baseline specifications required by the plasma wakefield experiments. Tolerances and errors were investigated. A 3 GHz travelling wave structure designed by using CST code. Particles were tracked by using the field maps acquired from these electromagnetic simulations. These results are presented in comparison with the generic accelerating structure model within PARMELA.

INTRODUCTION The AWAKE project is a proton driven plasma wakefield acceleration experiment by utilising the driver proton beam from CERN's SPS injector and a custom photo injector for the witness (trailing) electron beam [1, 2]. The layout of the injector consists of an S-band standing wave RF gun (SW), previously used in CERN's PHIN photo injector [3], followed by laser optics to direct the laser onto the cathode. Beamline continues with beam current and position monitors and a pepper pot emittance measurement system suitable for a beam subject to space charge effects. A new S-band booster section (accelerating travelling wave structure, ATS) was designed by using CST suite [4] and introduced in the model to boost the beam energy to a region adjustable between 16 – 20 MeV. ATS is followed by a quadrupole triplet and a downstream screen to perform quadrupole scans for emittance measurement. The tracking studies have been performed by using PARMELA [5]. For ATS the model provided by PARMELA and field maps extracted from CST were used and compared..

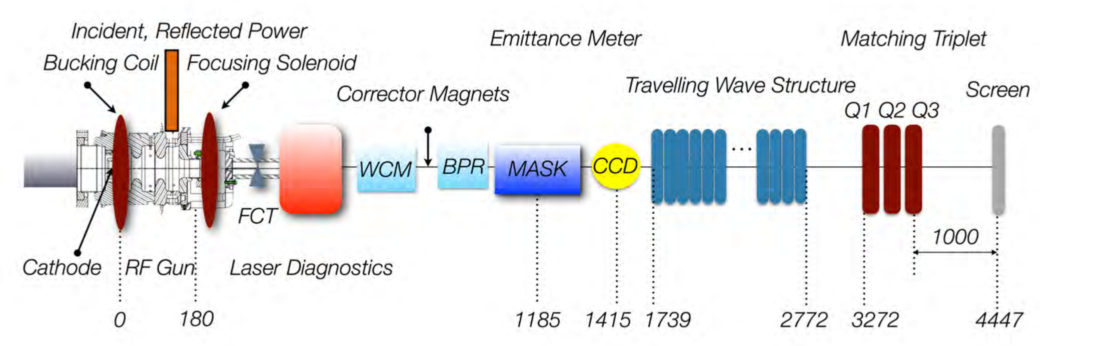

AWAKE Photoinjector and booster linac.

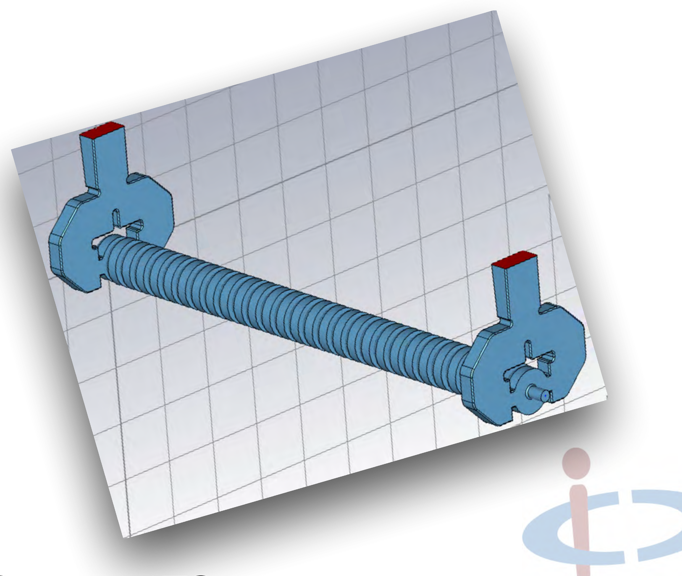

S-band ATS
Accelerating Travelling Wave Structure
15 MV/m, 2π

Emittance Diagnostics and Space Charge Limits

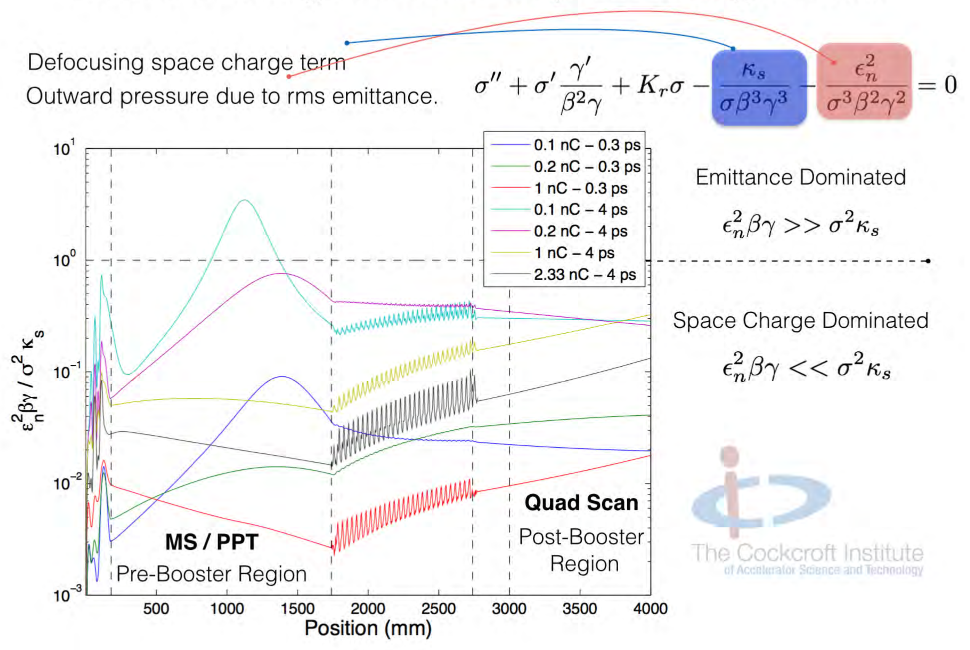

In order to maintain the balance between the emittance growth and the energy spread within ATS, a 10° off-crest phase was chosen for the baseline design by using the CST maps of the current design while the SW is optimised for the highest energy. In addition, the same beam dynamics conditions can be met with on-crest RF phase in the case of the PARMELA model for a travelling wave structure. The space charge component of the emittance is compensated using the field produced by two solenoids located around the SW. Slightly different working points to satisfy the constant envelope condition were determined for the field distributions from PARMELA and CST models.

In PARMELA, two field maps must be provided for a travelling wave structure; one produced with Neumann boundary condition (cosine map) and the other with Dirichlet boundary condition (sine map). These fields which are shifted in phase by 90° are fed into PARMELA by using the TRWCFIELD command. A single TRWAVE line is used to represent the entire ATS including the bore tubes with lengths equal to a cell length at each end of ATS to account for the fringe fields.

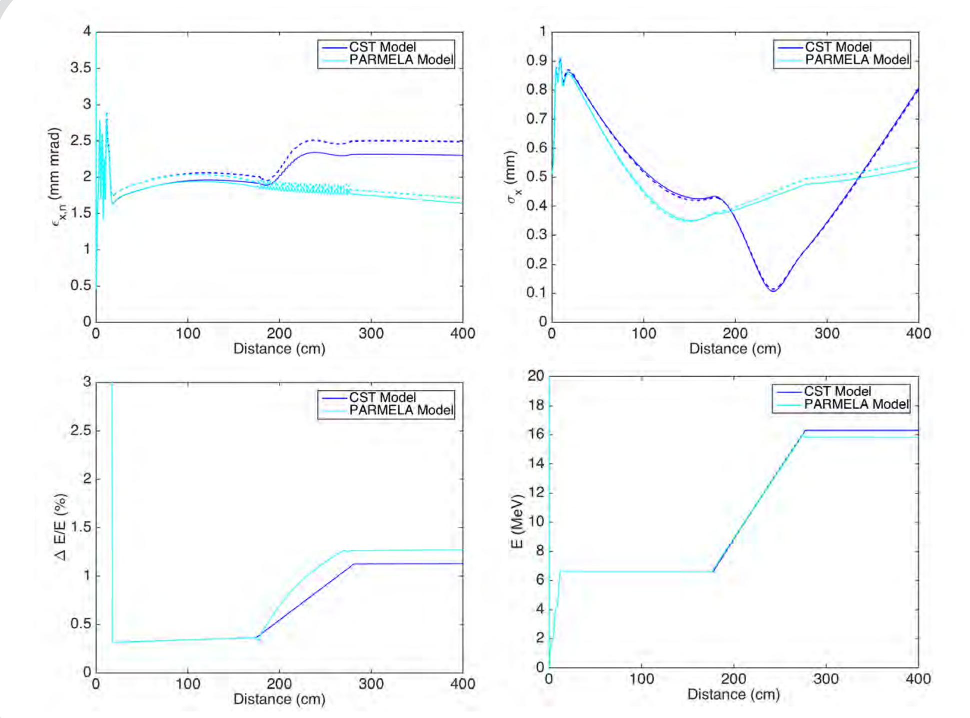

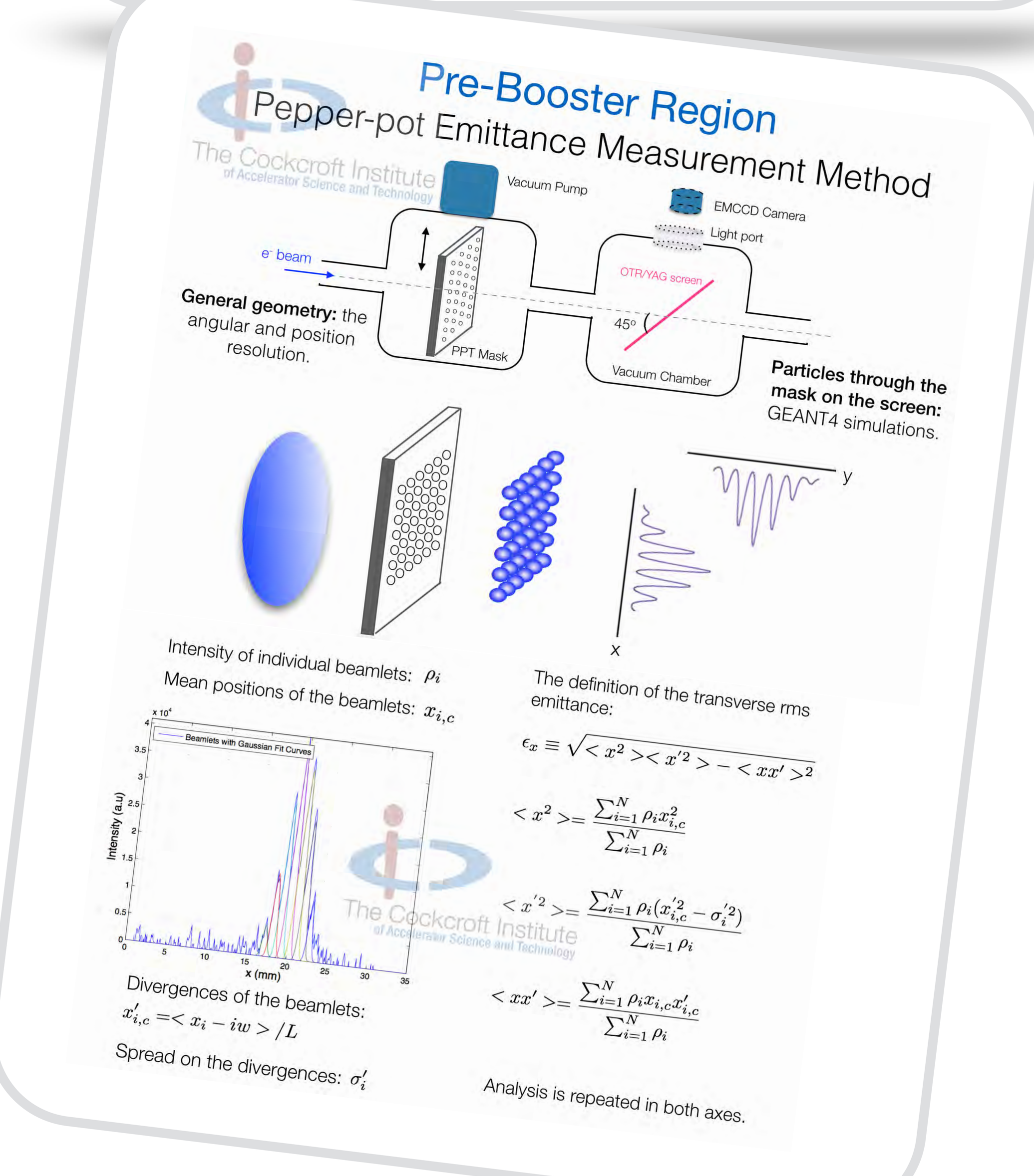

Post-Booster Region
Quad Scan

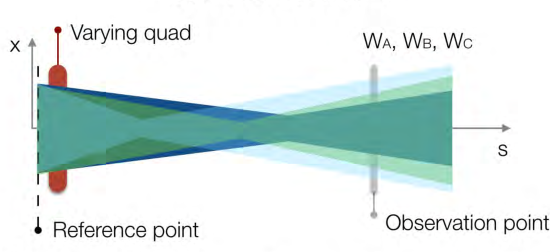

$$\sigma_{k,11} = (l^2 l_q^2 \sigma_{11})k^2 + (2ll_q\sigma_{11} + 2l^2 l_q \sigma_{12})k + (\sigma_{11} + 2l\sigma_{12} + l^2\sigma_{22})$$

A B C

- Fit the square of the beam size to a second degree polynomial curve and get the parameters A, B and C.

$$\epsilon^2 = \sigma_{22}\sigma_{11} - \sigma_{12}^2$$

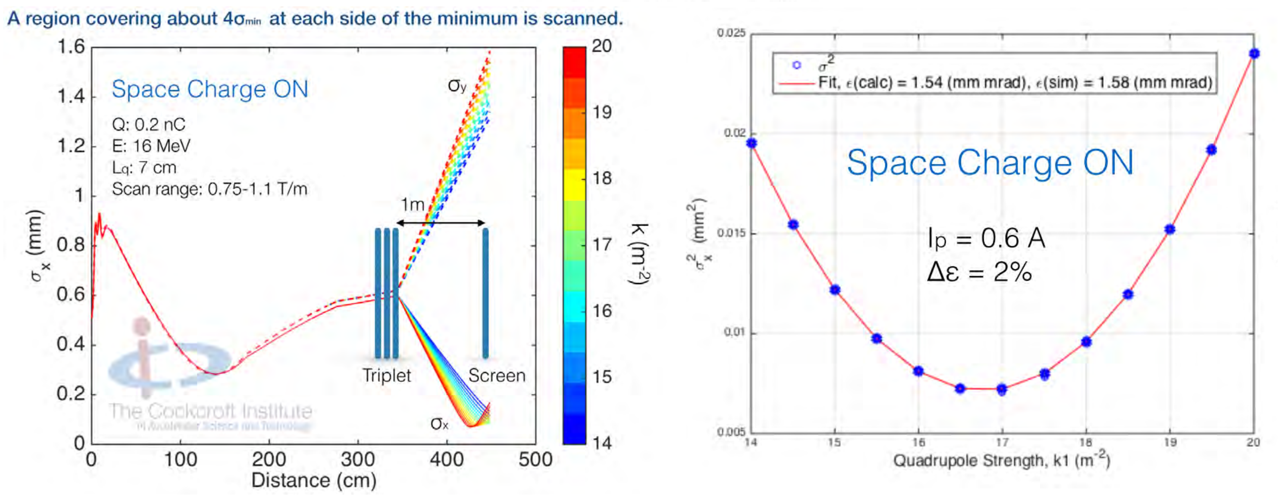

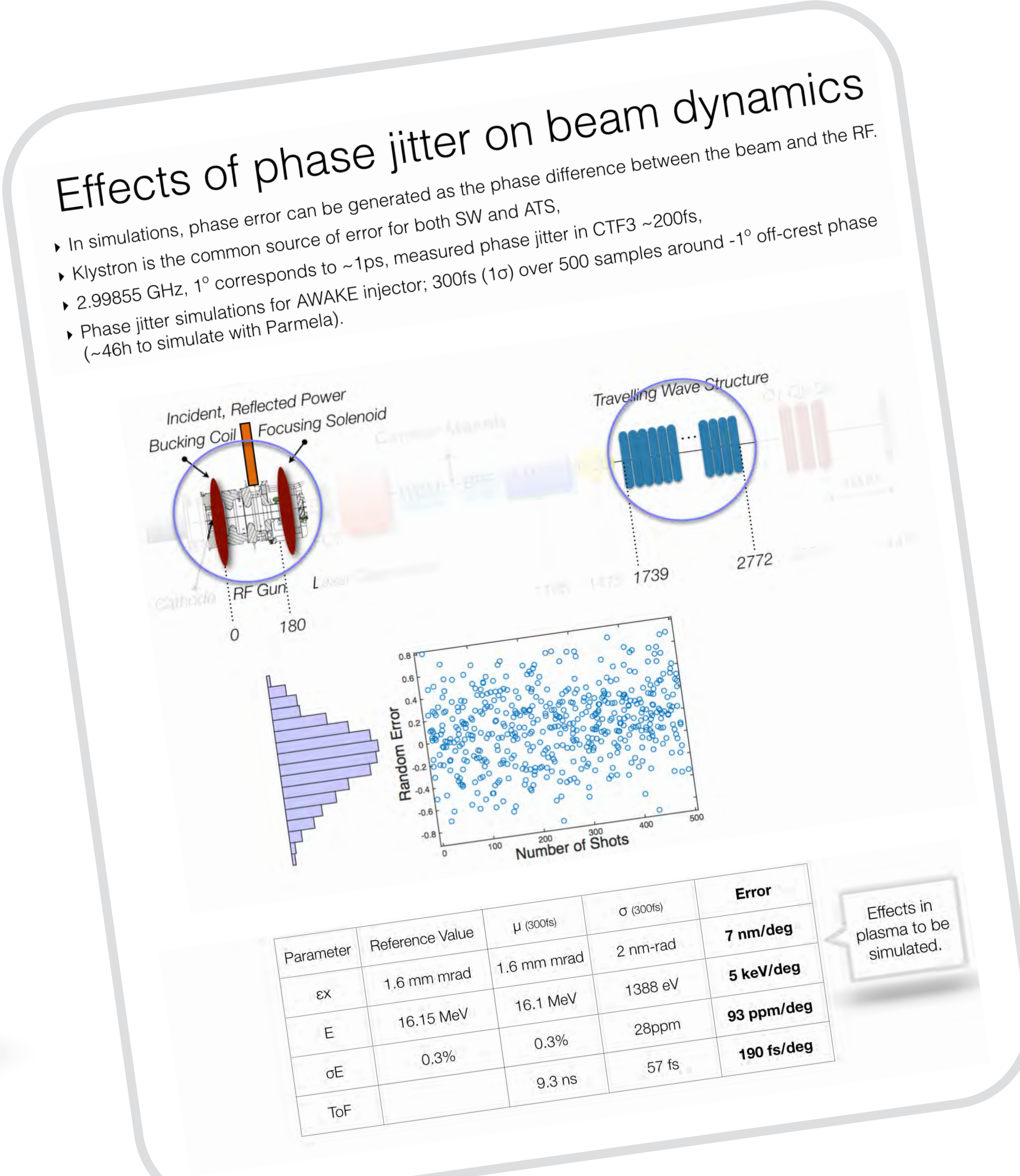

Alternative/Complementary Methods to Quad Scan

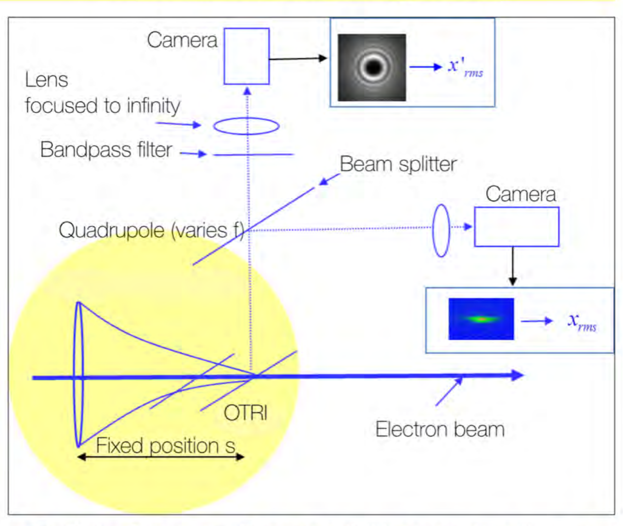

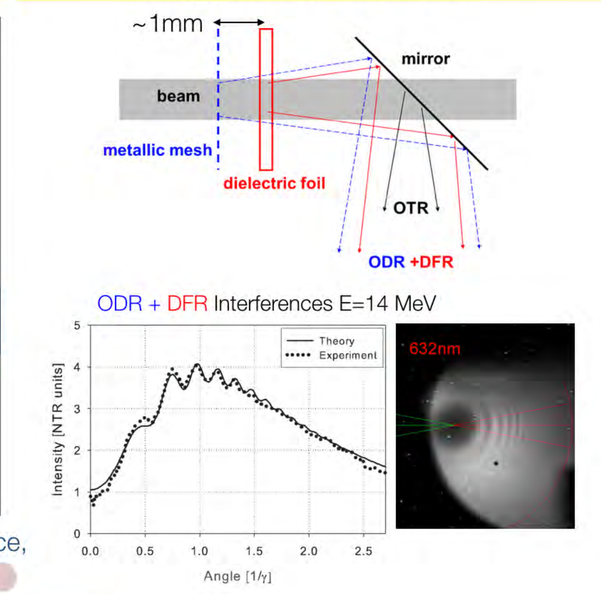

- Both techniques: Fringe visibility provides divergence,
- OTRI: foils well separated for high E,
- ODR-DFRI: foils close together - low E.

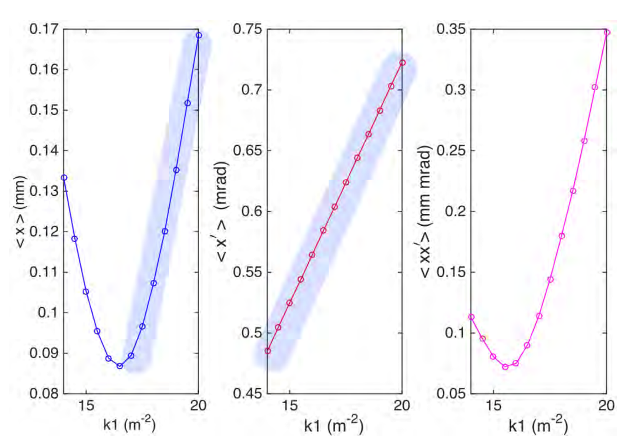

The Optical Diffraction Radiation Dielectric Foil Radiation Interference (ODR-DFRI) technique which is a modified version of the Optical Transition Radiation Interference (OTRI) [8] technique adapts the latter to lower beam energies and has the advantage of single shot operation to measure the rms emittance. The technique can be used in conjunction with a new algorithm developed to use sparse data from a quad scan to measure the rms emittance of space charge dominated beams [9]. Thus, the lower limit of measurable divergence values is 0.3 mrad for the injector. As seen in the figure, the divergence values range from 0.5 and upwards implying that the ODR-DFRI technique could have been implemented for this system as a complementary technique to the conventional quadrupole scan in case of more severe space charge limitations.

REFERENCES
[1] [1] A.Caldwell et al., CERN-SPSC-2013-013 (2013).
[2] O.Mete et al., Proc. of IPAC2014, MOPRI50 (2014).
[3] R.Roux, et al., CARENote-2004-034-PHIN (2004).
[4] www.cst.com
[5] L.M. Young, LA-UR-96-1835 (2005).
[6] www.mathworks.co.uk
[7] R.G.Olave et al., Proc.of IPAC2013, WEPAC43(2013).
[8] R.Fiorito et al., PRSTAB 9, 052802 (2006).
[9] K.Poorrezaie, et al., PRSTAB, 16, 082801 (2013).

ACKNOWLEDGMENTS
This work was supported by the Cockcroft Institute Core Grant and STFC. Authors would like to express their gratitude to Janet Susan Smith and Stefano Mazzoni for useful communications on feasibility of beam diagnostics equipment during the course of this study.

INTRA-BEAM SCATTERING EFFECTS IN ELENA*

J. Resta-López, J. R. Hunt, C. P. Welsch,
Cockcroft Institute and The University of Liverpool, UK

Abstract

Intra-Beam Scattering (IBS) is one of the main limiting processes for the performance of low energy ion storage rings, such as the Extra Low ENergy Antiproton ring (ELENA) that is being constructed at CERN. IBS effects limit the achievable equilibrium 6D beam phase space volume during the cooling process, as well as the stored beam intensity. In this contribution we analyse the IBS effects on the beam dynamics of the ELENA ring in detail. Numerical simulations using the codes BETACOOL and MAD-X have been performed to compute the beam life time and the equilibrium phase space parameters with electron cooling in the presence of IBS.

INTRODUCTION

ELENA [1] is a small synchrotron equipped with an electron cooler, which is currently being constructed at CERN to further decelerate antiprotons from the Antiproton Decelerator (AD) [2] from 5.3 MeV to 100 keV kinetic energy with a beam population of $\sim 10^7$ cooled antiprotons. Electron cooling will be used to counteract the emittance and the momentum spread blow-up caused by the deceleration process. This will increase the intensity of antiprotons delivered to the antihydrogen experiments at the AD by one to two orders of magnitude.

The ELENA cycle is schematically shown in Fig. 1. There are two cooling plateaus: the first cooling plateau lasts approximately 8 s at 35 MeV/c momentum, and the second one is applied for 2 s at 13.7 MeV/c. In both cases the cooling is applied to a coasting beam. A third cooling at 13.7 MeV/c will be applied to bunched beams prior to extraction.

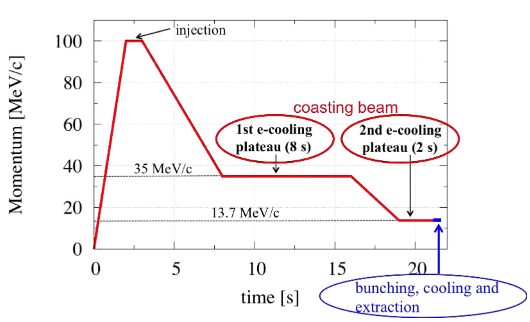

Figure 1: ELENA cycle.

A particular challenge for low energy ion storage rings, such as ELENA, is the question of achievable beam life time and stability. To address this question, we are investigating the long-term beam dynamics in ELENA considering different effects limiting the achievable phase space volume obtained under electron cooling. Among these effects, IBS and rest gas scattering are important sources of beam heating.

For ELENA with the nominal vacuum pressure $P = 3 \times 10^{-12}$ Torr, it has been estimated that the effect of rest gas scattering would be practically negligible with respect to IBS [3,4]. Therefore, in this paper we focus mainly on the study of the IBS effects.

IBS can be defined as a beam heating effect produced by multiple small-angle Coulomb scatterings of charged particles within the accelerator beam itself. It causes an exchange of energy between the transverse and longitudinal degree of freedom, thus leading to the growth of the beam phase space dimensions. The theory of IBS is extensively described in the literature, e.g. [5–8], and many of these IBS models are implemented in the simulation code BETACOOL [9,10]. This code allows us to calculate the evolution of beam distributions in the transverse and longitudinal phase space under the action of cooling and different scattering effects, and has been successfully benchmarked against experimental data, see e.g. [11].

IBS becomes stronger when the phase space volume of the beam is reduced by cooling, thus limiting the achievable final emittances, which are determined by an equilibrium state between IBS and cooling. In the next sections we investigate the beam evolution for the two ELENA cooling plateaus in the presence of IBS.

BEAM EVOLUTION

Beam dynamics simulations are performed using the code BETACOOL [9, 10], using the nominal beam parameters and electron cooling parameters adopted from [1,12] and the ELENA ring lattice with working point $Q_x \simeq 2.3$, $Q_y \simeq 1.3$ [13] in MAD-X format [14].

The simulations are based on a Monte-Carlo method (model beam algorithm of BETACOOL), with the following conditions: 1000 modelled macroparticles; electron cooling considering a cylindrical uniform electron beam distribution with transverse temperature $k_B T_{e\perp} = 0.01$ eV and longitudinal temperature $k_B T_{e\parallel} = 0.001$ eV; the cooling friction force is computed using the Parkhomchuk's model for a magnetised electron distribution [15]; rest gas and IBS effects are also included. For the IBS, the Martini model [7] is used. More details can be found in [4].

First Cooling Plateau

Let us consider first initial Gaussian distributions with relatively large rms transverse emittances and momentum

* Work supported by the EU under Grant Agreement 624854 and the STFC Cockcroft Institute core Grant No. ST/G008248/1.

spread: $(\epsilon_x, \epsilon_y) = (8,8)\ \pi$ mm·mrad, $\Delta p/p = 0.1\%$. Figure 2 shows the time evolution of these parameters during the first cooling plateau for 10 simulated random seeds.The corresponding beam profile distributions at different times of the cooling process are shown in Fig. 3. The beam distribution quickly deviates from a Gaussian profile and a very dense core appears.

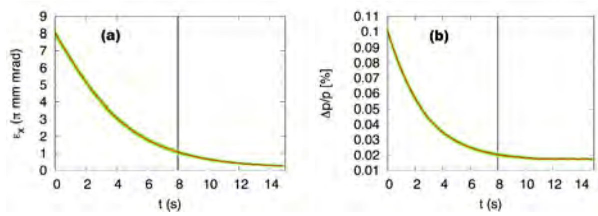

Figure 2: Evolution of the rms horizontal emittance (a) and momentum spread (b) over the first cooling plateau. The rms vertical emittance evolution is similar to (a).

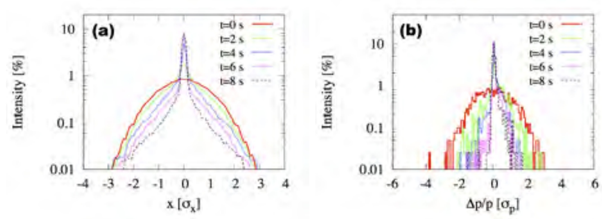

Figure 3: Horizontal (a) and momentum spread (b) distribution for different times during the first cooling.

Core-tail Development: For relatively large beam sizes at the beginning of the cooling, the beam distribution develops a very dense core and highly populated tails. This is due to the strength of the electron-antiproton friction force as a function of the relative velocity. Figure 4 shows the distribution of modelled antiprotons in the $(x, \Delta p/p)$ space at the beginning and at the end of the first cooling plateau. The parabolic momentum spread of the electrons due to space charge is also represented. Because of this space charge effect, antiprotons at large amplitudes experience a weaker friction force than those in the centre.

It is necessary to point out that in the case of cooling with large initial beam sizes, where the distribution quickly deviates from a Gaussian, the use of a standard IBS model, such as the Martini model, is probably underestimating the IBS effect for the core, thus leading to an overcooling of the core, as observed in Fig. 3. In the past, this was already noticed in [16]. Standard models of IBS are based on the growth of the rms beam parameters of Gaussian distributions. However, in the case of a non-Gaussian beam with a very dense core and large tails, it would be more correct to apply IBS induced kicks based on diffusion coefficients which are different for particles inside and outside of the core. Different IBS models for non-Gaussians distributions have been proposed in the literature [16–20], and implemented in the code BETACOOL [21].

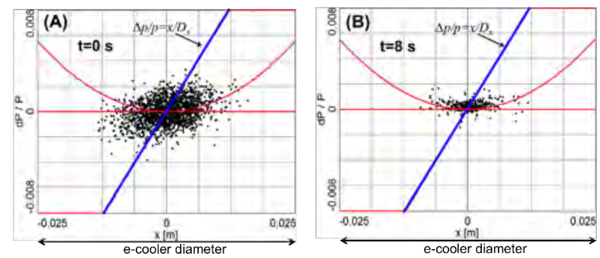

Figure 4: Distribution of an ensemble of 1000 modelled antiprotons in the cooler at $t = 0$ s (A) and at $t = 8$ s (B) for the first cooling plateau. The parabola represents the momentum spread of the electrons due to space charge charge. The straight blue line represents the dispersion line $\Delta p/p = x/D_x$ for the antiproton beam.

Applying an IBS core-tail model [16, 17], we have recalculated the time evolution of the ELENA beam distribution during cooling at 35 MeV/c, and compared it with the previous result where the IBS Martini model was applied (Fig. 5). The cooling of the core is smoother if an IBS core-tail model is applied and, probably, it describes more accurately the actual process.

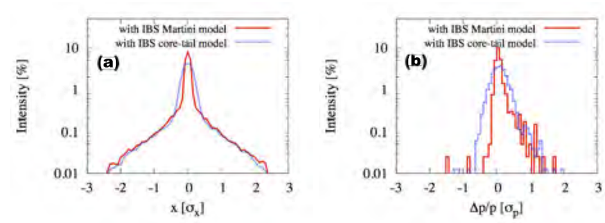

Figure 5: Horizontal (a) and momentum spread (b) distribution at $t = 8$ s for the first cooling plateau ($p = 35$ MeV/c), comparing the results using two different models of IBS: Martini model (solid red line) and a core-tail model (dotted blue line). The vertical distribution presents similar features to (a).

Second Cooling Plateau

For the second cooling plateau of a coasting antiproton beam at 13.7 MeV/c, Fig. 6 depicts the rms emittance and momentum spread as a function of time. For simplicity, in this case, we have adopted an initial Gaussian beam distribution with rms emittances $(\epsilon_x, \epsilon_y) = (2.8, 2.8)\ \pi$ mm·mrad and 0.05% momentum spread. These initial values take into account the adiabatic emittance increase by a factor $(\beta\gamma)_{35\ \mathrm{MeV}/c}/(\beta\gamma)_{13.7\ \mathrm{MeV}/c} \simeq 2.55$ because of the deceleration ramp from 35 MeV/c to 13.7 MeV/c. See Table 1 for a summary of the beam parameter values at the beginning and at the end of each cooling plateau.

Cooling of Bunched Beams

Before ejection, further cooling applied to bunched beams at 13.7 MeV/c momentum (for ~ 0.2–0.3 s) is planned to counteract IBS effects and reduce the phase space volume of

Table 1: Beam Parameters (rms Quantities) and Growth Rate Contributions from IBS $(1/\tau_x, 1/\tau_y, 1/\tau_p)_{\mathrm{IBS}}$ and E-cooling $(1/\tau_x, 1/\tau_y, 1/\tau_p)_{\mathrm{COOL}}$ before and after Cooling. The type of antiproton beam (coasting or bunched) and the cooling time are indicated. These results are the average over 10 modelled random seeds. For the growth rates, the negative sign indicates cooling.

Cycle step	ϵ_x, ϵ_y [π mm·mrad]	$\Delta p/p$ [%]	$(1/\tau_x, 1/\tau_y, 1/\tau_p)_{\mathrm{IBS}}$ [s^{-1}]	$(1/\tau_x, 1/\tau_y, 1/\tau_p)_{\mathrm{COOL}}$ [s^{-1}]
Cooling at 35 MeV/c, coasting beam, 8 s				
Start	8.0, 8.0	0.1	1.7×10^{-4}, -2.5×10^{-5}, 8.3×10^{-4}	-0.2, -0.2, -0.5
End	1.1, 1.1	0.02	0.02, -0.02, 0.7	-1.4, -1.4, -3.1
Cooling at 13.7 MeV/c, coasting beam, 2 s				
Start	2.8, 2.8	0.05	0.03, -0.009, 0.3	-1.1, -1.1, -1.9
End	0.52, 0.33	0.033	1.6, 1.8, 3.0	-2.5, -2.3, -4.5
Cooling at 13.7 MeV/c, bunched beam, 0.3 s				
Start	0.78, 0.49	0.049	2.6, 3.4, 0.7	-2.2, -2.0, -1.9
End	0.9, 0.55	0.043	1.7, 2.2, 1.7	-2.1, -2.0, -1.9

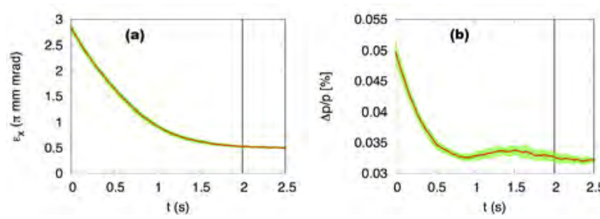

Figure 6: Evolution of the rms horizontal emittance (a) and momentum spread (b) over the second cooling plateau. The rms vertical emittance evolution is practically similar to (a).

bunches required by the experiments. Figure 7 compares the beam evolution between the cases with and without cooling for bunched beams. The cooling will keep transverse emittances $< 1\ \pi$ mm·mrad and momentum spread $< 0.05\%$. In the bunching process we have assumed 50% emittance blow-up. Initial and final values of emittances, momentum spread and growth rates are written in Table 1.

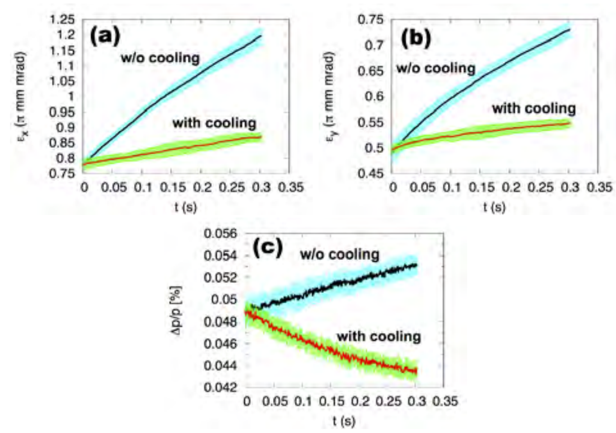

Figure 7: Evolution of the rms horizontal emittance (a), vertical emittance (b) and momentum spread (c) for bunched beams prior to extraction. The cases with and without cooling are compared.

OUTLOOK

IBS is one of the main heating processes limiting the achievable phase space volume during the beam cooling in low energy ion rings. In ELENA, it becomes significantly stronger at the second cooling plateau (p = 13.7 MeV/c) of the cycle and for cooling of bunched antiproton beams.

In this paper, BETACOOL simulations of the e-cooling process in ELENA are presented to describe the features of the beam evolution in the presence of IBS. The convenience of applying an IBS core-tail model is also discussed when large initial beam sizes are assumed at the beginning of the cooling process, as we have assumed here for the case of the cooling at 35 MeV/c.

Table 1 summarises the values of rms emittances and momentum spread as well as the IBS growth rates and cooling rates before and after the electron cooling.

It is also worth mentioning that for simplicity we have assumed initial Gaussian beam profiles. However, in practice, the distribution of the beam injected from the AD could have a dense core with significant non-Gaussian tails [22]. This characteristic will be taken into account in future studies.

ACKNOWLEDGMENTS

We gratefully acknowledge A. V. Smirnov for providing us with the latest version of the code BETACOOL, all our colleagues from the ELENA team at CERN for very fruitful discussions, and in particular C. Carli for useful discussions and comments on many aspects of this work.

REFERENCES

[1] V. Chohan (editor), "Extra Low Energy Antiproton ring (ELENA) and its Transfer Lines, Design Report," CERN-2014-002 (2014).

[2] S. Maury (editor), “Design Study of the Antiproton Decelerator: AD,” CERN/PS 96-43 (AR), 1996.

[3] C. Carli et al., “Review of Rest Gas Interaction at Very Low Energies Applied to the Extra Low Energy Antiproton Ring ELENA,” Proc. of IPAC2014, TUPRI028, Dresden, Germany, 2014.

[4] J. Resta-Lopez at al., “Simulation studies of the beam cooling process in presence of heating effects in the Extra Low ENergy Antiproton ring (ELENA),” to be published in JINST.

[5] A. Piwinski, “Intra-Beam Scattering,” Proc. of the 9th International Conference on High Energy Accelerators, Stanford, CA, 1974, p. 405.

[6] J. Bjorken, S. Mtingwa, “Intrabeam Scattering,” Part. Accel. **13**, 115 (1983).

[7] M. Martini, “Intrabeam Scattering in the ACOL-AA Machines,” CERN-PS-AA-84-9, 1984.

[8] A. Piwinski, “Intra-Beam Scattering,” CERN Report 92-01 (1992), p. 226.

[9] A. Sidorin, Nucl. Instrum. Meth. A **558** (2006) 325.

[10] `http://betacool.jinr.ru`

[11] A. I. Papash et al., Phys. Rev. ST-AB **16** (2013) 060101.

[12] G. Tranquile et al., “The ELENA Electron Cooler: Parameter Choice and Expected Performance,” Proc. of COOL2013, WEPPO16, Murren, CH, 2013.

[13] P. Belochitskii, “ELENA Project Status,” Proc. of COOL2013, THPMIHA02, Murren, CH, 2013.

[14] `http://mad.web.cern.ch/mad/`

[15] V. V. Parkhomchuk, Nucl. Instrum. Meth. A **441** (2000) 9.

[16] A. V. Fedotov, “IBS for Ion Distribution Under Electron Cooling,” Proc. of PAC05, Knoxville, Tennessee, USA, 2005.

[17] A. V. Fedotov, A. O. Sidorin, A. Smirnov, “IBS for Non-Gaussian Distributions,” BNL-94081-2010-CP (2010).

[18] A. Burov, “Electron Cooling against IBS for High Energy Colliders,” FERMILAB-TM-2213 (2003).

[19] G. Parzen, BNL Tech. Note C-AD/AP/150 (2004).

[20] P. Zenkevich, O. Boine-Frankenheim, A. Bolshakov, Nucl. Instrum. Meth. A **561** (2006) 284.

[21] BNL BETACOOL report, Dec. 2007: `http://betacool.jinr.ru/reports`

[22] C. Carli, private communication.

Intra-beam Scattering Effects in the Extra Low ENergy Antiproton ring (ELENA)

Javier Resta-Lopez,
James Hunt, Carsten Welsch,
Cockcroft Institute, The University of Liverpool

IPAC 2015
Richmond, Virginia, USA

Outline

- Context
- ELENA overview
- Emittance dilution and lifetime limiting processes
  - Rest gas
  - IBS
- Beam evolution
- Summary and Future plans

Context

Antiproton Decelerator (AD) at CERN

The AD provides low-energy antiprotons (5.3 MeV kinetic energy) for different experiments dedicated to the production of antihydrogen and measurement of its properties

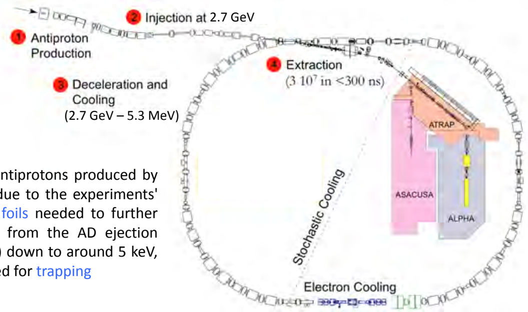

≈ 99.9% of the antiprotons produced by the AD are lost due to the experiments' use of degrader foils needed to further decelerate them from the AD ejection energy (5.3 MeV) down to around 5 keV, the energy needed for trapping

Context

Antiproton Decelerator (AD) and ELENA at CERN

ELENA will bring a 10 to 100-fold increase in the experiments' efficiency, as well as the possibility to accommodate an extra experimental area to investigate gravitation with antihydrogen (GBAR)

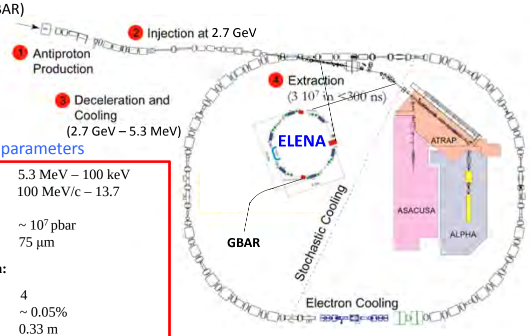

Basic ELENA beam parameters

Energy range	5.3 MeV – 100 keV
Momentum range	100 MeV/c – 13.7 MeV/c
Intensity	~ 10^7 pbar
Transverse acceptance	75 µm
Parameters at ejection:	
Number of bunches	4
$\Delta p/p$ (rms)	~ 0.05%
Bunch length (rms)	0.33 m
ε_x, ε_y (rms)	~ 1 π mm mrad

ELENA overview

Schematic layout

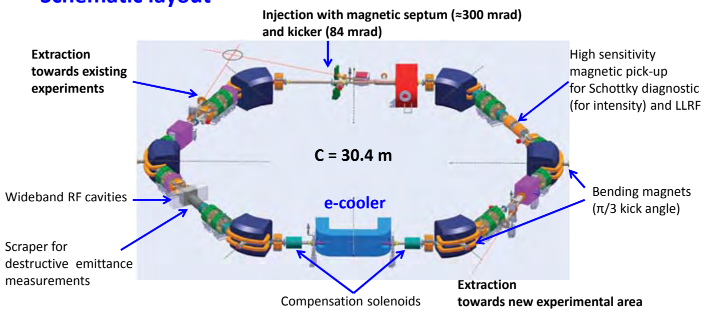

The e-cooler must be able to produce a cold and relatively intense electron beam:

$$k_B T_\perp < 0.1 \text{ eV}, \quad k_B T_\parallel < 0.001 \text{ eV} \qquad n_e \approx 1.5 \times 10^{12} \text{ m}^{-3}$$

Details in ELENA TDR, CERN-2014-002 (April 2014)

ELENA overview

Optics

Good tunability in the range $2 < Q_x < 2.5$ and $1 < Q_y < 1.5$

$Q_x \approx 2.3$, $Q_y \approx 1.3$

max $\beta_x \approx 12$ m
max $\beta_y \approx 6$ m
max $D_x \approx 1.7$ m
$<\beta_{x,y}> \approx 3$ m
$<D_x> \approx 1.2$ m

At e-cooler position:
$\beta_x \approx 2$ m
$\beta_y \approx 2$ m
$D_x \approx 1.5$ m

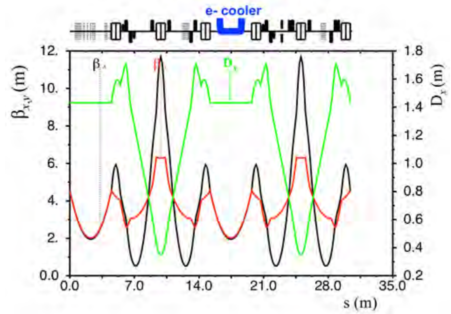

MADX model based on the specifications of the ELENA TDR

ELENA overview

ELENA cycle

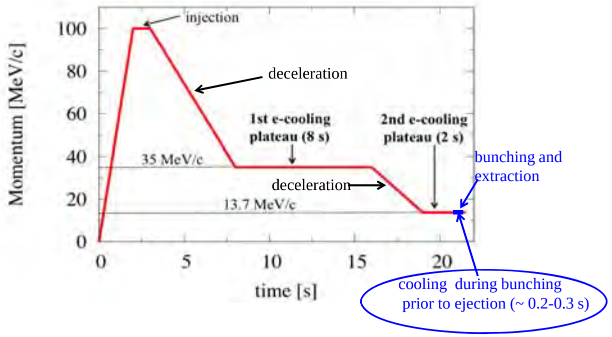

We have mainly focused on beam dynamics studies during the 1st and 2nd **e-cooling plateaus**

Emittance dilution and lifetime limiting processes

Heating processes:

- Interaction with the **rest gas**:
  - Nuclear scattering
  - Single Coulomb scattering } ⟶ particle loss if high scattering angle
  - Multiple Coulomb Scattering (MCS)
  - The ELENA vacuum pipe will be coated with Non-evaporable Getter (NEG) films
  - Expected residual gas composition: **95% H_2, 2% CO, 2% CO_2, 1% CH_4**
  - Nominal vacuum pressure for ELENA: **P=3x10^{-12} Torr**
  - **This pressure is a very safe limit in terms of both low MCS effect and very low rate of large angle scattering**
- **Intra-Beam Scattering (IBS):** Multiple small-angle Coulomb scatterings of charged particles within the accelerator beam itself. Exchange of energy between the transverse and longitudinal degrees of freedom

BETACOOL simulations

BETACOOL: [A. Sidorin et al., NIM A 558 (2006), 325]

- Calculation of the evolution of beam distributions under the action of cooling forces (in this case electron cooling) + different scattering effects
- Benchmarked against experimental data in different rings, e.g.

Experimental studies of IBS in RHIC and comparison with BETACOOL simulations

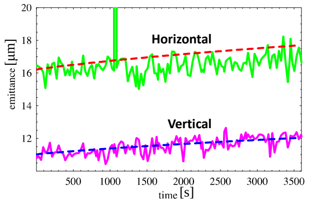

[A. V. Fedotov et al., Proc. of HB2006, WEBY03, Tsukuba, Japan, 2006]

BETACOOL simulations

Simulation conditions:

- Multiparticle simulations based on a Monte-Carlo method (model beam algorithm)
- 1000 modelled particles
- Coasting antiproton beam (at cooling plateaus) and bunched beam (before extraction)
- Electron cooling considering a cylindrical uniform electron beam distribution
- Cooling process + Rest gas + IBS (Martini model)
- Cooling friction force computed using the Parkhomchuk's model (magnetised electron distributions)

Beam evolution

1st cooling plateau, p=35 MeV/c, coasting beam

- **Electron cooling process in presence of rest gas and IBS**

Parameter evolution:

Simulated 10 random seeds for the evolution of a distribution of 1000 modelled particles

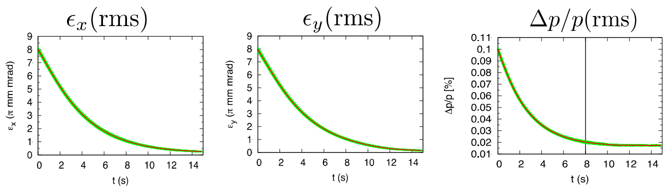

Step in cycle	ε_x, ε_y [π mm mrad] (rms)	Δp/p [%] (rms)
Start 1st cooling (35 MeV/c)	8.0, 8.0	0.1
After 8 s cooling (35 MeV/c)	**1.1, 1.1**	**0.02**

Conservative initial values

Beam evolution

1st cooling plateau, p=35 MeV/c, coasting beam

- **Electron cooling process in presence of rest gas and IBS**

Beam profile evolution:

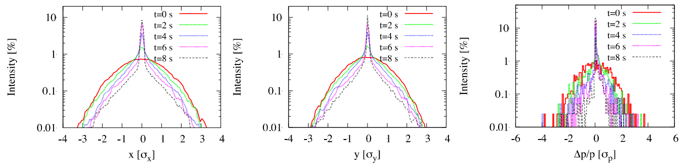

During the cooling process, the beam distribution quickly deviates from a Gaussian profile and a very dense core appears

Core overcooling. Underestimating IBS effect in the core?

Beam evolution

1st cooling plateau, p=35 MeV/c, coasting beam

- **Core-tail development:**

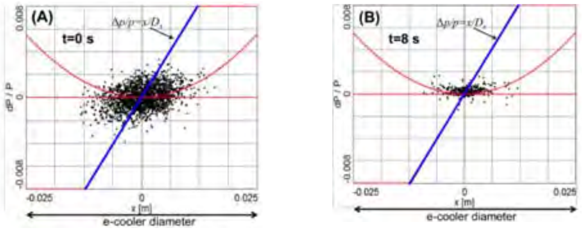

The parabola represents the momentum spread of the electrons due to space charge

For large initial beam size, particles in the tails experience weaker friction forces than in the core → development of core-tail particle distributions

Beam evolution

- **Core-tail development:**

Standard models of IBS, such as the Martini model, are based on the growth of the rms beam parameters of a Gaussian distribution. These models underestimate the IBS effect for non-Gaussian distributions.

Further investigation:

- Apply an IBS "core-tail" model (bi-Gaussian distribution): IBS induced kicks based on diffusion coefficients which are different for particles inside and outside of the core
- Apply a IBS "Local" model: can calculate correctly IBS for arbitrary distributions, but it takes a lot of computation time

[A. V. Fedotov, "IBS for Ion Distribution Under Electron cooling" Proc. PAC2005]

Beam evolution

1st cooling plateau, p=35 MeV/c, coasting beam

- **Core-tail development: IBS Martini model vs core-tail model:**

Beam distributions after 8 s cooling

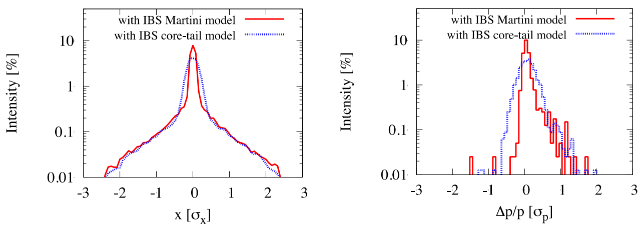

The cooling of the core is smoother if an IBS core-tail model (bi-Gaussian) is applied and, probably, it describes more accurately the actual process

Beam evolution

2nd cooling plateau, p=13.7 MeV/c, coasting beam

- **Electron cooling process in presence of rest gas and IBS**

Parameter evolution:

Simulated 10 random seeds for the evolution of a distribution of 1000 modelled particles

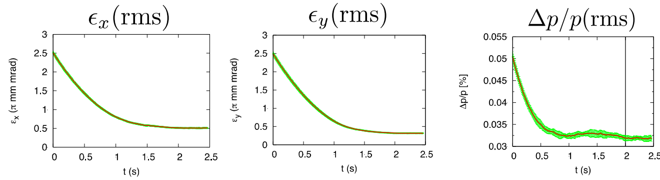

Step in cycle	ε_x, ε_y [π mm mrad] (rms)	Δp/p [%] (rms)
Start 2nd cooling (13.7 MeV/c)*	2.8, 2.8	0.05
After 2 s cooling (13.7 MeV/c)	**0.52, 0.33**	**0.033**

*Taking into account the adiabatic emittance increase by a factor ≈ 2.55 because of the deceleration from 35 MeV/c to 13.7 MeV/c

Beam evolution

2nd cooling plateau, p=13.7 MeV/c, coasting beam

- **Electron cooling process in presence of rest gas and IBS**
  Beam profile evolution:

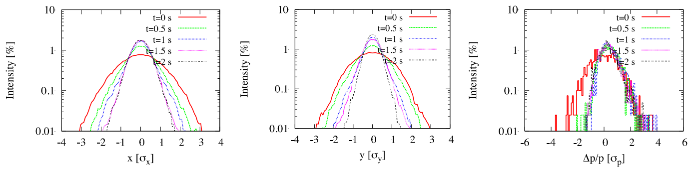

In this case, the cooling is more homogeneous for both core and tails, and after 2 s cooling the beam reaches the equilibrium

Beam evolution

Before extraction, p=13.7 MeV/c, bunched beam

- **Electron cooling process in presence of rest gas and IBS**
  Parameter evolution:
  Simulated 10 random seeds for the evolution of a distribution of 1000 modelled particles

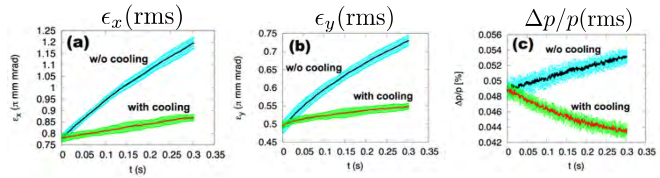

With cooling:

Step in cycle	ε_x, ε_y [π mm mrad] (rms)	Δp/p [%] (rms)
Start cooling (13.7 MeV/c)*	0.78, 0.49	0.049
After 0.3 s cooling (13.7 MeV/c)	0.9, 0.55	0.043

*Starting values assuming Debunching/bunching with 50% blow-up

Summary and Future plans

- For a better understanding of the long term beam dynamics in the ELENA ring, we have started a detailed investigation into the different cooling and heating processes which determine the beam lifetime and quality of the antiproton beam
- Here we have put special emphasis on the study of the cooling process in presence of IBS

Next steps:

- Comparison of equilibrium parameters using different models of IBS
- Simulations including e-cooler imperfections
- For simplicity we have assumed initial Gaussian beam profiles. However, in practice, the distribution of the beam injected from the AD could have a significant non-Gaussian shape. This characteristic will be taken into account in future studies.
- Identify potential aspects of the machine that could be optimised
- ELENA will be an ideal test-bench to compare experiments and simulations of e-cooling at very low energies

University of Liverpool — The Cockcroft Institute

Special thanks to:

Christian Carli, Alexander Smirnov, and all the ELENA team at CERN

Thank you

ELENA — QUASAR — BeaPhy

Intrabeam scattering

IBS theory extensively described in the literature, see e.g.

- A. Piwinski, Proc. of the 9th International Conference on High Energy Accelerators, 1974, p. 405: smooth lattice approximation
- J. Bjorken, S. Mtingwa (B-M), Part. Accel. 13 (1983) 115: using the scattering matrix formalism; valid for strong focusing machines; approximations valid for ultrarelativistic beams only
- M. Martini, CERN PS/84-9 (AA) 1984: (extended Piwinski's model) valid for strong focusing machines.
- M. Conte, M. Martini, Part. Accel. 17 (1985) 1: B-M theory adapted to include non-ultrarelativistic corrections
- and several approximations for practical purposes in some regimes of applicability (Wei, Parzen, Bane, Rao and Katayama, …), as well as refinements of the standard theories above, …

Reservoir

Context

- The **Antiproton Decelerator (AD)** at CERN provides low-energy antiprotons (5.3 MeV kinetic energy) for different experiments dedicated to the production of antihydrogen and measurement of its properties
- In today's set-up, about 99.9% of the antiprotons produced by the AD are lost due to the experiments' use of degrader foils needed to further decelerate them from the AD ejection energy (5.3 MeV) down to around 5 keV, the energy needed for trapping

From N. Madsen, Antiproton catching for antihydrogen experiments, ELENA Beam Physics and Performance Committee (19 July 2012):

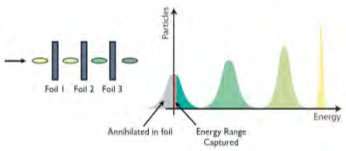

Energy straggling increases energy spread such that only few antiprotons can be captured

Context

Current setup:

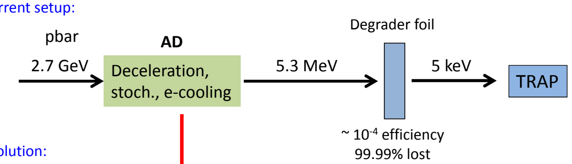

The solution:

- A small magnet ring that will fit inside the present AD hall – **ELENA**: 30 m circumference decelerator to slow the 5.3 MeV antiprotons from the AD to an energy of just 100 keV.

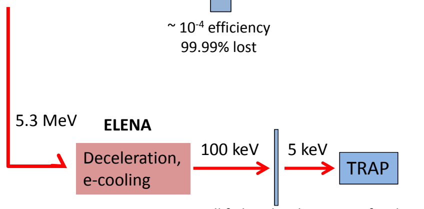

Still foil to decelerate to a few keV, but much reduced thickness

ELENA will bring a 10 to 100-fold increase in the experiments' efficiency, as well as the possibility to accommodate an extra experimental area to investigate gravitation with antihydrogen (GBAR)

ELENA overview

- **ELENA parameters**

For a coasting beam

Parameter	1st plateau	2nd plateau
Beam momentum	**35 MeV/c**	**13.7 MeV/c**
Initial $\Delta p/p$	0.1%	0.05%
Initial 1σ emittance	8 π mm mrad	2.8 π mm mrad
Beam intensity	$2.5\text{x}10^7$	$2.5\text{x}10^7$
Average beta function β_T	3 m	3 m
Average dispersion D_x	1.2 m	1.2 m
ELENA acceptance A_T	75 µm	75 µm
Vacuum pressure	$3\text{x}10^{-12}$ Torr	$3\text{x}10^{-12}$ Torr
Gas density n (at room T)	$9.6\text{x}10^{10}$ m^{-3}	$9.6\text{x}10^{10}$ m^{-3}

Electron cooler

- **ELENA e-cooler system parameters for the simulations**

From ELENA TDR, CERN-2014-002 (2014):

Parameter	Value
Momentum [MeV/c]	35 - 13.7
Velocity factor β=v/c	0.037 – 0.015
Electron beam energy [eV]	355 - 55
Electron current [mA]	5 - 2
Electron beam density [m^{-3}]	$1.38\text{x}10^{12}$ – $1.41\text{x}10^{12}$
B_{gun} [G]	1000
B_{drift} [G]	100
Expansion factor	10
Cathode radius [mm]	8
Electron beam radius [mm]	25
Twiss parameters [m]	β_x=2.103, β_y=2.186, D_x=1.498
Flange-to-flange length [mm]	1930
Drift solenoid length [mm]	1000
Effective length (good field region) [mm]	700
Electron beam transverse, longitudinal temperature [eV]	0.01, 0.001

Electron cooling

- **Friction force:**

The corresponding **friction force vs ion velocity**:

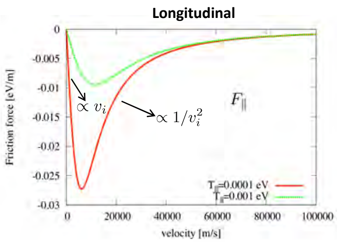

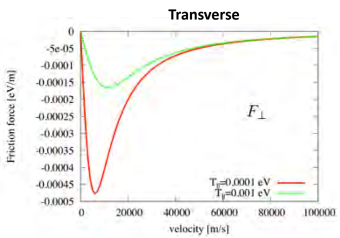

F peak (for T_{tr}=0.01 eV and T_{long}=0.0001 eV)= -0.027 eV/m, at v_i=6000 m/s
F peak (for T_{tr}=0.01 eV and T_{long}=0.001 eV)=-0.0095 eV/m, at v_i=11000 m/s

F peak (for T_{tr}=0.01 eV and T_{long}=0.0001 eV)= -0.00048 eV/m, at v_i=6000 m/s
F peak (for T_{tr}=0.01 eV and T_{long}=0.001 eV)=-0.00016 eV/m, at v_i=11000 m/s

Intrabeam scattering

IBS heating rates

$$\boxed{\frac{1}{\tau_x}, \frac{1}{\tau_y}, \frac{1}{\tau_p} \propto \frac{r_p^2 c}{32\pi\sqrt{\pi}\beta^3\gamma^4\epsilon_x\epsilon_y\sigma_p}\lambda}$$

$$\lambda = \begin{cases} N/C & \text{for coasting beams} \\ N_b/(2\sqrt{\pi}\sigma_s) & \text{for bunched beams} \end{cases}$$

IBS becomes stronger when the phase space volume of the beam is reduced by cooling, thus limiting the achievable final emittances

Beam dynamics

- **1st cooling plateau, p=35 MeV/c, coasting beam**
- **Electron cooling process in presence of rest gas and IBS**

IBS growth rates

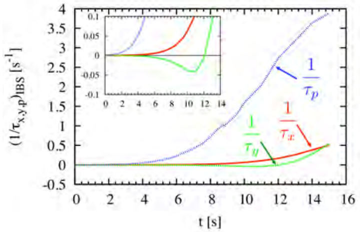

Cooling rates

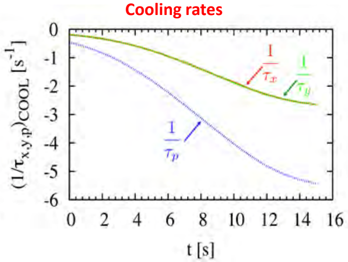

After 8s cooling, equilibrium is not yet reached
$(1/\tau_y)_{IBS}$ changes sign from negative (damping or cooling) to positive (heating) at t ≈13 s

Beam dynamics

- **2nd cooling plateau, p=13.7 MeV/c, coasting beam**
- **Electron cooling process in presence of rest gas and IBS**

IBS growth rates

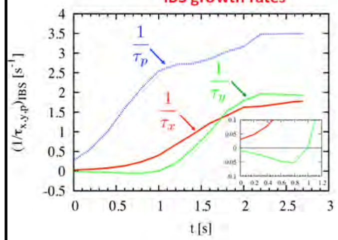

Cooling rates

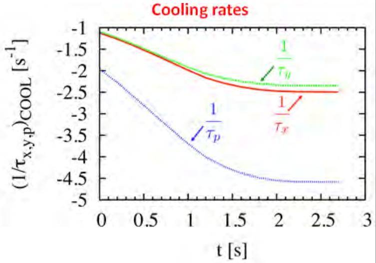

Equilibrium practically reached after 2 s cooling
$(1/\tau_y)_{IBS}$ changes sign from negative (damping or cooling) to positive (heating) at t ≈ 1 s

Beam dynamics

- **Electron cooling process in presence of rest gas and IBS**
  Invariant distributions

1st cooling plateau, p=35 MeV/c

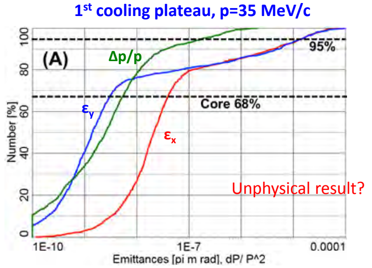

Core emittances (68%) ~ 10^{-8}, 10^{-9} π m rad
95% emittances ~ 10^{-5} π m rad

Very dense core
Long tails highly populated

Standard models of IBS, such as the Martini model, are based on the growth of the rms beam parameters of a Gaussian distribution. These models underestimate the IBS effect for beam distributions far from Gaussian.

Further investigation to prevent overcooling:

- Apply "core-tail" models
- Apply a "Local" model: it takes a lot of computation time!

Space charge

- Space charge limit N for a stored antiproton beam with **ΔQ=-0.1**

Incoherent tune shift due to space charge effects:

For a Gaussian distributed round beam:

$$\Delta Q_{sc} \approx -\frac{r_p N}{4\pi\beta^2\gamma^3\epsilon} B_f^{-1}$$

where B_f is a bunching factor:

$$B_f = \frac{\langle I \rangle}{\hat{I}} \begin{cases} 1 & \text{if coasting beam} \\ \frac{\sqrt{2\pi}\sigma_z}{C} h & \text{if bunched beam} \end{cases}$$

Here we have taken the rms emittance ϵ

h is the harmonic number

Bunched beam

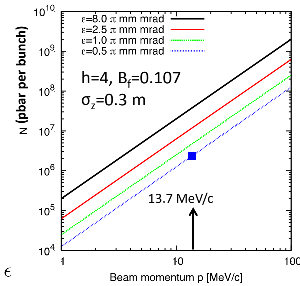

4 bunches, assuming $\varepsilon_{x,y}$≈0.5 π mm mrad
N_{total} ≈ 1x10^7

INVESTIGATIONS INTO DIELECTRIC LASER-DRIVEN ACCELERATORS USING THE CST AND VSIM SIMULATION CODES*

Y. Wei#, C.P. Welsch, Cockcroft Institute and University of Liverpool, UK
G. Xia, O. Mete, K. Hanahoe, Cockcroft Institute and University of Manchester, UK
J.D.A. Smith, Tech-X UK Ltd, Sci-Tech Daresbury, Warrington, UK

Abstract

Dielectric laser-driven accelerators (DLAs) based on gratings structures have received a lot of interests due to its high acceleration gradient up to GV/m and mature lithographic techniques for fabrication. This paper presents detailed numerical studies into the acceleration of relativistic and non-relativistic electrons in double gratings silica structures. The optimization of these structures with regards to maximum acceleration efficiency for different spatial harmonics is discussed. Simulations were carried out using the commercial CST and VSim simulation codes and results from both codes are shown in comparison.

INTRODUCTION

Dielectric laser-driven accelerators (DLA) have good potential to become a strong candidate for future electron accelerators. Due to a higher damage threshold than metals, these dielectric microstructures can support accelerating fields higher than what can be achieved in conventional accelerators. This can increase the acceleration gradients up to GV/m. An experiment has successfully demonstrated acceleration of relativistic electrons with an accelerating gradient of 250 MV/m in a fused silica double grating structure [1] and the acceleration of non-relativistic 28 keV electrons with a gradient of 25 MeV/m in a single grating structure was also observed [2].

This paper investigates dielectric laser-driven acceleration of electrons in a double grating structure exploiting the different spatial harmonics excited by the diffraction of the incident laser. The double grating structure was originally proposed by Plettner [3] and is shown in Figure 1. Each grating pillar adds a phase shift with respect to the adjacent vacuum space, which produces a longitudinally periodic oscillating electric field in the centre of the vacuum channel. Optimization studies into these structures by parameter variation studies have already been performed with the aim to increase the acceleration efficiency for highly relativistic electrons [4,5]. Here, we consider also the non-relativistic case where electrons are injected at an energy of 25 keV, corresponding to β=0.3, where β=v/c, v the electron velocity and c the speed of light. Different spatial harmonics were considered using the CST [6] and VSim [7] simulation codes to identify the optimum acceleration efficiency and comparing simulation results.

*This work is supported by the EU under Grant Agreement 289191 and the STFC Cockcroft Institute core grant No.ST/G008248/1.
#yelong.wei@cockcroft.ac.uk

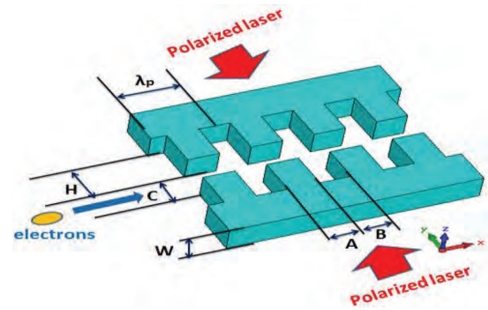

Figure 1. Schematics of a dielectric grating structure.

ACCELERATION OF HIGHLY RELATIVISTIC ELECTRONS

When a double grating structure is driven by two TM polarized laser beams from opposite sides, the diffraction of the incident laser at the grating excites different spatial harmonics which can all be used in principle to accelerate the electrons, see Figure 2.

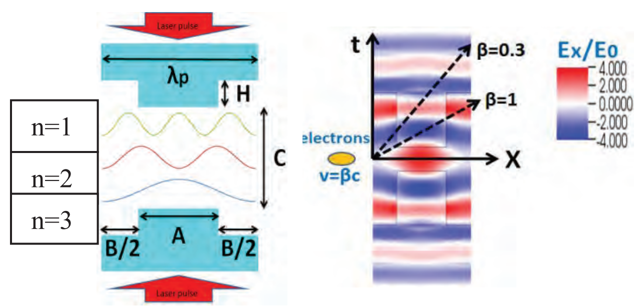

Figure 2. Illustration of the first, second and third spatial harmonics for the case that one grating period is illuminated by laser from two sides.

In the simulations an incoming plane wave with a wavelength of λ_0=1,550 nm was used to excite the grating structure from two sides. Silica (SiO_2, refractive index n=1.528) was chosen as grating material due to its good properties in terms of transparency and field damage threshold. Figure 3 shows the acceleration efficiency for different structure parameters for a grating period of λ_p = 1,550 nm. With an increase of the vacuum channel width C, the acceleration efficiency η gradually decreases, as can be seen in Figure 3(a). Figure 3(b) shows that the maximum acceleration efficiency can be achieved when the pillar height H=0.87λ_p. For further optimization the pillar ratio A/λ_p was varied and Figure 3(c) shows the resulting optimum acceleration efficiency of 0.25 and 0.26 as computed by VSim and CST, respectively.

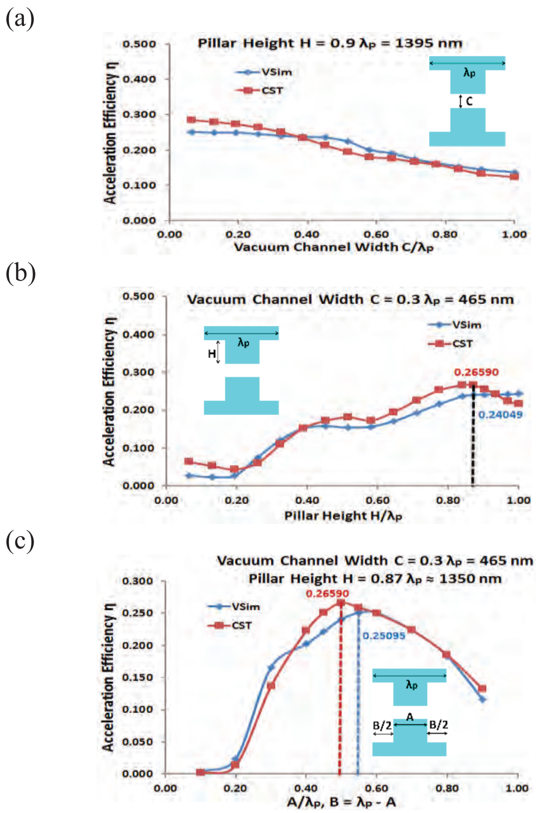

Figure 3. Acceleration efficiency $\eta = G/E_p$, where G is the average acceleration gradient and E_p the peak electric field in the grating structure as a function of vacuum channel width C (a), pillar height H (b) and pillar ratio A/λ_p (c).

Table 1. Optimum Parameters for Relativistic Electrons at a Fixed Channel Width $C=0.3\lambda_p=465$ nm

	VSim	CST
Pillar height H/λ_p	0.87	0.87
Pillar ratio A/λ_p	0.55	0.50
Acceleration efficiency η	0.25	0.26
Maximum gradient G (GV/m)	2.175	2.262

The damage threshold for silica is about 1 J/cm^2 for laser pulses of 100 fs [8]. This is equivalent to an electric field of E_{th}=8.7 GV/m and hence the maximum gradient is about 0.25·8.7=2.175 GV/m and 0.26·8.7=2.262 GV/m according to VSim and CST, respectively, see Table 1.

A laser system with 2 mJ pulse energy and 1 ps width would generate an input field E_0=2 GV/m and hence a gradient of about 2 GV/m for a 10 mm long and 0.04 mm high double grating structure. In this configuration even gradients as high as 2.0 GV/m would still not damage the silica structure.

ACCELERATION OF NON-RELATIVISTIC ELECTRONS

In the case of non-relativistic electrons the grating period λ_p, the laser wavelength λ_0 and the electron velocity β=v/c have to be matched, yielding the synchronicity condition $\lambda_p = n\ \beta\ \lambda_0$ [9]. Here, n is the numbers of laser cycles per electron passing one grating period, v is the speed of the electron and c is again the speed of light. Different spatial harmonics will be excited in the double grating structure, providing several principle options to accelerate the electrons. This will be studied in the following.

First Spatial Harmonics

First, a grating period of $\lambda_{p1}=0.3\lambda_0$ was chosen. In this case the first spatial harmonics is in synchronicity with the electrons along the double grating structure.

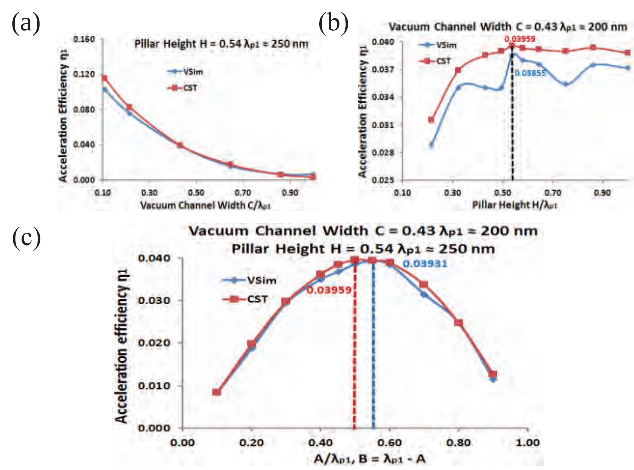

Figure 4. Acceleration efficiency as a function of vacuum channel width C (a), pillar height H (b) and pillar ratio A/λ_{p1} (c).

Figure 4(a) shows the effect from increasing the vacuum channel gap on the acceleration efficiency. Figure 4(b) shows that the maximum gradient appears if $H=0.54\lambda_{p1}$. Finally, an optimization of the pillar ratio A/λ_{p1} can be done to give the maximum acceleration efficiency, as shown in Figure 4(c). Optimum parameters are summarized in Table 2.

Table 2. Optimum Parameters for the 1st Spatial Harmonic as Calculated by VSim and CST for $C=0.43\lambda_{p1}\approx200$ nm

	VSim	CST
Pillar height H/λ_{p1}	0.54	0.54
Pillar Ratio A/λ_{p1}	0.55	0.50
Acceleration efficiency η_1	0.04	0.04
Maximum gradient G (GV/m)	0.348	0.348

Second Spatial Harmonics

Second, a grating period λ_{p2}=0.6λ_0, was considered, allowing electron acceleration by the second spatial harmonics.

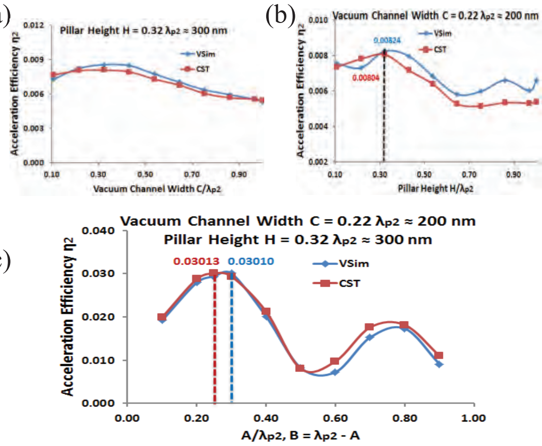

Figure 5. Acceleration efficiency as function of vacuum channel width C (a), pillar height H (b) and pillar ratio A/λ_{p2} (c).

Table 3. Optimum Parameters for the 2nd Spatial Harmonic Using C=0.22$\lambda_{p2}\approx$200 nm

	VSim	CST
Pillar height H/λ_{p2}	0.32	0.32
Pillar Ratio A/λ_{p2}	0.30	0.25
Acceleration efficiency η_2	0.03	0.03
Maximum gradient G (GV/m)	0.261	0.261

Third Spatial Harmonics

Third, a grating period λ_{p3}=0.9λ_0 was analysed, allowing to use the third spatial harmonic for acceleration .

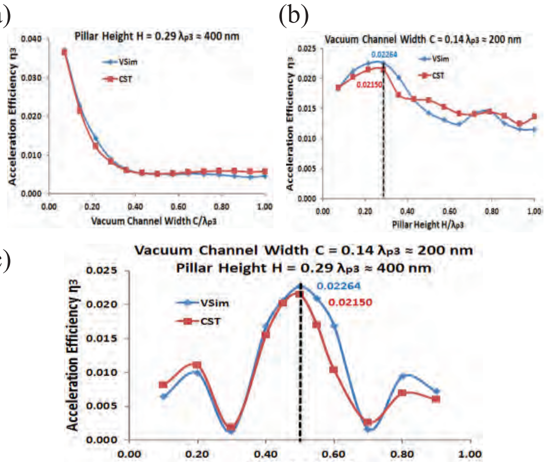

Figure 6. Acceleration efficiency as function of vacuum channel width C (a), pillar height H (b) and pillar ratio A/λ_{p3} (c).

Table 4. Optimum Parameters for the 3rd Spatial Harmonic at a Fixed C= 0.14$\lambda_{p3}\approx$200 nm

	VSim	CST
Pillar height H/λ_{p3}	0.29	0.29
Pillar Ratio A/λ_{p3}	0.50	0.50
Acceleration efficiency η_3	0.02	0.02
Maximum gradient G (GV/m)	0.174	0.174

CONCLUSION

The results from optimization studies to maximize the acceleration efficiency of highly relativistic and non-relativistic (β=0.3) electrons in a double grating structure were presented in this paper. Simulations were performed with the VSim and CST codes and very good agreements between the simulation results were found, giving confidence in the validity of the results. For highly relativistic electrons where λ_p=λ_0 the maximum gradient was found to be 2.175 GV/m and 2.262 GV/m, according to VSim and CST, respectively. As for non-relativistic electrons, an optimum compromise between acceleration efficiency and fabrication limitations, was identified in acceleration using the second spatial harmonics (λ_{p2}=0.6λ_0) to accelerate 25 keV (β=0.3) electrons. In this case accelerating gradients of up to 261 MV/m can be expected.

In a next step multistage DLA from the non-relativistic to highly relativistic regime will be investigated. It is also planned to carry out experimental studies into these structures using the available electron beam at Daresbury laboratory in the near future.

REFERENCES

[1] E. A. Peralta et al., Nature 503, 91 (2013).
[2] J. Breuer and P. Hommelhoff, Phys. Rev. Lett. 111, 134803(2013).
[3] T. Plettner, P. P. Lu, and R. L. Byer, Phys. Rev. STAB 9, 111301 (2006).
[4] A. Aimidula et al., Physics of Plasmas 21, 023110 (2014).
[5] A. Aimidula, et al., Nucl. Instr. Meth. A 740 (2014), p. 108-113.
[6] CST, available from www.cst.com
[7] VSim, available from www.txcorp.com
[8] M. Lenzner et al., Phys. Rev. Lett. 80, 4076-4079 (1998).
[9] T. Plettner et al., Phys. Rev. STAB 12, 101302 (2009).

Investigations into Dielectric Laser-driven Accelerators using the CST and VSim Simulation Codes

Yelong Wei, Carsten P. Welsch, *Cockcroft Institute and University of Liverpool, UK*
Guoxing Xia, Oznur Mete, Kieran Hanahoe, *Cockcroft Institute and University of Manchester, UK*
Jonathan D. A. Smith, *Tech-X UK Ltd, Sci-Tech Daresbury, Warrington, UK*

Abstract

Dielectric laser-driven accelerators (DLAs) have good potential to become a strong candidate for ultra-compact electron accelerators, because they can sustain high acceleration gradients up to GV/m. Recent proof-of-principle experiments have successfully demonstrated acceleration of electrons with accelerating gradients of up to 250 MV/m in such novel structures. This contribution presents detailed numerical studies into the acceleration of relativistic and non-relativistic electrons in double gratings silica structures. The optimization of these structures with regards to maximum acceleration efficiency for different spatial harmonics is discussed. Simulations were carried out using the commercial CST and VSim simulation codes and results from both codes are shown in comparison.

❖ Introduction

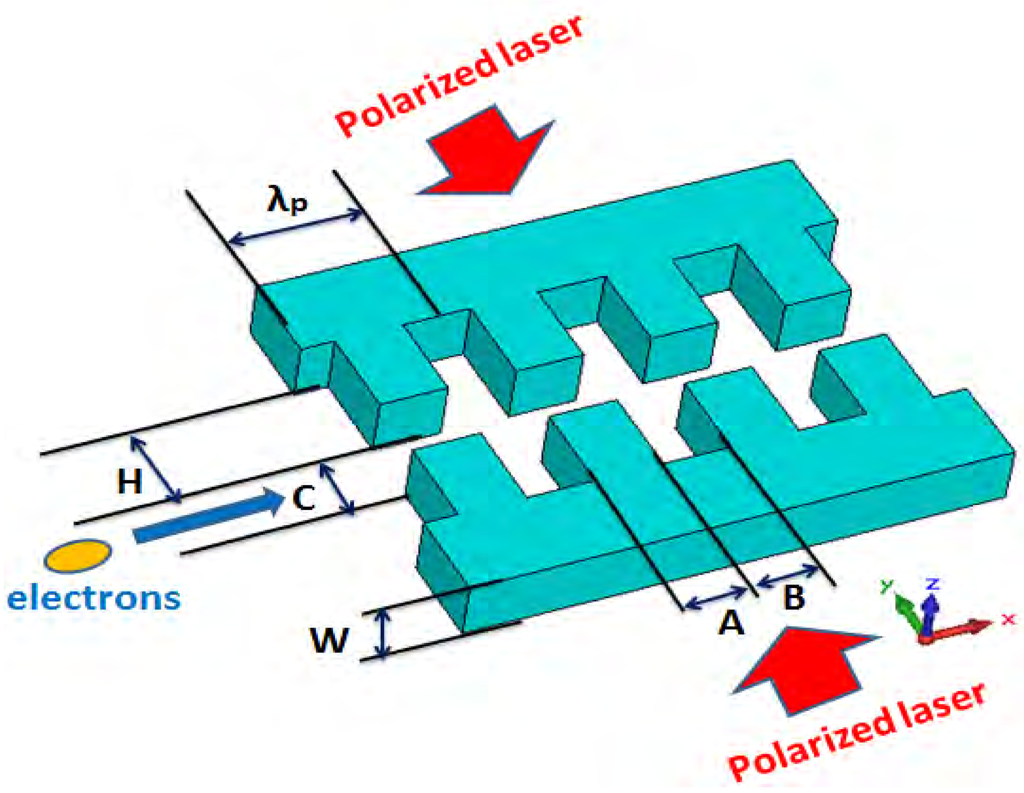

- Particles at any speed of β can be accelerated;
- It has higher acceleration efficiency and less deflection force compared to single grating acceleration of electrons;
- A symmetric profile of the accelerating fields;

❖ Principle

Grating period λ_p, laser wavelength λ_0 and electron velocity $\beta = v/c$ have to be matched, yielding the synchronicity condition

$$\lambda_p = n\,\beta\,\lambda_0$$

n is the numbers of laser cycles per electron passing one grating period.

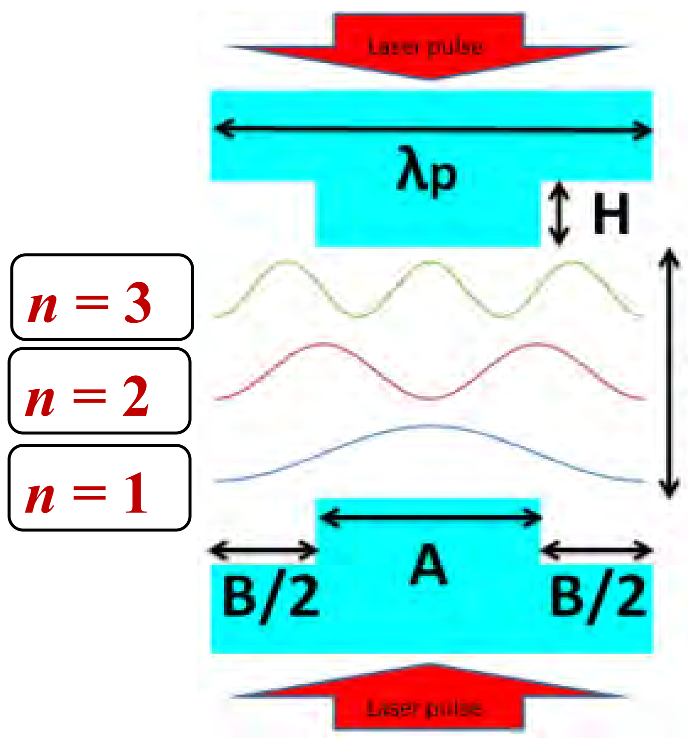

❖ Optimization on acceleration of highly relativistic electrons

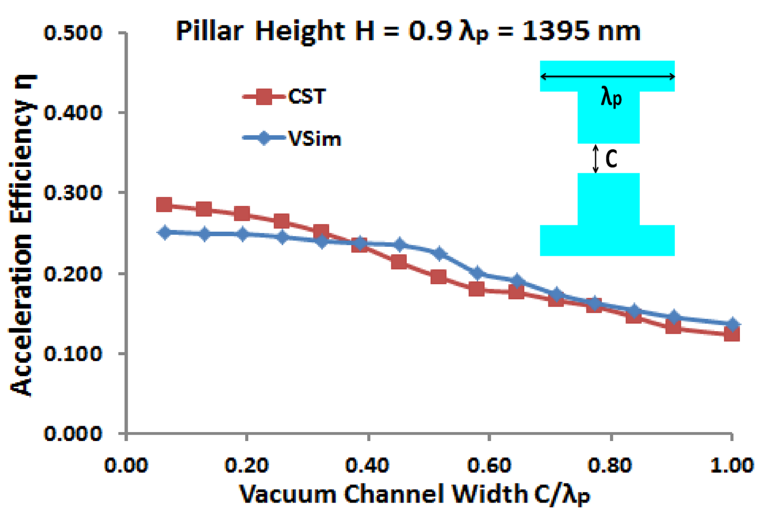

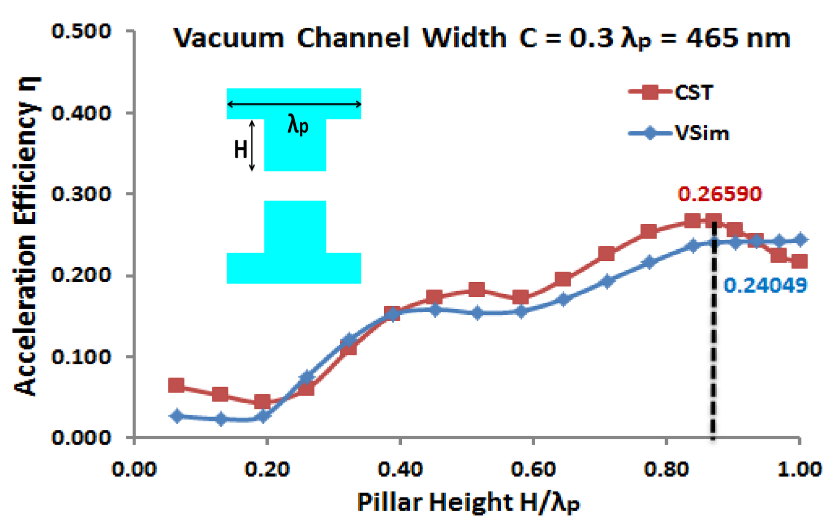

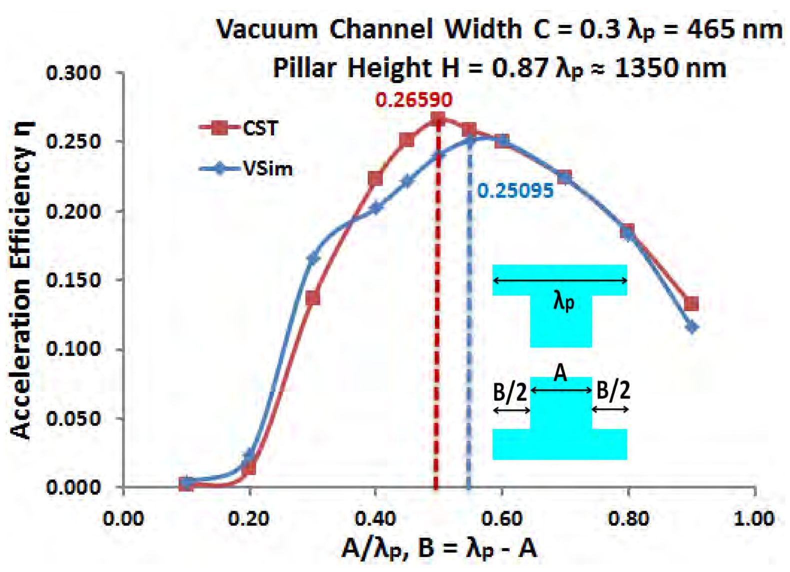

The grating period λ_p = 1550 nm; C=465 nm, H=1350 nm

Acceleration efficiency
- ❑ η=G/E_p= 0.26 ---CST
- ❑ η=G/E_p= 0.25 ---VSim

where G is the average acceleration gradient, E_p is the peak electric field in the grating structure

Laser system	
Wavelength λ_0	1550 nm
Pulse energy	several μJ
Pulse width	100 fs to several ps

The dielectric material is chosen as silica(SiO_2); The damage threshold is 1 J/cm^2 at laser pulses of 100 fs , which is equivalent to peak field of 8.7 GV/m; maximum achieved acceleration gradient is about

0.26*8.7=2.262 GV/m ---CST
0.25*8.7=2.175 GV/m ---VSim

❖ Acceleration of LOW β=0.3 electrons by first harmonics, *n*=1

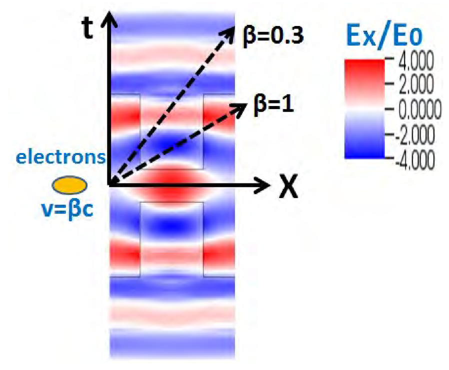

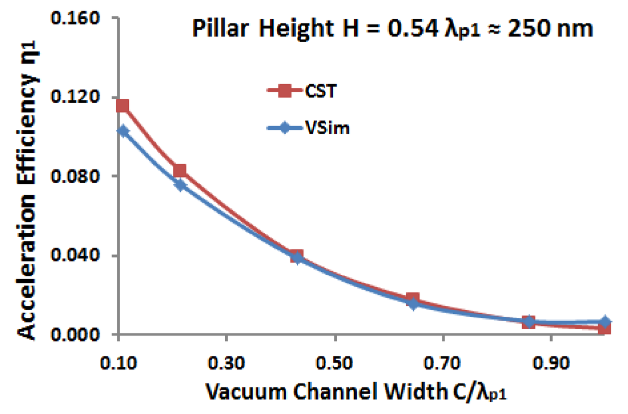

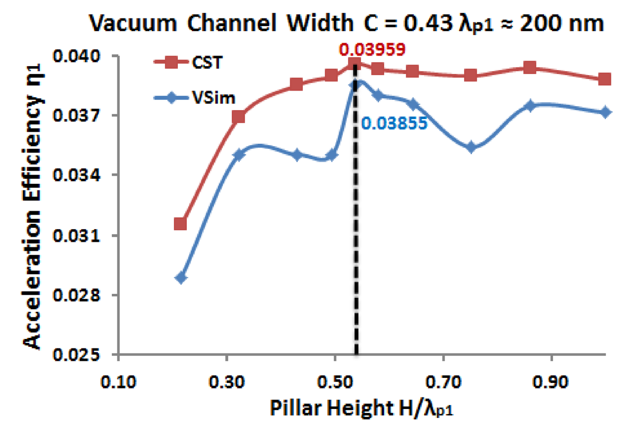

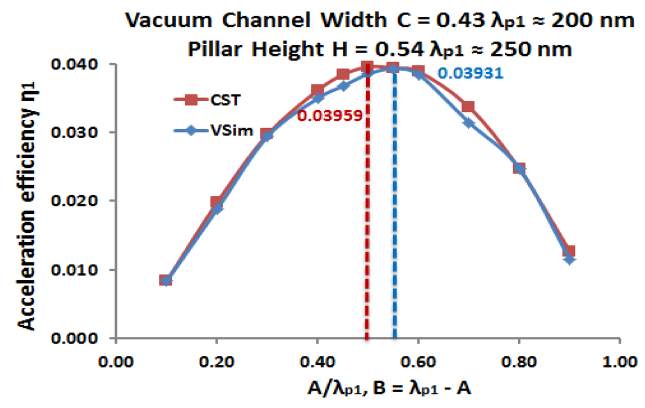

λ_{p1}= 465 nm; C=200 nm, H=250 nm

Acceleration efficiency
- ❑ η_1=G/E_p= 0.04 ---CST
- ❑ η_1=G/E_p= 0.04 ---VSim

❖ Acceleration of LOW β=0.3 electrons by second harmonics, *n*=2

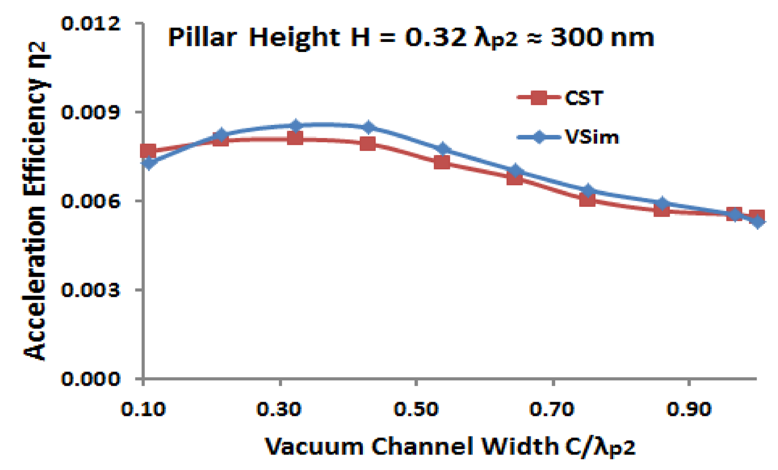

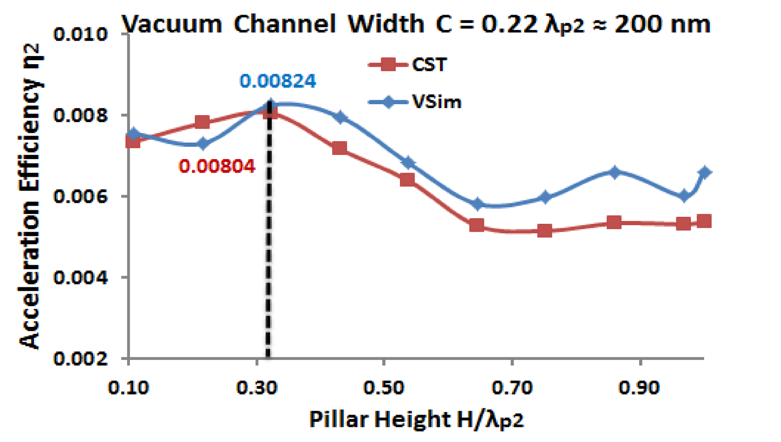

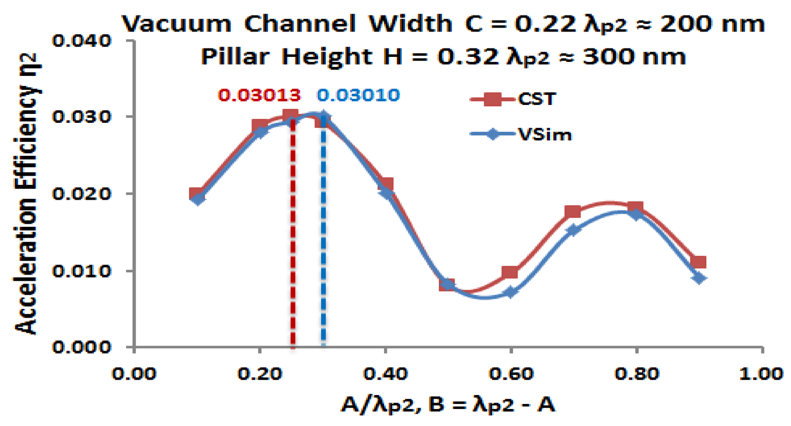

λ_{p2}= 930 nm; C=200 nm, H=300 nm

Acceleration efficiency
- ❑ η_2=G/E_p= 0.03 ---CST
- ❑ η_2=G/E_p= 0.03 ---VSim

❖ Acceleration of LOW β=0.3 electrons by third harmonics, *n*=3

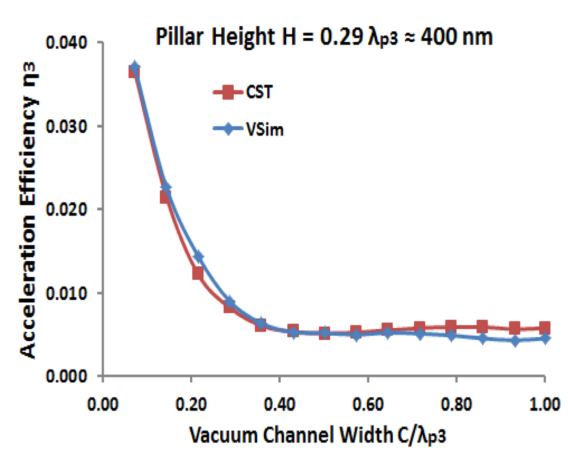

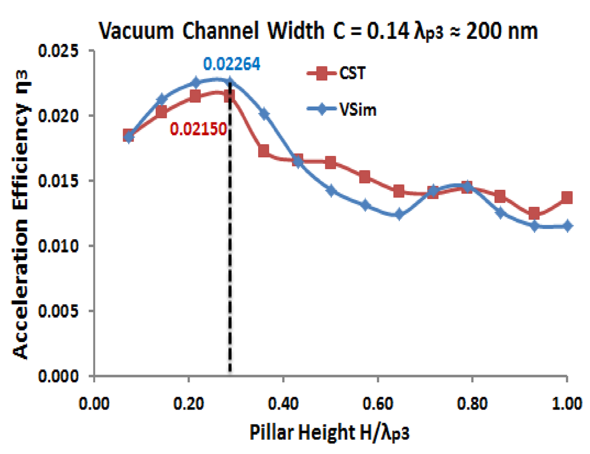

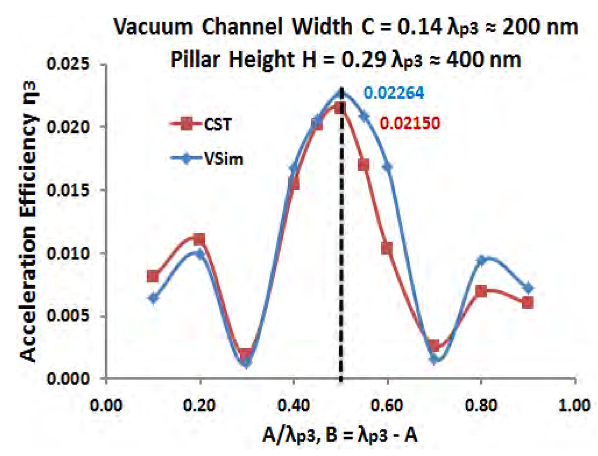

λ_{p3}= 1395 nm; C=200 nm, H=400 nm

Acceleration efficiency
- ❑ η_3=G/E_p= 0.02 ---CST
- ❑ η_3=G/E_p= 0.02 ---VSim

❖ Conclusion

- ❑ Acceleration Efficiency: **first harmonics > second harmonics > third harmonics;**
- ❑ Trade-off between fabrication limitation and acceleration efficiency, **second** harmonics has good potential for acceleration of 25 keV (β=0.3) electrons;
- ❑ If SiO_2 is chosen as the material, the achieved maximum gradient for **second** harmonics is **0.03*8.7=0.261 GV/m by CST and Vsim.**

❖ Outlook

- ❑ Do research on multistage DLA;
- ❑ Experimental studies for DLA;
- ❑ Investigate into new DLA structures

This work is supported by the EU under Grant Agreement No. 289191 and the STFC Cockcroft Institute core Grant No. ST/G008248/1

http://www.cockcroft.ac.uk
http://www.quasar-group.org
yelong.wei@cockcroft.ac.uk

Afterword

IPAC'15, the sixth International Particle Accelerator Conference, was held in historic Richmond, Virginia, USA from May 3-8, 2015 at the Greater Richmond Convention Center. The Group made a total of 9 contributions to the scientific program – all documented in this brochure – including posters on the most recent results from our gas jet setup, simulation studies into the optimization of dielectric laser accelerators, measurements using VELO and Novel Single Shot Bunch Length Diagnostic using Coherent Diffraction Radiation. A special highlight was a talk about Intra-beam Scattering Effects in ELENA by Marie Curie Senior Fellow Dr. Javier Resta-Lopez. He presented results from simulations that showed the impact of various factors on beam stability and lifetime in storage rings and how these might affect the quality of envisaged experiments. Dr. Resta-Lopez was joined at IPAC by Drs. Ralph Fiorito and Hao Zhang, Mr. Yelong Wei, QUASAR Group leader Prof. Carsten P. Welsch, as well as Dr. Ricardo Torres and Ms. Magda Klimontowska from our EU Project TEAM.

Ms. Klimontowska and Dr Torres presented the oPAC and LA³NET projects to the international accelerator community via a dedicated stand (see picture to the right), thus promoting the networks' Fellows and helping them attract future job opportunities. The stand displayed the projects' brochures, some selected videos produced by the Fellows and gave ample of opportunities for discussion with network partners and researchers from outside of the projects.

Our stand at IPAC 2015; from right to left: Ms. Magda Klimontowska and Dr. Ricardo Torres

The conference featured many interesting presentations, including talks about the AWAKE project and the HL-LHC upgrade – both projects in which the Group is already heavily involved in. The conference was found to be an ideal meeting point allowing for fruitful discussion with collaboration partners from all over the world.